MAGNETOPLASMADYNAMIC ARCJET THRUSTOR

Semi-Annual Report
2 May 1966 through 31 October 1966

AVSSD-0161-67

Prepared by

Avco Corporation
Space Systems Division
Research and Technology Laboratories
Wilmington, Massachusetts

31 March 1967

Contract NAS 3-8907

Prepared for

National Aeronautics and Space Administration
Lewis Research Center
Cleveland, Ohio

MAGNETOPLASMADYNAMIC ARCJET THRUSTOR

Semi-Annual Report
2 May 1966 through 31 October 1966

AVSSD-0161-67

Prepared by

Avco Corporation
Space Systems Division
Research and Technology Laboratories
Wilmington, Massachusetts

31 March 1967

Contract NAS 3-8907

Prepared for

National Aeronautics and Space Administration
Lewis Research Center
Cleveland, Ohio

TABLE OF CONTENTS

LIST OF ILLUSTRATIONS

LIST OF ILLUSTRATIONS (Continued)

I. INTRODUCTION

A. PROGRAM OBJECTIVES

The general objectives of Research and Development of a Magnetoplasmadynamic Arc Thrustor, conducted under Contract NAS3-8907 with the NASA/Lewis Research Center, are to conduct experimental and analytical investigations of the Magnetoplasmadynamic (MPD) Arcjet Thrustor. The scope of the program includes analysis and experimental evaluation of factors which establish the efficiency and reliability of the MPD arc thrustor. The work to be covered includes: (1) Parametric studies of the optimization of MPD thrustors, (2) analytical and experimental studies of the acceleration mechanism, (3) analysis of the cooling requirements, and (4) magnetic field coil design and cooling requirements.

B. PROGRAM ORGANIZATION

The program originates with the Spacecraft Technology Procurement Section of the NASA/Lewis Research Center. The NASA project manager is Mr. S. Domitz. The work on this contract is being performed by the Avco Research and Technology Laboratories in the Aero-Plasma Physics Directorate under Dr. R. R. John. Dr. S. Bennett is associate project manager. Other principal Avco/SSD participants are Dr. A. Tuchman, Dr. A. Malliaris, Mr. W. Powers, and Mr. G. Enos. The Avco-Everett Research Laboratory personnel who are directly assisting in the analytical effort

on this program are Dr. R. Patrick, Dr. J. Workman, and Mr. A. Schneiderman.

C. PROGRAM SCHEDULING

This report summarizes the first 6-month technical performance on the MPD program for the period 2 May 1966 through 31 October 1966. Expenditures of man-hours and contract costs, as well as the participation of engineering and scientific personnel, have been accounted in the monthly progress reports for the 6-month period.

D. TECHNICAL SUMMARY

An extensive comparison of MPD arcjet performance for liquid-cooled and radiation-cooled configurations has been made. Tests were conducted with ammonia propellant of 2"-, 3"-, and 4"-diameter radiation-cooled designs having tungsten anodes and cathodes. Comparative data were obtained with water-cooled engines of the same internal geometry. In addition, parametric variations in throat diameter, mass flow, magnetic field strength, and power level were carried out using water-cooled configurations to determine optimum performance conditions. A major conclusion derived from the experimental test program is that there is no significant difference in measured propulsion performance produced by the mode of engine cooling. The overall thrust efficiency in any case is poorer at very low mass flow rates resulting in high engine temperatures for the radiation engine. The maximum power input which can be tolerated with the radiation-cooled version varies approximately as the arcjet

linear dimension. It is also concluded, based on a series of tests with water-cooled configurations, that there is no strong dependence upon throat size or throat configuration, at least in the range of 0.5- to 0.85-inch throat diameter; outside of this range some flow instability develops at larger diameters and some lack of ability to handle the power develops at smaller diameters.

A radiation-cooled MPD arcjet design of 4-inch diameter appears to closely meet the objectives of the present study. A 75-hour lifetime test was performed on such an engine at the 3600-second, 34-percent overall efficiency level under exhaust environment conditions which were not optimum. Results of all tests performed indicate that at equivalent back pressures (about 100 microns), the performance of either the radiation or water-cooled MPD thrustor is substantially identical to test results reported by the NASA-Lewis Laboratory on comparable designs. The improved performance noted on the NASA-Lewis tests at very low back pressures therefore suggests about a 45-percent corresponding overall efficiency for the above test.

Analysis of the MPD arcjet discharge has been made using an analytical model of a j x B arc assuming one-dimensional, steady continuum fluid mechanics. The analysis considers the conservation relations for a three fluid gas (electrons, ions, and

neutrals) with appropriate transfer terms in mass, momentum, and energy for the three species. An applied axial magnetic field and an induced azimuthal field is assumed. The voltage characteristic is an empirical input. Transport coefficients and reaction rates are deduced from experimentally determined cross sections. Solutions are obtained through a set of first-order ordinary differential equations which are solved on a high-speed digital computer. Results for hydrogen gas typify the physical processes occurring in the MPD arc showing a strong discharge centered about the throat region of the nozzle. A low-pressure limit exists for the establishment of a high-current discharge and the current carried is pressure dependent.

A preliminary evaluation of a radiation-cooled magnetic field coil design and associated magnet subsystem was made to establish a technical approach to this requirement. Comparisons of the system weights for aluminum or copper magnets of 1-inch inner radius at 1 kilogauss shows a requirement of about 2 or 3 percent of the engine power-supply weight. Aluminum has a weight advantage at fields below 1 kilogauss and copper fields above 1 kilogauss. The total magnet- and power-supply weight within the approximations of the study is less than 50 pounds, and the operating temperature is below 500^{o}C. A Bitter type magnet design shows promise as an efficient and practical solution for a self-cooling design.

II. EXPERIMENTAL RESULTS

A. BACKGROUND

1. Power Range

On the basis of best present estimates[1-4], it appears that the development of power supplied within the next 10 to 15 year period will most likely be in the 5 to 50 kilowatt range. This power range has thus been selected for primary attention in MPD thrustor development.

2. MPD Thrustor Performance

A number of laboratories[6-14] have carried out MPD thrustor research. Although the devices differ in detail, the basic configuration is as indicated in figure 1. A summary performance curve[15] is given as figure 2. Apart from a continued interest in increasing the overall efficiency, the major problems now pertain to the development of a long-life radiation-cooled configuration and the determination of the effect of test environment on engine performance.

3. Propellant Characteristics

The most promising propellants presently under consideration for MPD thrustor operation are lithium and ammonia. The major advantage of lithium seems to reside in a smaller anode heating during operation; thus the thermal efficiency is higher, leading to possibly higher overall efficiencies, and the anode heat

rejection problem is less severe. The major advantage of ammonia is the avoidance of high temperatures in the feed system, and the fact that space flight qualified ammonia feed systems have been developed. Major emphasis in this program has been upon ammonia.

4. Magnet Assembly

In the power range 5-50 kilowatts MPD thrustors require external magnets. Although it is not definitively established, it appears that a solenoid of about 1 kilogauss axial field strength and inner radius of one or two inches is adequate. Development of a magnet configuration to provide this field at minimum weight and/or power is desired.

5. Conclusions

The main objective of this program is thus development of a long-lived, radiation-cooled, ammonia-fuelled MPD thrustor with minimum magnetic field requirement, for the power range 5 to 50 kilowatts.

B. EXPERIMENTAL VARIATION OF OPERATING PARAMETERS, WATER-COOLED

1. Introduction

A series of experiments has been performed on a sequence of water-cooled MPD arcjets operated with ammonia as the propellant. During the course of these measurements the quantities B, magnetic field strength, I, arc current, $\dot{m}$, metered ammonia mass flow,

Test	Current	Voltage	Power	Thrust	Mass Flow	Field Strength	Anode Power	Specific Impulse	Efficiency
	amps	volts	Kw	gm	gm/sec	kg	Kw	sec	%
1	300	100	30.	32.8	.0088	2.7	13.6	3720	19.5
2	400	100	40	48.3	.0088	2.7		5480	31.8
3	500	102	51.	65.6	.0088	2.7		7450	46.0
4	300	106	31.8	32.8	.0088	2.7	15.0	3720	18.4
5	300	125	37.5	36.3	.0068	2.7		5330	24.9
6	500	105	52.5	60.5	.0068	2.7	25.4	8900	49.3
7	400	102	40.8	50.2	.0068	2.7	19.5	7370	43.6
8	500	96	48.0	53.6	.0048	2.7	23.4	11100	60.
9	300	73	21.9	20.7	.0088	.9	11.7	2350	10.7
10	400	73	29.2	27.6	.0088	.9	15.0	3140	17.2
11	500	72	36.0	34.6	.0088	.9	17.6	3830	18.1
12	300	72	21.6	20.7	.0068	.9	11.1	3040	14.
13	400	70	28.0	27.6	.0068	.9	14.3	4060	19.2
14	500	71	35.5	34.6	.0068	.9	17.6	5090	23.8
15	300	60	18.0	13.8	.0048	.9	9.5	2880	10.6
16	400	68	27.2	24.2	.0048	.9	13.6	5040	21.5
17	500	81	40.5	34.6	.0048	.9	19.5	7210	29.6
18	500	73	36.5	27.6	.0027	.9	20.2	10200	33.5
19	400	65	26.0	22.4	.0027	.9	15.6	8260	34.3
20	300	62	18.6	13.8	.0027	.9	9.1	5100	18.2
21	300	105	31.5	31.1	.0088	3.6	13.0	3530	16.8
22	400	102	40.8	41.5	.0088	3.6	16.2	4710	23.1
23	500	101	50.5	58.8	.0088	3.6	20.2	6680	37.4
24	400	94	37.6	41.5	.0068	3.6	16.6	6100	32.4
25	500	94	47.0	53.7	.0068	3.6	19.5	7900	43.4
26	300	105	31.5	31.1	.0068	3.6	14.3	4570	22.6
27	300	140	42.0	38	.0048	3.6	16.2	7820	34.4
28	500	95	47.5	50.2	.0048	3.6	22.1	10400	53.
29	400	104	41.6	39.8	.0048	3.6	19.5	8300	38.1
30	300	165	49.5	36.3	.0027	3.6	29.3	13400	47.3
31	400	170	68.0	50.2	.0027	3.6	35.8	18600	66.
32	350	94	32.9	31.1	.0088	1.8	16.6	3530	16.
33	400	92	36.8	41.5	.0088	1.8	19.9	4710	25.5
34	500	86	43.0	50.2	.0088	1.8	22.8	5700	32.1
35	300	96	28.8	27.6	.0088	1.8	15.0	3130	17.4

TABLE I

Performance of X-7C-1 Engine

Test	Current amps	Voltage volts	Power Kw	Thrust gm	Mass Flow gm/sec	Field Strength kg	Anode Power Kw	Specific Impulse sec	Efficiency %
36	350	96	33.6	31.1	.0068	1.8	17.6	4570	20.3
37	400	95	38.0	39.8	.0068	1.8	20.2	5860	29.5
38	500	95	47.5	51.8	.0068	1.8	26.1	7610	40.0
39	300	100	30.0	27.6	.0068	1.8	15.6	4060	18.0
40	400	100	40.0	39.8	.0048	1.8	23.1	8300	39.6
41	500	102	51.0	48.4	.0048	1.8	29.3	10050	48.5

TABLE I

Test	Current amps	Voltage volts	Power Kw	Thrust gm	Mass Flow gm/sec	Field Strength kg	Anode Power Kw	Specific Impulse sec	Efficiency %
1	300	85	25.5	14.8	.0088	.9	16.1	1680	7.
2	400	87	34.8	25.1	.0088	.9	21.0	2850	9.8
3	500	81	40.5	35.4	.0088	.9	26.0	4020	14.8
4	300	87	26.1	14.8	.0068	.9	16.1	2180	6.
5	400	91	36.4	28.1	.0068	.9	22.4	3840	15.3
6	500	100	50.0	38.5	.0068	.9	31.7	5660	21.
7	300	125	37.5	23.6	.0048	.9	24.6	4920	14.8
8	400	123	49.2	35.4	.0048	.9	33.8	7370	25.5
9	500	120	60.0	41.5	.0048	.9	40.5	8640	28.7
10	300	115	34.5	28.1	.0163	1.8	16.9	1720	6.7
11	400	124	49.6	50.3	.0163	1.8	22.8	3080	15.
12	500	110	55.0	62.2	.0163	1.8	26.4	3810	20.7
13	300	137	41.1	37.1	.0163	1.8	17.6	2280	9.9
14	300	145	43.5	38.6	.0127	1.8	17.6	3040	13.
15	475	129	61.3	59.3	.0127	1.8	28.8	4660	21.7
16	400	125	50.0	44.4	.0127	1.8	23.6	3500	14.9
17	300	124	37.2	38.5	.0163	2.7	16.5	2360	11.7
18	400	126	50.4	56.3	.0163	2.7	22.8	3450	18.4
19	500	125	62.5	71.1	.0163	2.7	28.8	4360	23.8
20	300	160	48.0	44.4	.0127	2.7	21.1	3500	15.5
21	400	145	58.0	54.8	.0127	2.7	29.2	4320	19.6
22	500	140	70.0	73.1	.0127	2.7	35.1	5750	29.0

TABLE II

Performance of X-7C-2 Engine

Test	Current amps	Voltage volts	Power Kw	Thrust gm	Mass Flow gm/sec	Field Strength kg	Anode Power Kw	Specific Impulse sec	Efficiency %
1	400	135	54.0	46.7	.0088	1.8	12.0	5300	22.1
2	500	93	46.5	47.8	.0088	.9	23.8	5430	25.8
3	400	85	34.0	35.1	.0088	.9	18.9	3990	19.8
4	300	64	19.2	17.5	.0088	.9	11.7	1990	8.7
5	300	65	19.5	15.9	.0068	.9	11.7	2340	9.2
6	500	95	47.5	44.7	.0068	.9	22.8	6570	29.8
7	400	70	28.0	25.4	.0068	.9	15.6	3730	16.3
8	500	115	57.5	51.0	.0088	1.8	26.0	5800	24.7

TABLE III

Performance of X-7C-3 Engine

Test	Current	Voltage	Power	Mass Flow	Thrust	Field Strength	Anode Power	Specific Impulse	Efficiency
	amps	volts	Kw	gm/sec	gm	kg	Kw	sec	%
1	300	46	13.8	.068	34.6	.83	10.4	510	6.1
2	400	45	18.0	.068	38.1	.83	12.8	560	5.7
3	500	43	21.5	.068	43.3	.83	15.1	635	6.1
4	600	42	25.2	.068	48.4	.83	17.5	710	6.6
5	800	41.5	33.2	.068	58.8	.83	22.2	865	7.4
6	1000	41.5	41.5	.068	71.0	.83	26.6	1040	8.6
7	1200	41.5	49.8	.068	83.1	.83	30.2	1220	9.8
8	1400	41.5	58.2	.068	91.8	.83	32.9	1350	10.0
9	300	46	13.8	.068	34.6	.83	10.4	510	6.1
10	300	45.5	13.7	.053	25.9	.83	10.4	490	3.3
11	400	43	17.2	.053	27.6	.83	12.4	520	4.0
12	500	41.5	20.8	.053	34.6	.83	14.8	655	5.2
13	600	41	24.6	.053	38.1	.83	16.8	720	5.4
14	800	40	32.0	.053	50.2	.83	21.5	945	7.1
15	1000	40	40.0	.053	62.3	.83	25.2	1070	8.8
16	1200	40	48.0	.053	76.2	.83	28.2	1430	10.9
17	1400	38	53.2	.053	86.5	.83	30.2	1630	12.7
18	300	45.5	13.7	.053	25.9	.83	10.4	490	3.3
19	300	45.	13.5	.036	19.0	.83	10.4	530	3.5
20	400	42.	16.8	.036	22.4	.83	12.1	620	4.0
21	500	40.	20.0	.036	27.6	.83	14.5	765	5.1
22	600	39.	23.4	.036	31.1	.83	16.5	865	5.2
23	800	37.	29.6	.036	45.0	.83	20.2	1250	9.2
24	1000	36.	36.0	.036	55.4	.83	23.2	1540	11.4
25	1200	35.	42.0	.036	64.0	.83	25.2	1770	13.0
26	1400	34.	47.7	.036	72.7	.83	27.9	2010	14.8
27	300	45.	13.5	.036	19.0	.83	10.4	530	3.5
28	300	40.	12.0	.016	12.1	.83	9.0	760	3.7
29	400	36	14.4	.016	17.2	.83	10.7	1080	6.2
30	500	35	16.5	.016	19.0	.83	12.8	1190	6.6
31	600	33	19.8	.016	22.4	.83	14.5	1400	7.6
32	800	32	25.6	.016	31.1	.83	17.5	1940	11.3
33	1000	32	32.0	.016	38.1	.83	20.8	2380	13.6
34	1200	32.5	39.0	.016	46.7	.83	24.5	2910	16.8

TABLE IV

Performance of X-7C-4 Engine

Test	Current	Voltage	Power	Mass Flow	Thrust	Field Strength	Anode Power	Specific Impulse	Efficiency
	amps	volts	Kw	gm/sec	gm	kg	Kw	sec	%
35	1400	34.5	48.3	.016	51.9	.83	30.2	3240	16.8
36	300	40	12.0	.016	12.1	.83	9.4	760	3.7
37	300	40.5	12.2	.0127	12.1	.83	9.0	950	4.5
38	400	36	14.4	.0127	13.7	.83	10.7	1080	4.9
39	500	34	17.0	.0127	17.3	.83	12.1	1360	6.7
40	600	32	19.2	.0127	20.7	.83	14.1	1630	8.5
41	800	31	24.8	.0127	27.6	.83	16.8	2170	11.6
42	1000	32	32.0	.0127	34.6	.83	20.8	2720	14.2
43	1200	33	39.6	.0127	41.5	.83	25.9	3270	16.4
44	1400	37	51.8	.0127	46.7	.83	32.9	3670	15.9
45	300	40	12.0	.0127	12.1	.83	9.4	950	4.6
46	300	39	11.7	.0092	10.7	.83	8.4	1160	5.1
47	400	35	14.0	.0092	13.8	.83	10.4	1500	7.1
48	500	33	16.5	.0092	17.2	.83	12.1	1870	9.4
49	600	32	19.2	.0092	20.7	.83	14.1	2250	11.7
50	800	31	24.8	.0092	24.1	.83	17.5	2620	12.2
51	1000	32	32.0	.0092	29.3	.83	22.2	3180	14.0
52	1200	35	42.0	.0092	34.6	.83	28.2	3760	14.9
53	1400	36	50.4	.0092	39.8	.83	32.9	4330	16.4
54	300	45	13.5	.0092	17.3	.83	9.4	1880	11.4
55	300	38	11.4	.0088	12.1	.83	8.0	1380	7.1
56	400	36	14.4	.0088	15.5	.83	10.1	1760	9.1
57	500	35	17.5	.0088	20.7	.83	12.1	2350	13.4
58	600	44	26.4	.0088	34.6	.83	15.8	3930	24.8
59	800	47	37.6	.0088	41.5	.83	22.2	4720	25.0
60	1000	51	51.0	.0088	50.2	.83	28.2	5700	27.0
61	1200	39	46.8	.0088	41.5	.83	29.2	4720	20.0
62	1400	45	63.0	.0088	60.6	.83	33.6	6890	31.8
63	300	43	12.9	.0088	17.2	.83	8.4	1960	12.5
64	300	45	13.5	.0068	15.5	.83	8.4	2280	12.5
65	400	45	18.0	.0068	18.7	.83	10.7	2750	13.7
66	500	45	22.5	.0068	25.9	.83	13.1	3810	21.0
67	600	45	27.0	.0068	29.3	.83	16.1	4310	22.4
68	800	52	41.6	.0068	41.5	.83	22.5	6100	29.4

TABLE IV

Test	Current	Voltage	Power	Mass Flow	Thrust	Field Strength	Anode Power	Specific Impulse	Efficiency
	amps	volts	Kw	gm/sec	gm	kg	Kw	sec	%
69	1000	49	49.0	.0068	46.7	.83	27.9	6870	31.5
70	1200	42	50.4	.0068	45.0	.83	30.2	6620	28.4
71	1400	47	65.8	.0068	53.7	.83	33.6	7900	31.0
72	300	45	13.5	.0068	15.5	.83	8.4	2280	12.5
73	300	46	13.8	.0048	15.5	.83	8.0	3230	17.3
74	400	49	19.6	.0048	20.7	.83	11.1	4310	21.8
75	500	50	25.0	.0048	25.2	.83	14.1	5250	25.4
76	600	54	32.4	.0048	32.9	.83	17.5	6850	33.4
77	800	55	44.0	.0048	41.5	.83	23.2	8650	39.2
78	1000	53	53.0	.0048	48.4	.83	28.2	10100	44.2
79	1200	45	54.0	.0048	45.0	.83	31.2	9380	37.5
80	1400	44	61.6	.0048	46.7	.83	~	9730	35.5
81	300	45	13.5	.0048	15.5	.83	8.0	3230	17.8
82	300	54	16.2	.068	31.9	1.25	9.0	470	4.5
83	400	50	20.0	.068	38.3	1.25	11.4	560	5.2
84	500	49	24.5	.068	46.2	1.25	13.8	680	6.1
85	600	48	28.8	.068	54.2	1.25	16.1	800	7.2
86	800	47	37.6	.068	68.6	1.25	20.5	1010	8.8
87	1000	47	47.0	.068	84.5	1.25	25.2	1240	10.7
88	1200	46.5	55.8	.068	101	1.25	29.2	1480	12.9
89	1400	46.5	65.0	.068	115	1.25	33.2	1690	14.3
90	300	54	16.2	.068	31.9	1.25	9.4	470	4.5
91	300	53	15.9	.053	22.3	1.25	9.0	420	2.8
92	400	50	20.0	.053	28.6	1.25	11.8	540	3.7
93	500	47	23.5	.053	36.7	1.25	13.8	690	5.2
94	600	46	27.6	.053	43.1	1.25	16.1	810	6.1
95	800	45	36.0	.053	57.4	1.25	20.5	1080	8.3
96	1000	45	45.0	.053	71.8	1.25	24.9	1350	10.4
97	1200	44	52.8	.053	86.2	1.25	28.2	1620	12.8
98	1400	44	61.6	.053	104	1.25	31.6	1950	18.6
99	300	53	15.9	.053	22.3	1.25	9.7	420	2.8
100	300	52	15.6	.036	19.1	1.25	9.7	530	3.1
101	400	46	18.4	.036	22.3	1.25	11.8	620	3.6
102	500	44	22.0	.036	28.7	1.25	13.8	800	5.0

TABLE IV

Test	Current	Voltage	Power	Mass Flow	Thrust	Field Strength	Anode Power	Specific Impulse	Efficiency
	amps	volts	Kw	gm/sec	gm	kg	Kw	sec	%
103	600	43	25.8	.036	35.1	1.25	15.8	980	6.4
104	800	42	33.6	.036	49.5	1.25	19.8	1370	9.7
105	1000	41	41.0	.036	65.5	1.25	23.5	1810	14.0
106	1200	41	48.2	.036	75.0	1.25	26.2	2080	15.6
107	1400	40	56.0	.036	89.5	1.25	29.2	2480	19.1
108	300	51	15.3	.036	19.1	1.25	9.7	530	3.2
109	300	49	14.7	.016	14.3	1.25	9.0	890	4.2
110	400	42	16.8	.016	17.5	1.25	11.1	1090	5.5
111	500	41	20.5	.016	20.7	1.25	13.1	1290	6.3
112	600	38	22.8	.016	25.5	1.25	14.8	1590	8.5
113	800	36	28.8	.016	35.1	1.25	18.1	2190	12.9
114	1000	36	36.0	.016	44.7	1.25	21.8	2790	16.6
115	1200	37	43.2	.016	52.7	1.25	26.5	3290	19.3
116	1400	39	54.6	.016	63.8	1.25	31.2	3980	22.4
117	300	45	13.5	.016	14.3	1.25	9.0	890	4.5
118	300	44.5	13.3	.0127	12.7	1.25	8.7	1000	4.6
119	400	43	17.2	.0127	19.1	1.25	11.1	1500	8.0
120	500	42	21.0	.0127	25.5	1.25	13.8	2010	11.7
121	600	47	28.2	.0127	36.7	1.25	16.8	2890	18.1
122	800	37	29.6	.0127	33.5	1.25	19.1	2640	14.4
123	1000	36	36.0	.0127	43.1	1.25	22.5	3400	19.5
124	1200	37	44.4	.0127	47.8	1.25	27.6	3760	19.5
125	1400	39	54.7	.0127	57.5	1.25	32.6	4530	22.9
126	300	45	13.5	.0127	14.3	1.25	9.0	1130	5.7
127	300	46	13.8	.0092	14.3	1.25	8.7	1500	7.7
128	400	47	18.8	.0092	20.7	1.25	11.4	2040	11.9
129	500	50	25.0	.0092	28.7	1.25	14.4	2720	17.2
130	600	52	31.2	.0092	38.3	1.25	17.5	3390	24.6
131	800	52	41.6	.0092	47.8	1.25	22.5	5200	28.7
132	1000	39	39.0	.0092	46.3	1.25	24.2	5050	28.7
133	1200	40	48.0	.0092	51.1	1.25	29.2	5550	28.4
134	1400	42	58.8	.0092	60.7	1.25	33.2	6600	32.8
135	300	45	13.5	.0092	14.3	1.25	8.7	1500	7.9
136	300	45	13.5	.0088	14.3	1.25	8.7	1630	8.3

TABLE IV

Test	Current	Voltage	Power	Mass Flow	Thrust	Field Strength	Anode Power	Specific Impulse	Efficiency
	amps	volts	Kw	gm/sec	gm	kg	Kw	sec	%
137	400	45	18.0	.0088	19.1	1.25	11.1	2170	11.0
138	500	43	21.5	.0088	22.3	1.25	13.4	2530	12.6
139	600	52	31.2	.0088	35.1	1.25	16.8	3990	21.6
140	800	54	43.2	.0088	51.2	1.25	22.8	5810	33.1
141	1000	54	54.0	.0088	63.8	1.25	27.9	7250	41.2
142	1200	51	61.2	.0088	68.7	1.25	31.9	7800	42.
143	1400	46	64.4	.0088	67.1	1.25	~	7630	38.2
144	300	46	13.8	.0088	14.3	1.25	9.0	1630	8.1
145	300	49	14.7	.0068	14.3	1.25	9.0	2100	10.
146	400	47	18.8	.0068	19.1	1.25	11.4	2810	13.7
147	500	47	23.5	.0068	25.5	1.25	13.8	3250	23.6
148	600	49	29.4	.0068	31.9	1.25	17.1	4690	24.5
149	800	55	44.0	.0068	51.2	1.25	22.6	7520	42.
150	1000	57.5	57.5	.0068	67.2	1.25	29.0	9880	55.5
151	1200	49	58.8	.0068	52.3	1.25	32.2	9150	46.7
152	1400	46	64.4	.0068	60.6	1.25	~	8920	40.4
153	300	49	14.7	.0068	14.3	1.25	9.0	2100	10.
154	300	52	15.6	.0048	14.3	1.25	9.0	2980	13.1
155	400	52	20.8	.0048	20.7	1.25	11.8	4320	20.6
156	500	55	27.5	.0048	28.7	1.25	14.5	5980	30.0
157	600	57.5	34.5	.0048	38.3	1.25	17.8	7980	42.5
158	800	62.5	50.0	.0048	54.3	1.25	23.5	11300	59.0
159	1000	57.5	57.5	.0048	57.5	1.25	29.2	12000	57.5
160	1200	51	61.2	.0048	57.5	1.25	33.6	12000	54.0
161	1400	54	25.6	.0048	70.3	1.25	~	14600	65.5
162	300	51	15.3	.0048	14.3	1.25	8.7	2980	13.3
163	300	57	17.1	.068	33.5	1.66	8.4	490	4.6
164	400	54	21.6	.068	39.9	1.66	10.0	590	5.2
165	500	52	26.0	.068	47.9	1.66	14.1	705	6.2
166	600	52	31.2	.068	55.8	1.66	18.2	820	7.0
167	800	52	41.6	.068	75.0	1.66	21.5	1100	9.6
168	1000	52	52.0	.068	94.	1.66	26.2	1380	12.0
169	1200	51	61.2	.068	113.	1.66	31.0	1660	14.8
170	1400	50.5	70.7	.068	128	1.66	35.2	1880	16.3
171	300	59.	17.7	.068	33.5	1.66	9.0	490	4.5

TABLE IV

Test	Current	Voltage	Power	Mass Flow	Thrust	Field Strength	Anode Power	Specific Impulse	Efficiency
	amps	volts	Kw	gm/sec	gm	kg	Kw	sec	%
172	300	58	17.4	.053	23.9	1.66	9.4	450	3.0
173	400	52	20.8	.053	28.7	1.66	11.8	540	3.6
174	500	50	25.0	.053	36.7	1.66	13.8	690	4.9
175	600	49.5	29.7	.053	46.3	1.66	16.5	820	6.5
176	800	51	46.3	.053	67.2	1.66	20.8	1270	10.0
177	1000	51	51.0	.053	88.0	1.66	25.2	1650	13.7
178	1200	50	60.0	.053	103.0	1.66	29.6	1940	16.0
179	1400	47	65.8	.053	118.	1.66	33.6	2220	19.2
180	300	58	17.4	.053	23.9	1.66	9.4	450	3.0
181	300	57	17.1	.036	19.1	1.66	9.4	530	2.9
182	400	50	20.0	.036	23.5	1.66	11.8	650	3.7
183	500	50	25.0	.036	33.5	1.66	14.8	930	6.0
184	600	50	30.0	.036	39.9	1.66	16.8	1110	7.1
185	800	49	39.2	.036	57.5	1.66	21.5	1590	11.3
186	1000	50	50.0	.036	78.3	1.66	25.2	2170	16.3
187	1200	45	54.0	.036	91.	1.66	27.9	2520	20.4
188	1400	43	60.2	.036	104.	1.66	30.6	2880	24.0
189	300	57	17.1	.036	19.1	1.66	9.4	530	2.9
190	300	51	15.3	.016	12.7	1.66	9.0	790	3.1
191	400	50	20.0	.016	23.9	1.66	11.8	1490	8.5
192	500	50	25.0	.016	28.7	1.66	14.8	1790	9.9
193	600	50	30.0	.016	39.9	1.66	18.2	2490	15.9
194	800	50	40.0	.016	52.7	1.66	23.2	3290	20.8
195	1000	42	42.0	.016	51.2	1.66	26.2	3200	19.7
196	1200	42	50.4	.016	67.1	1.66	29.6	4200	26.8
197	1400	41	57.4	.016	75.0	1.66	34.2	4680	29.5
198	300	50	15.0	.016	12.7	1.66	9.4	790	3.2
199	300	50	15.0	.0127	14.3	1.66	9.4	1030	5.1
200	400	50	20.0	.0127	20.7	1.66	12.1	1630	8.1
201	500	51	25.5	.0127	28.7	1.66	14.8	2260	12.2
202	600	51	30.6	.0127	36.7	1.66	17.5	2890	16.6
203	800	51	40.8	.0127	49.5	1.66	23.5	3900	22.7
204	1000	53	53.0	.0127	67.1	1.66	28.6	5280	32.1
205	1200	49	58.8	.0127	68.7	1.66	33.0	5420	30.3
206	1400	45	64.0	.0127	70.3	1.66	-	5540	29.2

TABLE IV

Test	Current	Voltage	Power	Mass Flow	Thrust	Field Strength	Anode Power	Specific Impulse	Efficiency
	amps	volts	Kw	gm/sec	gm	kg	Kw	sec	%
207	300	50	15.0	.0127	14.3	1.66	9.0	1030	5.1
208	300	51	15.3	.0092	12.7	1.66	9.4	1380	5.5
209	400	51	20.4	.0092	20.7	1.66	11.4	2250	10.8
210	500	51	25.5	.0092	30.3	1.66	14.1	3300	19.7
211	600	52	31.2	.0092	33.5	1.66	17.5	3640	18.8
212	800	46	44.8	.0092	52.7	1.66	23.5	5720	32.3
213	1000	60	60.0	.0092	70.3	1.66	29.6	7640	43.
214	1200	50	60.0	.0092	65.6	1.66	34.6	7140	37.5
215	1400	50	70.0	.0092	68.7	1.66	40.2	6870	35.2
216	300	50	15.0	.0092	12.7	1.66	9.4	1380	5.6
217	300	50	15.0	.0088	12.7	1.66	9.0	1440	5.9
218	400	45	18.0	.0088	17.5	1.66	11.1	1990	9.3
219	500	43	21.5	.0088	23.9	1.66	16.5	2720	14.5
220	600	43	25.8	.0088	30.3	1.66	19.5	3440	19.4
221	800	49	39.2	.0088	49.5	1.66	22.2	5620	34.1
222	1000	58	58.0	.0088	68.7	1.66	32.2	7800	43.3
223	1200	59	20.8	.0088	83.1	1.66	35.6	9450	53.3
224	1400	51	71.4	.0088	72.0	1.66	41.2	8180	39.6
225	300	50	15.0	.0088	12.7	1.66	9.0	1440	5.9
226	300	50	15.0	.0068	12.7	1.66	8.7	1870	7.6
227	400	45	18.0	.0068	15.9	1.66	11.1	2340	10.0
228	500	45	22.5	.0068	20.7	1.66	13.5	3040	13.4
229	600	47	28.2	.0068	33.5	1.66	16.1	4930	28.1
230	800	43	34.4	.0068	47.8	1.66	22.5	7030	47.0
231	1000	50	50.0	.0068	70.3	1.66	28.9	10300	70.0
232	1200	55	66.0	.0068	70.3	1.66	36.7	10300	52.8
233	1400	53	74.2	.0068	70.3	1.66	42.9	10300	47.1
234	300	50	15.0	.0068	12.7	1.66	8.7	1870	7.6
235	300	48	14.4	.0048	11.2	1.66	8.0	2340	8.7
236	400	49	19.3	.0048	14.3	1.66	10.8	2980	10.6
237	500	55	27.5	.0048	30.3	1.66	14.5	6310	33.4
238	600	55	33.0	.0048	36.7	1.66	16.8	7650	40.8
239	800	61	48.8	.0048	59.1	1.66	23.6	12300	71.7
240	1000	64	64.0	.0048	78.2	1.66	29.2	16200	95.5
241	1200	64	76.8	.0048	88.0	1.66	-	18300	101.

TABLE IV

Test	Current amps	Voltage volts	Power Kw	Mass Flow gm/sec	Thrust gm	Field Strength kg	Anode Power Kw	Specific Impulse sec	Efficiency %
242	1400	64	89.6	.0048	86.2	1.66	~	17900	83.
243	300	50	15.0	.0048	12.7	1.66	8.0	2640	10.7
244	300	65	19.5	.068	35.2	2.08	9.0	520	4.5
245	400	55	22.0	.068	41.5	2.08	12.1	610	5.5
246	500	55	27.5	.068	52.8	2.08	14.5	780	7.2
247	600	55	33.0	.068	62.3	2.08	18.1	910	8.3
248	800	55	44.0	.068	83.2	2.08	23.2	1220	11.1
249	1000	55	55.0	.068	105	2.08	24.8	1540	14.1
250	1200	55	66.0	.068	127	2.08	31.9	1860	17.2
251	1400	55	77.0	.068	14.0	2.08	35.2	2050	18.0
252	300	65	19.5	.068	35.2	2.08	9.3	520	4.5
253	300	65	19.5	.053	28.6	2.08	9.3	540	3.8
254	400	54	21.6	.053	33.5	2.08	12.8	630	4.7
255	500	50	25.0	.053	39.9	2.08	16.1	750	5.8
256	600	50	30.0	.053	51.2	2.08	18.8	960	7 9
257	800	51	40.8	.053	70.3	2.08	23.2	1320	12.1
258	1000	51	51.0	.053	101	2.08	28.2	1900	18.1
259	1200	51	61.2	.053	118	2.08	31.2	2220	20.6
260	1400	51	71.4	.053	135	2.08	34.5	2540	23.1
261	300	63	18.9	.053	30.3	2.08	10.1	570	4.6
262	300	52	15.6	.036	31.9	2.08	10.7	880	8.7
263	400	52	20.8	.036	41.5	2.08	13.8	1150	11.0
264	500	50	25.0	.036	51.	2.08	16.5	1410	13.9
265	600	50	30.0	.036	59.	2.08	18.1	1630	15.5
266	800	48	38.4	.036	78.	2.08	22.2	2160	21.1
267	1000	49	49.0	.036	84.5	2.08	25.9	2340	19.5
268	1200	46	55.2	.036	99	2.08	29.2	2740	23.6
269	1400	45	63.0	.036	111	2.08	33.6	3070	26.2
270	300	63	18.9	.036	31.9	2.08	10.7	880	7.2
271	300	53	15.9	.016	14.3	2.08	9.4	890	3.8
272	400	51	20.4	.016	19.1	2.08	12.1	1190	5.4
273	500	50	25.0	.016	28.7	2.08	14.8	1800	9.9
274	600	50	30.0	.016	36.7	2.08	17.8	2290	13.5
275	800	42	33.6	.016	44.8	2.08	21.2	2800	18.0

TABLE IV

Test	Current	Voltage	Power	Mass Flow	Thrust	Field Strength	Anode Power	Specific Impulse	Efficiency
	amps	volts	Kw	gm/sec	gm	kg	Kw	sec	%
276	1000	42	42.0	.016	55.9	2.08	26.2	3490	22.4
277	1200	43	51.6	.016	67.2	2.08	31.2	4200	26.2
278	1400	45	63.0	.016	81.5	2.08	38.5	5150	31.7
279	300	52	15.6	.016	14.3	2.08	10.0	890	3.9
280	300	53	15.9	.0127	14.3	2.08	10.0	1120	4.9
281	400	51	20.4	.0127	22.3	2.08	12.8	1760	9.2
282	500	51	25.5	.0127	31.9	2.08	15.5	2510	15.0
283	600	52	31.2	.0127	38.3	2.08	18.1	3020	17.8
284	800	55	44.0	.0127	57.5	2.08	23.5	4530	28.4
285	1000	50	50.0	.0127	64	2.08	28.2	5050	31.1
286	1200	45	54.0	.0127	67.2	2.08	35.2	5290	31.6
287	1400	46	64.4	.0127	78.3	2.08	41.8	6160	36.1
288	300	50	15.0	.0127	14.3	2.08	10.7	1120	5.2
289	300	52	15.6	.0092	11.1	2.08	9.4	1210	4.1
290	400	50	20.0	.0092	19.1	2.08	12.1	2080	9.5
291	500	46	23.0	.0092	23.9	2.08	14.8	2690	13.0
292	600	45	27.0	.0092	28.7	2.08	16.8	3120	16
293	800	48	38.4	.0092	44.7	2.08	22.8	4850	27.2
294	1000	55	55.0	.0092	70.3	2.08	30.2	7650	47
295	1200	51	61.2	.0092	72.0	2.08	~	7830	44.2
296	1400	52	72.8	.0092	79.8	2.08	~	8680	45.8
297	300	47	14.1	.0092	11.1	2.08	~	1210	4.6
298	300	46	13.8	.0088	9.6	2.08	9.4	1090	3.7
299	400	44	17.2	.0088	14.3	2.08	11.8	1620	6.5
300	500	42	21.0	.0088	19.1	2.08	13.8	2170	9.5
301	600	41	24.4	.0088	25.5	2.08	16.1	2900	14.5
302	800	41	32.8	.0088	38.3	2.08	21.2	4350	24.4
303	1000	45	45.0	.0088	52.7	2.08	27.9	5980	33.7
304	1200	40	48.0	.0088	70.3	2.08	35.2	8000	56.2
305	1400	51	71.4	.0088	81.5	2.08	43.6	9260	51.0
306	300	45	13.5	.0088	9.6	2.08	--	1090	3.8
307	300	45	13.5	.0068	12.7	2.08	--	1870	8.4
308	400	47	18.8	.0068	19.1	2.08	--	2810	13.7
309	500	46	23.0	.0068	22.3	2.08	--	3280	15.3

TABLE IV

Test	Current	Voltage	Power	Mass Flow	Thrust	Field Strength	Anode Power	Specific Impulse	Efficiency
	amps	volts	Kw	gm/sec	gm	kg	Kw	sec	%
310	600	45	27.0	.0068	27.1	2.08	-	3980	19.2
311	800	46	36.8	.0068	43.1	2.08	-	6340	35.7
312	1000	45	45.0	.0068	49.5	2.08	-	7280	38.5
313	1200	50	60.0	.0068	70.3	2.08	-	10300	58.3
314	1400	56	78.4	.0068	73.5	2.08	-	10800	48.7
315	300	47	14.1	.0068	12.7	2.08	-	1870	8.1
316	300	50	15.0	.0048	12.7	2.08	8.7	3020	10.8
317	400	50	20.0	.0048	17.5	2.08	11.1	4170	15.3
318	500	51	25.5	.0048	23.8	2.08	14.8	5310	22.2
319	600	52	31.2	.0048	35.1	2.08	18.5	6500	39.6
320	800	60	48.0	.0048	55.8	2.08	24.9	10000	65.0
321	1000	66	66.0	.0048	81.5	2.08	30.2	13700	100
322	1200	70	84.0	.0048	111.	2.08	35.8	23000	147
323	1400	66	92.4	.0048	110	2.08	45.3	22900	131
324	300	50	15.0	.0048	12.7	2.08	9.4	3020	10.8
325	300	70	21.0	.068	44.7	2.50	9.0	660	6.7
326	400	58	23.2	.068	51.1	2.50	12.1	750	7.9
327	500	58	29.0	.068	60.6	2.50	15.1	890	8.9
328	600	58	34.8	.068	76.7	2.50	18.1	1120	11.9
329	800	60	48.0	.068	102	2.50	23.5	1500	15.3
330	1000	60	60.0	.068	127	2.50	27.9	1860	19.0
331	1200	60	72.0	.068	143	2.50	33.0	2100	20.0
332	1400	60	84.0	.068	168	2.50	-	3460	23.8
333	300	73	21.9	.068	44.7	2.50	9.0	660	6.4
334	300	68	20.4	.053	33.5	2.50	9.3	630	5.0
335	400	55	22.0	.053	36.7	2.50	12.8	690	5.6
336	500	53	26.5	.053	47.8	2.50	16.8	900	7.8
337	600	53	31.8	.053	57.4	2.50	18.8	1080	9.4
338	800	55	44.0	.053	86.2	2.50	23.6	1620	15.3
339	1000	55	55.	.053	111	2.50	27.6	2090	20.3
340	1200	55	66.	.053	137	2.50	31.2	2580	25.8
341	1400	55	77.	.053	153	2.50	34.2	2880	27.6
342	300	66	19.8	.053	33.5	2.50	10.0	630	5.1
343	300	57	17.1	.036	23.8	2.50	11.4	660	4.4

TABLE IV

Test	Current	Voltage	Power	Mass Flow	Thrust	Field Strength	Anode Power	Specific Impulse	Efficiency
	amps	volts	Kw	gm/sec	gm	kg	Kw	sec	%
344	400	53	21.2	.036	25.5	2.50	14.1	710	4.1
345	500	51	25.5	.036	33.5	2.50	16.1	930	5.9
346	600	51	30.6	.036	51.1	2.50	19.1	1420	11.4
347	800	51	40.8	.036	76.6	2.50	22.9	2130	19.2
348	1000	51	51.0	.036	101	2.50	26.9	2800	26.7
349	1200	51	61.2	.036	122	2.50	29.9	3380	32.5
350	1400	50	70.0	.036	135	2.50	34.2	3640	34.8
351	300	55	16.5	.036	23.8	2.50	10.7	660	4.5
352	300	52	15.6	.016	14.3	2.50	12.1	890	4.0
353	400	49	19.6	.016	22.3	2.50	14.1	1400	7.6
354	500	46	23.0	.016	27.1	2.50	15.5	1700	9.6
355	600	45	27.0	.016	39.9	2.50	17.8	2490	17.8
356	800	45	36.0	.016	54.2	2.50	21.5	3400	24.5
357	1000	45	45.0	.016	70.2	2.50	26.2	4380	32.8
358	1200	45	54.0	.016	83.0	2.50	33.6	5180	38.3
359	1400	50	70.0	.016	102	2.50	40.2	6350	44.6
360	300	53	15.9	.016	14.3	2.50	10.8	890	3.9
361	300	50	15.0	.0127	12.7	2.50	11.4	1000	3.8
362	400	46	18.4	.0127	19.1	2.50	13.4	1500	7.5
363	500	45	22.5	.0127	25.5	2.50	15.5	2010	10.9
364	600	45	27.0	.0127	31.9	2.50	16.8	2510	14.3
365	800	45	36.0	.0127	47.8	2.50	21.5	3760	24.0
366	1000	45	45.0	.0127	67.0	2.50	27.9	5260	37.7
367	1200	50	60.0	.0127	83.0	2.50	34.9	6540	43.5
368	1400	50	70.0	.0127	99.0	2.50	42.9	7790	53.0
369	300	50	15.0	.0127	12.7	2.50	11.4	1000	3.8
370	300	50	15.0	.0092	11.1	2.50	10.0	1210	4.3
371	400	48	19.2	.0092	19.1	2.50	12.8	2080	10.0
372	500	45	22.5	.0092	27.1	2.50	14.8	2940	17.0
373	600	44	26.4	.0092	30.2	2.50	17.5	3280	18.0
374	800	45	36.0	.0092	46.2	2.50	22.2	5020	31.0
375	1000	50	50.0	.0092	62.2	2.50	28.9	6760	40.5
376	1200	55	66.0	.0092	78	2.50	35.9	8500	48.2
377	1400	55	77.0	.0092	91	2.50	45.2	9900	56.0

TABLE IV

Test	Current	Voltage	Power	Mass Flow	Thrust	Field Strength	Anode Power	Specific Impulse	Efficiency
	amps	volts	Kw	gm/sec	gm	kg	Kw	sec	%
378	300	49	14.7	.0092	11.1	2.50	11.4	1210	4.3
379	300	50	15.0	.0088	12.7	2.50	10.7	1440	5.9
380	400	48	19.2	.0088	15.9	2.50	12.4	1810	7.3
381	500	45	22.5	.0088	22.3	2.50	14.8	2540	12.1
382	600	45	27.0	.0088	28.7	2.50	17.5	3260	16.6
383	800	50	40.0	.0088	46.3	2.50	24.9	5260	29.3
384	1000	56	56.0	.0088	70.3	2.50	31.9	8000	48
385	1200	53	63.5	.0088	94.3	2.50	40.2	10700	76.5
386	1400	61	85.4	.0088	103	2.50	46.8	11700	68.0
387	300	48	14.4	.0088	12.7	2.50	10.7	1440	6.1
388	300	50	15.0	.0068	12.7	2.50	10.1	1870	7.6
389	400	50	20.0	.0068	19.1	2.50	12.8	2810	12.9
390	500	49	24.5	.0068	25.5	2.50	15.8	3750	18.7
391	600	50	30.0	.0068	36.7	2.50	19.5	5400	31.7
392	800	58	46.4	.0068	59.1	2.50	26.6	8700	53.2
393	1000	63	63.0	.0068	83	2.50	33.6	12200	77.3
394	1200	69	82.7	.0068	107	2.50	40.2	15700	98.0
395	1400	70	98.0	.0068	132	2.50	48.6	19300	125
		65	91.0	.0068	118	2.50		17300	108
396	300	50	15.0	.0068	12.7	2.50	10.7	3310	15.3
397	300	55	16.5	.0048	15.9	2.50	10.7	3310	15.3
398	400	55	22.0	.0048	22.3	2.50	13.4	4650	22.6
399	500	58	29.0	.0048	31.9	2.50	16.5	6650	35.2
400	600	60	36.0	.0048	41.5	2.50	19.5	8650	48.0
401	800	65	52.0	.0048	60.6	2.50	25.6	12600	71.
402	1000	70	70.0	.0048	94.2	2.50	30.6	19600	94.
403	1200	75	90.0	.0048	121	2.50	36.8	25200	163
404	1400	72	101.0	.0048	129	2.50	45.3	26900	165
405	300	55	16.5	.0048	15.9	2.50	10.7	3310	15.3

TABLE IV

Test	Current	Voltage	Power	Mass Flow	Thrust	Field Strength	Anode Power	Specific Impulse	Efficiency
	amps	volts	Kw	gm/sec	gm	kg	Kw	sec	%
1	300	54	16.2	.068	35.1	2.08	10.2	520	5.4
2	400	52	20.8	.068	44.7	2.08	13.4	660	6.8
3	500	51	25.5	.068	47.8	2.08	16.5	700	6.3
4	600	51	30.6	.068	52.7	2.08	19.0	770	6.4
5	800	50.5	40.4	.068	65.5	2.08	25.0	960	7.5
6	1000	50	50.0	.068	76.7	2.08	30.1	1200	8.3
7	300	53	15.9	.068	35.1	2.08	10.2	520	5.5
8	300	52	15.6	.053	25.5	2.08	10.2	480	3.8
9	400	50	20.0	.053	30.3	2.08	13.6	570	4.2
10	500	49	24.5	.053	35.1	2.08	16.5	660	4.6
11	600	48	28.8	.053	39.9	2.08	19.4	750	5.0
12	800	47	37.6	.053	51.1	2.08	24.7	960	6.3
13	1000	46	46.0	.053	63.8	2.08	29.8	1200	8.0
14	300	51.5	15.4	.053	25.5	2.08	10.2	480	3.8
15	300	48.5	14.5	.036	17.5	2.08	9.8	490	2.8
16	400	46	18.4	.036	23.9	2.08	13.6	660	4.1
17	500	46	23.0	.036	28.7	2.08	16.2	800	4.8
18	600	45.5	27.3	.036	35.1	2.08	19.0	980	6.0
19	800	45	36.0	.036	47.8	2.08	24.1	1320	8.5
20	1000	42	42.0	.036	57.5	2.08	27.6	1600	10.5
21	300	48.5	14.5	.036	17.5	2.08	9.8	490	2.8
22	300	45	13.5	.016	12.7	2.08	9.5	790	3.6
23	400	43	17.2	.016	17.5	2.08	12.0	1090	5.3
24	500	42	21.0	.016	25.5	2.08	14.0	1590	9.3
25	600	40	24.0	.016	31.9	2.08	15.8	1990	12.7
26	800	35	28.0	.016	36.7	2.08	18.4	2290	14.5
27	1000	34	34.0	.016	38.3	2.08	22.8	2390	13.0
28	300	46	13.8	.016	12.7	2.08	9.5	790	3.6
29	300	45	13.5	.0127	12.7	2.08	8.9	1000	4.5
30	400	44	17.6	.0127	22.3	2.08	11.4	1750	8.5
31	500	42	21.0	.0127	27.1	2.08	13.4	2130	13.2
32	600	40	24.0	.0127	33.6	2.08	15.2	2640	17.8
33	800	35	28.0	.0127	35.1	2.08	17.8	2760	16.7
34	1000	34	34.0	.0127	38.3	2.08	23.1	3020	16.3
35	300	45	13.5	.0127	12.7	2.08	8.9	1000	4.5

TABLE V
Performance of X-7C-5 Engine

Test	Current amps	Voltage volts	Power Kw	Mass Flow gm/sec	Thrust gm	Field Strength kg	Anode Power Kw	Specific Impulse sec	Efficiency %
36	300	43	12.9	.0092	11.1	2.08	8.9	1210	5.0
37	400	43	17.2	.0092	19.1	2.08	9.8	2080	11.1
38	500	44	22.0	.0092	25.5	2.08	12.0	2770	15.4
39	600	40	24.0	.0092	31.9	2.08	14.3	3470	16.6
40	800	35	28.0	.0092	33.6	2.08	18.4	3650	17.5
41	1000	36	36.0	.0092	38.3	2.08	24.7	4160	21.3
42	300	43	12.9	.0092	11.1	2.08	8.9	1210	5.0
43	300	44	13.2	.0088	14.3	2.08	8.9	1620	8.1
44	400	43	17.2	.0088	20.7	2.08	8.9	2350	13.0
45	500	42	21.0	.0088	28.7	2.08	10.8	3260	20.4
46	600	41	24.6	.0088	33.6	2.08	12.0	3820	24.0
47	800	36	29.6	.0088	35.1	2.08	19.6	3990	21.7
48	1000	38	38.0	.0088	39.9	2.08	26.0	4540	21.8
49	300	43	13.9	.0088	14.3	2.08	8.9	1620	8.1
50	300	42	12.6	.0068	14.3	2.08	8.0	2100	11.5
51	400	42	16.8	.0068	19.1	2.08	11.4	2810	15.3
52	500	42	21.0	.0068	23.9	2.08	14.0	3510	19.2
53	600	42	25.2	.0068	30.3	2.08	16.5	4450	25.8
54	800	41	32.8	.0068	35.1	2.08	21.8	5160	26.6
55	1000	40	40.0	.0068	38.3	2.08	27.2	5630	27.1
56	300	40	12.0	.0068	14.3	2.08	8.2	2100	11.5
57	300	41	12.3	.0048	11.1	2.08	8.0	2310	10
58	400	44	17.6	.0048	15.9	2.08	11.1	3310	14.4
59	500	46	23.0	.0048	23.9	2.08	14.6	4970	24.8
60	600	46.5	27.9	.0048	28.7	2.08	17.4	5970	29.4
61	800	44	35.2	.0048	31.9	2.08	22.5	6640	29.0
62	1000	45	45.0	.0048	36.8	2.08	29 8	7670	30.1
63	300	36	10.8	.0048	8.0	2.08	7.6	1660	6.0
64	300	36	10.8	.068	25.5	.83	7.3	370	4.3
65	400	35	14.0	.068	27.1	.83	8.9	400	3.7
66	500	38	19.0	.068	35.2	.83	12.0	520	4.6
67	600	37	22.2	.068	38.3	.83	13.6	560	4.7
68	800	36	28.8	.068	44.8	.83	17.4	660	4.9
69	1000	36	36.0	.068	54.4	.83	22.2	800	5.8
70	300	45	13.5	.068	27.1	.83	8.9	400	3.8

TABLE V

Test	Current amps	Voltage volts	Power Kw	Mass Flow gm/sec	Thrust gm	Field Strength kg	Anode Power Kw	Specific Impulse sec	Efficiency %
71	300	44	13.2	.053	22.3	.83	9.2	420	3.4
72	400	43	17.2	.053	25.5	.83	12.4	480	3.4
73	500	42	21.0	.053	28.7	.83	15.2	540	3.5
74	600	41	24.6	.053	31.9	.83	17.1	600	3.8
75	800	40	32.0	.053	41.5	.83	21.8	780	4.9
76	1000	38	38.0	.053	51.2	.83	25.0	960	6.3
77	300	43	12.9	.053	22.3	.83	9.5	420	3.5
78	300	43	12.9	.036	14.3	.83	10.2	400	2.1
79	400	41	16.4	.036	15.9	.83	12.4	440	2.0
80	500	38	19.0	.036	20.7	.83	14.0	580	3.0
81	600	36	21.6	.036	22.3	.83	16.5	620	3.1
82	800	35	28.0	.036	30.3	.83	19.6	840	4.4
83	1000	33	33.0	.036	36.7	.83	23.5	1020	5.5
84	300	41	12.3	.036	14.3	.83	9.8	400	2.2
85	300	36	10.8	.016	8.0	.83	7.95	500	1.8
86	400	35	14.0	.016	9.6	.83	10.1	600	2.0
87	500	35	17.5	.016	12.7	.83	13.0	790	2.8
88	600	35	21.0	.016	17.5	.83	15.2	1090	4.4
89	800	34	27.2	.016	23.9	.83	18.7	1490	6.3
90	1000	26	26.0	.016	15.9	.83	21.0	990	2.9
91	1000	29	29.0	.016	22.3	.83	21.6	1390	5.1
92	1000	33	33.0	.016	28.7	.83	22.2	1790	7.5
93	300	32	9.6	.016	8.0	.83	7.6	500	2.0
94	300	30	9.0	.0127	3.2	.83	6.7	250	.4
95	400	32	12.8	.0127	6.4	.83	9.8	500	1.2
96	500	33	16.5	.0127	9.6	.83	12.3	750	2.1
97	600	35	21.0	.0127	14.3	.83	15.5	1130	3.7
98	800	34	28.2	.0127	22.3	.83	19.0	1760	6.7
99	1000	34	34.0	.0127	31.9	.83	23.8	2510	11.3
100	300	30	9.0	.0127	3.2	.83	7.3	250	.4
101	300	56	16.8	.068	38.3	2.50	11.4	560	6.2
102	400	55	22.0	.068	47.8	2.50	14.9	700	7.4
103	500	54	27.0	.068	54.4	2.50	18.1	800	7.8
104	600	54	32.4	.068	62.3	2.50	20.9	910	10.2
105	800	53	42.4	.068	75.0	2.50	27.2	1100	9.4
106	1000	53	53.0	.068	89.5	2.50	31.4	1310	10.7
107	300	56	16.8	.068	38.3	2.50	11.1	560	6.2

TABLE V

Test	Current amps	Voltage volts	Power Kw	Mass Flow gm/sec	Thrust gm	Field Strength kg	Anode Power Kw	Specific Impulse sec	Efficiency %
108	300	53	15.9	.053	31.9	2.50	11.7	600	5.8
109	400	52	20.8	.053	38.3	2.50	14.5	720	6.4
110	500	52	26.0	.053	44.8	2.50	17.4	850	7.0
111	600	51	30.6	.053	51.2	2.50	20.6	960	7.8
112	800	50.5	40.4	.053	64.0	2.50	26.3	1200	9.2
113	1000	50	50.0	.053	76.7	2.50	30.7	1440	10.7
114	300	53	15.9	.053	31.9	2.50	11.7	600	5.8
115	300	51	15.3	.036	19.1	2.50	11.1	530	3.2
116	400	48	19.2	.036	25.5	2.50	14.2	710	4.5
117	500	48	24.0	.036	31.9	2.50	17.4	890	5.6
118	600	48	28.8	.036	38.3	2.50	20.0	1160	6.8
119	800	47	37.6	.036	51.2	2.50	25.0	1420	9.3
120	1000	45	45.0	.036	64.0	2.50	28.5	1770	12.1
121	300	49	14.7	.036	19.1	2.50	10.8	530	3.3
122	300	45	13.5	.016	12.7	2.50	11.1	790	3.6
123	400	43	17.2	.016	19.1	2.50	13.0	1190	6.4
124	500	42	21.0	.016	27.1	2.50	14.9	1670	10.5
125	600	41	24.6	.016	31.9	2.50	16.5	1990	12.5
126	800	38	30.4	.016	39.9	2.50	20.0	2500	15.7
127	1000	37	37.0	.016	46.3	2.50	25.0	2890	17.4
128	300	43	12.9	.016	12.7	2.50	10.4	790	3.8
129	300	43	12.9	.0127	9.6	2.50	10 8	750	2.7
130	400	41	16.4	.0127	15.9	2.50	12.4	1250	5.8
131	500	40.5	20.3	.0127	25.5	2.50	14.0	2000	12.1
132	600	40.5	24.3	.0127	35.1	2.50	15.8	2760	19.1
133	800	40	32.0	.0127	44.7	2.50	20.6	3520	23.6
134	1000	39	39.0	.0127	47.9	2.50	26.3	3760	22.2
135	300	43	12.9	.0127	9.6	2.50	10.4	750	2.7
136	300	43	12.9	.0092	8.0	2.50	10.2	870	2.6
137	400	40	16.0	.0092	14.3	2.50	12.0	1560	6.7
138	500	39	19.5	.0092	22.3	2.50	13.6	2430	13.3
139	600	41	24.6	.0092	31.9	2.50	16.5	3470	20.6
140	800	42	33.6	.0092	40.0	2.50	22.5	4350	24.8
141	1000	41	41.0	.0092	44.7	2.50	28.2	4870	25.4
142	300	41	12.3	.0092	8.0	2.50	10.4	870	2.7
143	300	41	12.3	.0088	8.0	2.50	9.8	910	2.8
144	400	39	15.6	.0088	14.3	2.50	11.4	1620	7.2
145	500	37	18.5	.0088	20.7	2.50	13.0	2350	12.7

TABLE V

Test	Current amps	Voltage volts	Power Kw	Mass Flow gm/sec	Thrust gm	Field Strength kg	Anode Power Kw	Specific Impulse sec	Efficiency %
146	600	37	22.2	.0088	28.7	2.50	15.2	3260	20.3
147	800	42	33.6	.0088	40.0	2.50	22.5	4550	26.1
148	1000	41	41.0	.0088	43.2	2.50	29.8	4900	24.8
149	300	40	12.0	.0088	8.0	2.50	9.8	910	3.0
150	300	40	12.0	.0068	8.0	2.50	9.5	1170	3.8
151	400	38	15.2	.0068	11.1	2.50	11.4	1630	5.7
152	500	36	18.0	.0068	15.6	2.50	13.0	2300	9.6
153	600	37	22.2	.0068	21.9	2.50	15.5	3220	15.3
154	800	46	36.8	.0068	38.3	2.50	24.7	5630	28.3
155	1000	44	44.0	.0068	41.5	2.50	30.4	6100	27.6
156	300	38	11.4	.0068	8.0	2.50	9.5	910	3.1
157	300	39	11.7	.0048	6.4	2.50	9.2	1330	3.5
158	400	37	14.8	.0048	12.8	2.50	11.0	2660	11.0
159	500	38	19.0	.0048	19.1	2.50	13.3	3980	19.2
160	600	42	25.2	.0048	25.5	2.50	17.4	5310	25.8
161	800	49	39.2	.0048	40.9	2.50	25.6	8330	39.3
162	1000	46.5	46.5	.0048	41.5	2.50	31.0	8640	37.1
163	300	38	11.4	.0048	6.4	2.50	9.2	1330	36.0
164	300	51	15.3	.068	37.8	1.66	10.4	560	6.6
165	400	49	19.6	.068	41.5	1.66	14.0	610	6.2
166	500	49	24.5	.068	44.8	1.66	16.8	660	7.0
167	600	48	28.8	.068	51.2	1.66	20.6	750	6.4
168	800	46	36.8	.068	57.6	1.66	25.6	850	6.4
169	1000	45	45.0	.068	70.3	1.66	30.4	1030	7.8
170	300	51	15.3	.068	37.8	1.66	10.8	560	6.6
171	300	48	14.4	.053	28.7	1.66	11.0	540	5.2
172	400	46	18.4	.053	31.9	1.66	14.0	600	5.0
173	500	45	22.5	.053	33.6	1.66	16.8	630	4.5
174	600	44	26.4	.053	41.5	1.66	20.0	780	5.8
175	800	43.5	34.8	.053	49.6	1.66	25.6	940	6.5
176	1000	43	43.0	.053	59.2	1.66	30.1	1120	7.4
177	300	48	14.4	.053	28.7	1.66	10.4	540	5.2
178	300	46	13.8	.036	19.1	1.66	10.8	530	3.5
179	400	43	17.2	.036	20.7	1.66	14.0	570	3.3
180	500	42	21.0	.036	25.5	1.66	16.5	710	4.1
181	600	42	25.2	.036	31.9	1.66	19.4	880	5.4
182	800	41	32.8	.036	40.0	1.66	23.8	1110	6.5
183	1000	39	39.0	.036	49.6	1.66	26.6	1370	8.5

TABLE V

Test	Current	Voltage	Power	Mass Flow	Thrust	Field Strength	Anode Power	Specific Impulse	Efficiency
	amps	volts	Kw	gm/sec	gm	kg	Kw	sec	%
184	300	44	13.2	.036	19.1	1.66	10.8	530	3.7
185	300	40	12.0	.016	8.0	1.66	9.5	500	3.3
186	400	38	15.2	.016	14.3	1.66	11.7	890	4.0
187	500	36	18.0	.016	17.5	1.66	13.6	1090	5.2
188	600	35	21.0	.016	20.7	1.66	15.2	1290	6.2
189	800	32	25.6	.016	27.1	1.66	18.4	1690	8.6
190	1000	31.5	31.5	.016	31.9	1.66	22.8	1980	9.7
191	300	40	12.0	.016	8.0	1.66	9.5	500	3.3
192	300	37	11.1	.0127	6.4	1.66	8.6	500	1.4
193	400	35	14.0	.0127	11.1	1.66	10.2	870	3.3
194	500	34	17.0	.0127	14.3	1.66	12.0	1120	4.6
195	600	32	19.2	.0127	19.1	1.66	14.0	1500	7.2
196	800	31	24.8	.0127	25.5	1.66	17.4	2010	10.0
197	1000	31	31.0	.0127	31.9	1.66	22.2	2510	12.4
198	300	36	10.8	.0127	6.4	1.66	8.9	500	1.5
199	300	35	10.5	.0092	4.8	1.66	8.2	520	1.1
200	400	34	13.6	.0092	9.6	1.66	9.8	1040	3.5
201	500	33	16.5	.0092	15.9	1.66	11.4	1720	8.0
202	600	32	19.2	.0092	19.1	1.66	13.3	2070	10.0
203	800	32	25.6	.0092	25.5	1.66	16.4	2770	13.2
204	1000	33	33.0	.0092	30.3	1.66	23.1	3300	14.6
205	300	35	10.5	.0092	4.8	1.66	8.6	520	1.1
206	300	35.5	10.7	.0088	4.8	1.66	8.3	540	1.0
207	400	34	13.6	.0088	9.6	1.66	9.5	1090	3.7
208	500	32	16.0	.0088	14.3	1.66	11.7	1620	7.0
209	600	31.5	18.9	.0088	17.5	1.66	13.0	1990	8.8
210	800	32	25.6	.0088	25.5	1.66	17.8	2900	13.8
211	1000	35	35.0	.0088	31.9	1.66	24.4	3630	15.8
212	300	33	9.9	.0088	4.8	1.66	7.3	540	1.3
213	300	33	9.9	.0068	4.8	1.66	7.3	710	1.6
214	400	32	12.8	.0068	8.0	1.66	8.9	1170	3.5
215	500	32	16.0	.0068	14.3	1.66	10.8	2100	9.1
216	600	32	19.2	.0068	17.5	1.66	13.0	2580	11.2
217	800	33	26.4	.0068	22.3	1.66	18.4	3280	13.3
218	1000	37	37.0	.0068	30.3	1.66	26.6	4450	17.5
219	300	33	9.9	.0068	4.8	1.66	7.6	710	1.6

TABLE V

Test	Current	Voltage	Power	Mass Flow	Thrust	Field Strength	Anode Power	Specific Impulse	Efficiency
	amps	volts	Kw	gm/sec	gm	kg	Kw	sec	%
220	300	32	9.6	.0048	3.2	1.66	7.0	670	1.1
221	400	31	12.3	.0048	8.0	1.66	8.9	1660	5.2
222	500	31	15.5	.0048	12.7	1.66	11.4	2650	10.0
223	600	32	19.2	.0048	15.9	1.66	14.0	3320	13.2
224	800	39	31.2	.0048	23.9	1.66	21.8	4980	18.3
225	1000	44	44.0	.0048	31.9	1.66	30.0	6650	23.2
226	300	32	9.6	.0048	3.2	1.66	7.3	670	1.1
227	300	32	9.6	.0027	3.2	1.66	6.7	1180	1.9
228	400	36	14.4	.0027	8.0	1.66	9.8	2960	7.9
229	500	42	21.0	.0027	14.3	1.66	13.3	5280	17.3
230	600	46	27.6	.0027	20.7	1.66	17.4	7650	27.6
231	800	49	39.2	.0027	27.1	1.66	25.4	10000	34.6
232	1000	51	51.0	.0027	33.5	1.66	33.3	12400	39.2
233	300	34	10.2	.0027	3.2	1.66	8.0	1180	1.8
234	300	55	16.5	.068	39.9	2.50	10.8	590	6.8
235	300	54	16.2	.053	33.5	2.50	11.1	630	6.3
236	300	51.5	15.5	.036	23.9	2.50	11.1	660	4.9
237	300	43	12.9	.016	15.9	2.50	10.8	990	5.9
238	300	41	12.3	.0127	12.7	2.50	9.8	1000	5.0
239	300	40	12.0	.0092	11.1	2.50	9.2	1210	5.4
240	300	37	11.1	.0052	11.1	2.50	8.9	2140	10.3
241	300	40	12.0	.0035	11.1	2.50	8.6	3180	14.1
242	300	43	12.9	.0029	12.7	2.50	8 6	4380	20.7
243	300	45	13.5	.0024	14.3	2.50	8.9	5960	30.3
244	300	50	15.0	.00185	15.9	2.50	9.2	8600	43.7
245	300	60	18.0	.00125	20.7	2.50	8.3	16500	91.0
246	300	71	21.3	.0007	25.5	2.50	8.6	36650	210.
247	400	45	18.0	.0035	15.9	2.50	12.8	4540	19.2
248	400	46	18.4	.0029	17.5	2.50	12.8	6030	27.7
249	400	50	20.0	.0024	19.1	2.50	12.8	8950	36.5
250	400	54	21.6	.00185	22.3	2.50	12.8	12000	62.8

TABLE V

Test	Current amps	Voltage volts	Power Kw	Mass Flow gm/sec	Thrust gm	Field Strength kg	Anode Power Kw	Specific Impulse sec	Efficiency %
251	400	65	27.0	.00125	31.9	2.5	13.8	25500	145
252	400	44	17.6	.0035	15.9	2.5	12.8	4540	19.7
253	500	45	22.5	.0035	19.1	2.5	15.4	5460	22.2
254	500	49	24.5	.0029	23.9	2.5	16.5	9750	38.5
255	500	53	26.5	.0024	27.1	2.5	16.5	11300	55.5
256	500	61	30.5	.00185	31.9	2.5	16.8	17200	86.7
257	500	68	34.0	.00125	35.1	2.5	17.8	38100	14.0
258	500	49	24.5	.0035	22.3	2.5	16.8	6380	28.0
259	600	52	31.2	.0035	31.9	2.5	19.9	9100	44.8
260	600	55	33.0	.0029	33.6	2.5	19.9	11600	56.7
261	600	57	34.2	.0024	35.1	2.5	20.2	14600	72.3
262	600	65	39.0	.00185	36.7	2.5	21.5	19800	89.8
263	600	74	44.4	.00125	47.9	2.5	22.1	38300	19.8
264	600	54	32.4	.0035	31.9	2.5	19.9	9100	43.3
265	800	58	46.4	.0035	47.9	2.5	28.5	13700	68.
266	800	60	48.0	.0029	47.9	2.5	28.8	16500	79.3
267	800	62	49.6	.0024	51.2	2.5	28.8	21300	105
268	800	67.5	54.0	.00185	56.1	2.5	30.2	30300	151
269	800	74	59.2	.00125	59.2	2.5	30.8	47400	227
270	800	57.5	46.0	.0035	47.9	2.5	27.6	13700	68.
271	1000	59	50.0	.0035	59.2	2.5	36.2	16900	81.
272	1000	61	61.0	.0029	60.7	2.5	36.2	21000	100.
273	1000	65	65.0	.0024	62.3	2.5	37.6	25900	120.
274	1000	71	71.0	.00185	65.5	2.5	39.3	35300	157
275	1000	80	80.0	.00125	67.2	2.5	41.8	53700	217
276	1000	56	56.0	.0035	59.2	2.5		13700	86.

TABLE V

and d, a characteristic thrustor dimension, have been systematically varied. The dependent variables V, arc voltage, and P_{amb}, the environmental tank pressure, have also varied but have not been controlled.

The data obtained in this sequence of tests are given in Tables I-V. A discussion of this data follows.

2. Engine Configuration

Five engines were tested in the sequence. These engines have been designated X-7C-1 through X-7C-5. The engines have a common anode housing, magnet, and cathode assembly. They differ in the i.d. of the straight throat section. A sketch of the X-7C series engines is given in figure 3, and a photograph in figure 4. For comparison, the X-2C engine which has been operated under a wide variety of conditions, is sketched in figure 5. The essential difference is that the X-2C cathode lies upstream of a true throat, while the X-7C configuration is a straight one.

Throat dimensions for the X-7C series are listed in Table VI.

TABLE VI

Throat Dimensions of X-7C Engines

Engine	Throat Diameter
X-7C-1	0.85"
X-7C-2	1.25"
X-7C-3	1.05"
X-7C-4	0.60"
X-7C-5	0.40"

Note: Throat diameter of X-2C = 0.5"

3. Discussion of Results

The X-7C engines are numbered in the order in which they were fabricated and tested. After operation of the X-7C-1 with 0.85" throat, the X-7C-2 with 1.25" throat was fabricated. This operated erratically in the power and mass flow ranges tested. The X-7C-3 was intended as intermediate between the X-7C-1 and X-7C-2, with a throat of 1.05". This also operated erratically. At this point smaller thrustors were used, and these operated stably at 0.60" (X-7C-4) and 0.40" (X-7C-5). For data analysis we have concentrated upon the X-7C-1, 4, and 5, in the belief that the erratic operation of the X-7C-2 and 3 did not produce reliable data.

Anode Fall Voltage

The anode fall voltage, V_{an}, is defined as

$$V_{an} = \frac{P_{an}}{I}$$

where P_{an} is the power delivered to the anode coolant, in watts, and I is the arc current in amperes. Based on the data of Tables I-V, the anode fall voltage decreases with current and increases with magnetic field. There is no clear cut variation with throat diameter, although there is an indication that there may be an optimum for diameters near 0.6", with generally higher anode fall voltages at 0.4" and 0.85". The first two statements are exemplified in figure 6, drawn from Table IV, and the final observation is indicated in Table VII below.

TABLE VII

Variation of Anode Fall Voltage with Throat Diameter;

$\dot{m}$ = 0.036 gm/sec

I amp	B Kilogauss	Anode Fall Voltage		
		d = 0.4" volts	d = 0.6" volts	d = 0.85" volts
600	0.83	29.2	27.5	35.4
	1.66	34.2	28	39.4
1000	0.83	24.9	23.2	33.6
	1.66	28.3	25.2	29.6

Total Arc Voltage

The total arc voltage increases in general with B with case exceptions, and with the throat diameter. The behavior with arc current is not entirely monotonic; the voltage is higher at low currents (order of 300 amperes) than at intermediate currents (order of 800-1000 amperes), but then varies little with further current increase, occasionally even rising one or two percent of 1400 amperes. The behavior of arc voltage with B and I is shown in figure 7, and the variation with throat diameter is indicated in Table VIII.

TABLE VIII

Variation of Arc Voltage with Throat Diameter;

$\dot{m}$ = 0.036 gm/sec

I amp	B Kilogauss	Arc Voltage		
		d = 0.4" volts	d = 0.6" volts	d = 0.85" volts
600	0.83	36	39	57
	1.66	42	50	69
1000	0.83	33	36	64
	1.66	39	50	50

Thermal Efficiency

The thermal efficiency is defined by

$$\varepsilon_t = \frac{\text{Power Input - Power to Engine Coolant}}{\text{Power Input}}$$

It is not evident from the definition, but is true as a practical matter, that

$$\varepsilon_t = \frac{V - V_{an}}{V}$$

the reason for this being that the heating of the cathode coolant is quite small relative to the heating of the anode coolant, so that

Power to Engine Coolant = Power to Anode + Power to Cathode

$$\approx \text{Power to Anode} = I\, V_{an}$$

Thus, the behavior of thermal efficiency with respect to variation in I, B, and throat diameter can be understood by reference to the behavior of V and V_{an}.

From figures 6 and 7, V_{an} falls with increasing current at a rate greater than the rate at which V falls, so that ε_t increases, in general, with current. Further, the increase in V with B is, for the most part (but not always) more pronounced than the rise in V_{an} with B, so the thermal efficiency usually increases as B is increased. Finally, referring to Tables VII and VIII, since the arc voltage increases fairly steadily with throat diameter, while the anode fall has a minimum (for the engines tested) at 0.6", the thermal efficiency is poorest for the 0.4" engine, and about the same, on the average for the other two. Figure 8 displays the variation of thermal efficiency as a function of current and magnetic field, while Table IX indicates the dependence of thermal efficiency on throat diameter.

TABLE IX

Variation of Thermal Efficiency with Throat Diameter;

$\dot{m}$ = 0.036 gm/sec

I amp	B Kilogauss	Thermal Efficiency		
		d = 0.4"	d = 0.6"	d = 0.85"
600	0.83	18.9	29.5	38
	1.66	18.6	44	42.9
1000	0.83	24.6	35.6	47.6
	1.66	30.1	49.6	40.8

Thrust

The thrust as measured by a displacement type thrust stand in an environmental tank, with an ambient pressure of the order of 100μ, increases in general with current, magnetic field, and throat diameter. (Indeed, for the portion of the thrust which is of magnetic origin, then a dependence of the form I B ℓ is anticipated). This behavior of measured thrust is displayed in Table X below.

From Table X, except for anomalies displayed by the X-7C-1 engine at 1.66 kilogauss, the increase of thrust with I, B, and d is smooth.

TABLE X

Variation of Thrust with I, B, and Throat Diameter

$\dot{m}$ = 0.036 gm/sec

I amp	B Kilogauss	Thrust, grams		
		d = 0.4"	d = 0.6"	d = 0.85"
600	0.83	22.3	31.1	51.1
	1.66	31.9	39.9	60.7
	2.50	38.3	51.1	79.8
1000	0.83	36.7	55.4	89.3
	1.66	49.6	78.3	76.8
	2.50	64.0	101	111
1400	0.83		72.7	121
	1.66		104	111
	2.50		135	169

Efficiency

It is difficult to frame conclusions concerning the efficiency because of the uncertainties introduced by the test environment. The ambient pressure is of the order of 100μ, and ample evidence exists that engine performance is sensitive to ambient pressure at least at pressures in excess of 1μ (and perhaps below). Thus, it is really not known what the true mass flow is. For this reason, for all the comparisons made above,

the mass flow has been set at 0.036 gm/sec so that the back pressure is not a variable. It is anticipated that the trends in voltage, thrust, etc., would be maintained at a lower back pressure, but probably with different absolute values of these quantities. It is believed to be permissible to treat the efficiency data in the same way; the mass flow rate is fixed, and it is understood that the absolute values of efficiency and I_{sp} may be in error owing to interaction with the test environment.

With these provisions, figure 9 has been prepared in which efficiency is plotted versus I_{sp} for the three test engines. Several factors are apparent from these data.

(i) there are no large differences. The 0.6" engine is consistently more efficient than the other two, and it is interesting to note that this engine had consistently the smaller anode fall.

(ii) higher I_{sp} values are achieved with the larger engines. The mass flows are fixed and the points plotted are for the same range of I and B. Since the thrust and voltage both increase with engine size, fixing I, B and $\dot{m}$ and varying engine size has the effect of allowing larger thrusts (hence higher I_{sp} and larger voltage (hence higher input power) for the larger engines. In principle this could be compensated for by reducing $\dot{m}$ for the smaller engines, but for this comparison we have tried to keep $\dot{m}$ fixed.

C. ENGINE PERFORMANCE AS A FUNCTION OF PROPELLANT FLOW RATE

During the parametric variation reported above, it was possible to operate the engines at a wide range of ammonia flow rates. Interesting effects were found which had not been noted earlier in a more restricted range of ammonia flow rates.

Basically, it was observed that over a range of relatively high mass flow rates the engine performance was insensitive to flow rate and in agreement with performance measured earlier for the X-2C engine at flow rates in the same range (0.029 to 0.058 gm/sec). However, it was also observed that at flow rates below 0.020 gm/sec, the measured performance was not as good as at the higher flow rates.

Drawing on the data of Table IV (d = 0.6") figures 10 and 11 have been prepared. Figure 10 shows, for B = 2.5 kilogauss efficiency as a function of specific impulse for ammonia flow rates in the range 4.8 to 68 x 10^{-3} gm/sec. Data for the flow rates 36, 53, and 68 x 10^{-3} gm/sec cluster together and agree with earlier measurements at 29 and 58 x 10^{-3} gm/sec on an X-2C engine (d = 0.5"). However, for 4.8 to 16 x 10^{-3} gm/sec, lower efficiencies are observed.

Figure 11 is similar to figure 10, but is drawn for B = 0.83 kilogauss. Again, as the mass flow rate reaches low values the performance falls off substantially.

The effect is an important one, although it should be stressed that owing to our incomplete understanding of the interaction of the thrustor with the test environment it may be unrepresentative of what would occur in a hard vacuum. The importance lies in the fact that if, as appears to be the case in our laboratory, there is a minimum mass flow for efficient MPD operation, then there is a minimum power which must be used. For,

$$P_{min} = \frac{4.8 \times 10^{-2} \dot{m}_{min} I_{sp}^2}{\varepsilon_o}$$

where P_{min} is the minimum input power in watts and ε_o is the overall efficiency. If, for example, the minimum mass flow rate is 20×10^{-3} gm/sec, and the desired I_{sp} is 4,000 sec with a 40% overall efficiency, then P_{min} = 38.4 Kw. To achieve the same I_{sp} and efficiency at lower power, the mass flow rate must be reduced.

Thus, there is a tendency for performance at low currents and low magnetic fields to be less attractive than that obtained at higher currents and magnetic fields, with the apparent conclusion that low power operation is unattractive. We point out that this is based on the mass flow rate effect, which may be environmentally produced.

The question arises as to the detailed manner in which the performance falls off at lower mass flow rates. That is, for fixed I, B, and engine size, as $\dot{m}$ is reduced, does the thrust fall off more rapidly below $\dot{m} = 20 \times 10^{-3}$ gm/sec than above, or does the voltage rise more rapidly? In the first case the input power would remain relatively unchanged but the thrust power would not rise with I_{sp} sufficiently rapidly to keep on the efficiency - I_{sp} curve for higher mass flow rates. In the second case the thrust power would rise but the input power could rise at a great enough rate (with decreasing $\dot{m}$) to reduce efficiency.

Table XI displays the behavior of the operating parameters as $\dot{m}$ is reduced at fixed I and B, for the 0.6" diameter throat engine (K-7C-4).

TABLE XI

Variation of Mass Flow Rate for X-7C-4 Engine

(d = 0.6") I = 1000 amperes, B = 1.66 Kilogauss

$\dot{m}$ gm/sec	V volts	Pin Kw	T gm	I_{sp} sec	ε_o %
.068	52	52	94	1,380	12
.053	51	51	88	1,650	13.7
.036	50	50	78.3	2,170	16.3
.016	42	42	51.2	3,200	19.7
.0127	53	53	67.1	5,280	32.1
.0092	60	60	70.3	7,640	43.0
.0088	58	58	68.7	7,800	43.3
.0068*	50	50	70.3	10,300	70
.0048*	64	64	78.2	16,200	95.5

*$\varepsilon_o > \varepsilon_t$, definitely indicating entrainment.

From Table XI, for mass flows of 0.068 to 0.036 gm/sec the thrust falls slightly with mass flow decrease, and the input power is nearly constant. For mass flows of 0.0127 gm/sec and below the thrust and input power vary erratically with mass flow rate, and show no marked trends, suggesting that the true mass flow rate is perhaps not being varied. At 0.016 gm/sec both the thrust and voltage are minimum.

While it is dangerous to draw conclusions from data on imperfectly understood interactions, it is possible to hypothesize that at high mass flows the interaction with the environment is negligible, at low mass flows this interaction dominates completely, and in the range 0.010 to 0.020 gm/sec both the input mass flow and the environment contribute to the measured performance. If this is true, then it is likely that the qualifying terms "low," "high," and "intermediate" take on different meanings depending upon the environment. Thus, we have attempted to draw conclusions from our data based on a flow rate of 0.036 gm/sec, which seems a reasonable compromise between avoiding interaction with the environment and not requiring excessively high input powers. In a lower ambient pressure facility the "safe" mass flow may be substantially lower, permitting valid operation at much lower input power levels.

D. PERFORMANCE OF RADIATION COOLED ENGINES

1. Comparison of Radiation and Water-Cooled Engines

A radiation cooled engine which shows considerable merit has been designated X-7C-R, shown in figures 12, 13 and 14.

The tungsten anode and cathode are self-cooling and boron nitride insulators are used for interior insulation. On this model, the outside diameter was 4 inches and the throat diameter 0.8 inch. A water-cooled counterpart (X-7C-1) was tested separately to evaluate the effects of cooling mode.

On the basis of tests made on these engines, it has been concluded that there is no significant difference in thrust performance due to the cooling mode. To illustrate this point, figure 15 compares directly the efficiency versus I_{sp} for two engine configurations, one water-cooled and one radiation-cooled, but each having a 4-inch outside diameter and a 0.8 inch throat.

However, there is an apparent difference in operating parameters between the two engines which is not yet understood. At fixed I, B, and $\dot{m}$, there is a significant difference in V and thrust, of such a nature that the ratio T/V is not greatly affected; thus, the efficiency versus I_{sp} curve is not much changed although the detailed operating points are.

Examining Table XII, it is clear that in general the water cooled X-7C-1 ran at a higher voltage than did the radiation cooled X-7C-R, and, under some conditions, at a higher thrust. Indeed, the effect is as though the characteristic dimension of

TABLE XII

Comparison of Radiation Cooled X-7CR and Water Cooled X-7C-1

I	$\dot{m}$	B	Voltage			Thrust		
			X-7C-R	X-7C-1	X-7C-4	X-7C-R	X-7C-1	X-7C-4
400	0.036	0.88	42	60	42	19.9	33.5	22.4
		1.25	50	57	46	28.6	31.9	22.3
		1.66	57	66	50	41.5	36.7	23.5
		2.08	76	75	52	44.7	39.3	41.5
		2.50	69	85	53	46.5	46.3	25.5
500		0.88	39	57	40	26.5	39.9	27.6
		1.25	50	54	44	39.8	38.3	28.7
		1.66	57	66	50	52.7	49.5	33.5
		2.08	64	76	50	54.2	55.8	51
		2.50	65	85	51	56.5	63.9	33.5
600		0.88	38	57	39	33.2	51.1	31.1
		1.25	49	52	43	51.1	43.2	35.1
		1.66	51	69	50	54.3	60.7	39.9
		2.08	57	76	50	63.8	72	59
		2.50	60	86.5	51	70	79.8	51.1

the X-7C-R is smaller than that of the water cooled version. For comparison, we have included also in Table XII the data for the X-7C-4 engine with 0.6" throat. It can be seen that the voltage and, usually, the thrust for the X-7C-R thrustor are bracketed by the values for the X-7C-1 and X-7C-4 thrustors.

In summary, it appears that there are differences in operating point between radiation and water cooled engines, but no outstanding differences in overall propulsion performance. At low values of B the X-7C-R behaved like the X-7C-4 (0.6" throat) and at high values of B like the X-7C-1 (0.85" throat).

2. Effect of Scale-Down

A scaled-down version of the X-7C-R radiation-cooled engine was made to evaluate performance of a lighter version of the radiation-cooled design. A 3-inch diameter MPD arcjet was tested over a range of mass flow, magnetic field strength and currents to define the performance. Results of these tests are presented in figures 16 and 17.

The overall efficiency and specific impulse compares in essence with previous data on a water-cooled version. However, the maximum attainable current and the minimum mass flow were more limited due to higher engine temperatures. At comparable conditions, the engine temperature was generally 200-300^{o}C higher than on the larger 4-inch diameter engine. The maximum

specific impulse achieved with this engine is below the range of immediate interest.

The 3-inch engine was fabricated from a tungsten billet which was apparently defective as evidenced by the development of a crack on the cathode end of the engine prior to test. This became worse during test and power cycling. Three different runs developed two other cracks through the throat of the engine. The condition of interior parts, insulation and cathode, was found to be generally good after test.

The problem of fractures developing on the anode, on both the 4-inch diameter as well as the 3-inch diameter engines during thermal cycling suggests either an extension beyond the ultimate tensile strength of the tungsten strength of the tungsten or the development of a crystalline structure which degrades the tensile properties. The material used for the anode is sintered tungsten with a few percent thoria doping. No indication of recrystallization has been found, which would lead to the development of failures in tungsten.

It has been demonstrated on a previous program[19] that radiation-cooled thrustors can handle power levels of at least 30 Kw for periods of at least 700 hours with proper design for cooling. On that program higher engine temperatures were reached without anode failures, though with smaller diameter engines. The larger dimension of the present engines may introduce a limitation by the internal stresses developed.

a. Operating Voltage

The voltage current characteristic of the 3-inch radiation engine parallels the performance of the water-cooled version as shown in figure 17 but displays about a 10-volt decrement which is presently unexplained. The cathode employed on this test was barium-calcium-aluminate impregnated tungsten rather than the usual thoriated tungsten used on other tests. A combination of this fact and the hot anode may produce the observed voltage change.

b. Operating Temperature

The external surface temperature of the radiating engine was determined from readings with an optical pyrometer which were corrected for the tungsten emissivity and window absorption. The temperature for the 3- and 4-inch diameter thrustors are plotted in figure 18 versus arc power. While some hysteresis is noted in the increasing power values over those for decreasing power, the data generally follow the fourth power relation shown as expected. At lower mass flow values, a rise in temperature occurs.

c. Low-Power Engine Tests

A series of tests were conducted on the L-2 model engine which primarily had been utilized for alkali metal propellant tests. The engine had a 2-inch outside diameter and a 0.5-inch throat. A photo of the arcjet assembly and mounting

bracket is shown in figure 19. The construction details of the engine are given in figure 20. It comprises a tungsten exhaust nozzle fitted and molybdenun-vanadium (2150°C) brazed to a molybdenum section which is held by the mounting bracket, as seen in figure 19. The thoriated tungsten cathode and boron-nitride insulators extend beyond the water-cooled bracket and incorporate metallic C-ring seals.

This engine was installed on a thrust balance and mounted within an aluminum test tank. The magnetic field was produced by a water-cooled solenoid coil and a water-cooled shield ring was mounted inside the coil so as to enclose the engine. The magnetic field had a maximum value of 2 kilogauss. Since this engine is a relatively low-power design all tests were made at this peak value of magnetic field to keep the voltage high, and, correspondingly, to reduce the engine current at a given power level. Data were obtained at various mass flow conditions at increasingly high current levels. The procedure followed in the tests was one of progressively raising the power on the engine until ultimately some indication of failure in the cathode-anode region was evident.

Tests of the engine were halted after erosion was observed when the power was increased to about 14 Kw. However, the damage to the engine was found to be relatively superficial, occurring for the most part as a fracturing at the forward edge of the boron nitride insulator separating the cathode and

anode. This effect did not recur on the second test when the changes in power were more gradual.

The performance of the engine was low, providing about 1800 seconds specific impulse at 10 percent overall efficiency for the lowest ammonia flow rate utilized. The overall thrust efficiency variation with the specific impulse is shown in figure 21. The efficiencies are generally below 10 percent and show a lower trend with decreasing propellant mass flow at any given specific impulse. The results were generally lower than the best data on water-cooled MPD arcjets.

The integrity of the engine, while not extensively tested for endurance, seemed satisfactory below the maximum power input attained of 22.5 Kw. During the tests a large temperature gradient was evident across the brazed joint separating the tungsten and molybdenum sections. The conditions which limited further testing was local melting of molybdenum directly behind the tungsten throat. Some melting and attrition of the cathode and the C-rings was also found.

d. Power Capability

The radiation engines which have been tested establish some bound to the maximum power input which can be achieved without material loss. The performance of the three radiation engines which have been tested define a size to maximum power behavior as shown in figure 22. If the conduction process from the internal to external surface is considered bound by the onset of melting, then the maximum power will be approximately dependent on the scale dimension as observed.

E. ENGINE LIFE DEMONSTRATION

An endurance test on a radiation-cooled version of the MPD arcjet was made using a 4-inch diameter X-7CR engine (figure 12) with ammonia propellant. The test involved only one power cycle from startup to shutdown. Initially, operation was conducted at progressively higher power values in steps of 100 amperes from 200 to the duration test value of 900 amperes. Operation at 1000 amperes was attempted but produced some material erosion. The endurance test was begun at a power level of 36 Kw, specific impulse of 3600 seconds, and overall thrust efficiency of 34 percent. A mass flow of .023 gm/sec and a magnetic field strength of 2.5 kilogauss were utilized. The background exhaust pressure was about 90 microns.

The maximum external engine temperature for the radiation engine was approximately 2000^{o}K, shown operating in figure 23.

The test was conducted for 75 hours (uninterrupted) at the power and mass flow condition set. However, certain malfunctions of support equipment occurred which affected the test results. Loss of the transducer signal, due to an overheated cable, after a few hours operation, did not allow a continuous monitoring of thrust. However, a more serious condition developed when an observation window developed a crack which could not be sealed efficiently. As a result, the background environment became air-contaminated to an extent which caused slow oxidation of the radiating engine parts, particularly the high-temperature nozzle

end of the engine. This condition had not been observed on any previous tests on this program with a controlled background. In fact, former experience with tungsten body radiation cooled arcjet thrustors (Reference 19) which operated at higher temperatures and for prolonged periods of up to 30 days, did not display oxidation.

In spite of the short comings of the test the 4-inch diameter radiation engine shows considerable promise. The anode block did not exhibit any thermal structural cracks as had occurred on other tests at lower current levels with cycling. The power, specific impulse and overall thrust efficiency values which had been achieved offer reasonable propulsion conditions. The operation of the engine at the stated conditions. The operation of the engine at the stated conditions in an improved vacuum, where increased thrust has been demonstrated (Reference 18), would project the performance close to the 5000-second, 50 percent overall efficiency figure.

III. MPD ARCJET ANALYSIS

A computational procedure has been developed for analyzing the magnetic annular arc discharge of an MPD arc thrustor. The calculation requires the voltage characteristic as an empirical input but otherwise is self-consistent and does not rely on other experimental data. Hopefully, at a future date, this restriction can be removed.

The hydrodynamic model considers a quasi one-dimensional steady flow down the axis of the annular nozzle; i.e., the effect of area change is considered, but radial radiations are neglected. The azimuthal velocity of each gas species is treated, but no azimuthal variations are considered. The analysis assumes an applied constant axial magnetic field and an induced azimuthal field due to the radial currents. Hydrogen gas is the working medium with four species considered: H_2, H, H^+, and e. The ion H_2^+ is assumed to go to $H^+ + H$ in times short compared to those of interest. Conservation equations for mass, momentum, and energy are written for each of the four species along with the appropriate Maxwell relations. The transport coefficients and reaction rates for all processes have been duduced from experimentally determined cross sections.

Boundary conditions are applied both upstream corresponding to the incoming cold neutral gas and downstream at the respective sonic point for each species. The requirement that the flow proceed through each sonic singularity in a regular manner eliminates the necessity of further boundary conditions on the supersonic flow. A set of first-order ordinary differential equations

is obtained which is solved by a Runge-Kutta procedure on a high-speed digital computer.

Results have been obtained for several sets of parameters corresponding to usual MPD arc operating conditions. In figure 24, the behavior of several key parameters (current density and axial velocity) is shown for a typical calculation. In each case, the calculations show a strong discharge centered about the throat region of the nozzle and several millimeters in thickness. The thickness of the zone appears to be controlled primarily by diffusion of the ion-electron pairs in the neutral background and a simple hand calculation assuming only this process gives results comparable to the computer output. The primary flow process is a strong heating of the neutral gas by the discharge in the subsonic regime. For a given geometry and mass flow, in fact, the energy of the subsonic part of the discharge appears to be directly proportional to the heating required to bring the gas to the sonic point. Thus, in each case, one is able to establish a relationship between current and incoming Mach number. This effect at higher pressure is shown in figure 25.

The simplest geometry to analyze is one with electrode surfaces extending infinitely far upstream. However, a high-current solution exists for this model only above a certain incoming gas pressure (typically 10-20 mm Hg). Below this pressure, something that resembles a glow discharge is the only result. The high-

current mode can be extended in each case to slightly lower pressures by insulating the electrodes at various positions upstream of the nozzle throat. This result, however, may correspond to an experimentally unstable discharge. A simple relationship for estimating the low-pressure limit has been derived which appears to agree both with the computer results and with experimental observations of discharge blowoff.

The strong expansion that occurs in the supersonic flow regime very quickly leads to large ratios of the cyclotron-to-collision frequency for the electrons, thus effectively terminating the radial discharge. Up to the present time, the calculation scheme does not take into account wave or collective phenomena which could modify the results for the current pattern in the supersonic flow. Part of the current analytical effort is directed towards better understanding the important processes in the supersonic expansion.

Much of the present work involves analyzing the computer results to find simple general relationships such that the effect of different experimental parameters on the flow may be easily seen. Of particular interest is the effort to theoretically predict the voltage characteristic.

IV. MAGNET DESIGN CONSIDERATIONS

A. CURRENT STATUS

The MPD arcjet thrustor has been under evaluation at Avco/SSD in configurations which utilized externally applied magnetic fields in the discharge region. The thrustors have been operated in the 10 to 50-Kw range; externally applied magnetic field strengths have ranged from 250 gauss up to 4 kilogauss.

To date, little effort has been expended in fabricating a magnetic field coil configuration for optimum magnet power utilization. Field coils have been made simply by winding copper tubing around a mandrel. Some of the more obvious advantages of this method for laboratory evaluation of magnetic field effects upon engine operation are the following:

1. The coils may be water-cooled. The cooling permits the use of very high currents in the coils for achieving the high magnetic field strengths desired for evaluations.

2. Fabrication is extremely simple. New coil configurations may be fabricated in just a few hours.

3. Magnetic field strength distribution may be varied almost at will. Several magnet coils may be wrapped around the same mandrel and on top of previous coils. The several coils may be operated so that their fields are aiding or bucking each other, producing different ratios of the axial magnetic field strength, B_z, to the radial field strength, B_r.

4. Tubing is readily available, and no machining is required for the fabrication of coils.

5. Insulation of turns from each other is accomplished by sliding shrink-on tubing over the copper tubing.

The experimental results have indicated that engine operation is not appreciably affected by magnetic field strength distributions, and that the magnetic field produced by a solenoidal magnet coil is equally as effective as any other distribution tested. Insofar as field strength is concerned, our results have indicated that increases of magnetic field strength above approximately 1 kilogauss do not significantly improve either engine efficiency or specific impulse obtained.

The next section outlines some of the work which has been done at Avco/SSD to determine the weight penalties associated with a properly designated magnet subsystem. In view of the experimental results just mentioned, the following assumptions have been made for the purpose of the discussion:

a. The required magnetic field distribution can be obtained with a solenoidal magnet coil.

b. For reference purposes, the field strength at the core center may be taken as the basic design parameter.

c. The field strength at the core center will be of the order of 1 kilogauss.

d. The inner radius of the magnet coil will be of the order of 1 inch.

B. RADIATION-COOLED MAGNETS

Approximate evaluations have been made of the weights of radiation-cooled magnet systems. Copper and aluminum have been considered as the solenoid materials. The following sections, although preliminary, form the basis for a complete evaluation of magnet subsystem weight requirements.

1. Solenoidal Electromagnets

The axial field strength at the center of the solenoid is given by the Fabry relation, which has the form[21]:

$$B_z = G \left(\frac{P\lambda}{\rho r_i}\right)^{\frac{1}{2}} \qquad (1)$$

where B_z (kilogauss) is the magnetic field strength, G is a geometric factor which depends upon the coil geometry (i.e., ratio of outside to inside radii $r_o/r_i \equiv \alpha$, and length-to-diameter ratio, $\ell/2\ r_i \equiv \beta$), P (megawatts) is the power input, λ is the fraction of the coil occupied by the conductor, ρ (ohm-cm) is the resistivity of the coil material, and r_i (cm) is the inside radius of the coil.

The geometric factor, G, is a relatively weak function of the radii ratio, α, and the coil length-to-diameter ratio, β. Its maximum value is about 0.20 and corresponds to values of both α and β in the range 2 to 3. For the purposes of the following

semiquantitative discussion, G will be assumed a constant equal to the maximum value of 0.20 and both α and β will be assumed to be of the order 2 to 3. From the viewpoint of the following analysis, these quantities have only a second-order effect on the calculated results, and by preselecting values of G, α, and β the problem of estimating magnet system weights is considerably simplified. In a later section, consideration will be given to two different coil designs and the effects of coil design upon the value of the geometric factor, G, and the magnet system weight.

Substituting G = 0.20 into Equation (1), the Fabry relation can be written

$$P = 6.25 \times 10^{-2} \rho r_i B_z^2 / \lambda \qquad (2)$$

with dimensions: input power, P(Kw), resistivity, ρ (10^{-6} ohm-cm), inner radius, r_i (in.), axial field strength, B_z (kilogauss), and the fraction of coil occupied by the conductor, λ, (dimensionless). Equation (2), with the dimensional units as indicated, is used for the remainder of this discussion.

From the Fabry relation in the form of Equation (2), the solenoid power requirement is seen to be proportional to the square of the required axial field strength, directly proportional to the solenoid material resistivity and inner radius, and inversely proportional to the packing fraction, λ. The resistivity of the solenoid material is a function of temperature, increasing with an

increase in coil temperature. For the purposes of the present discussion, it is assumed that the temperature within the entire coil is a constant, and in a later section it will be shown that a coil design for which this assumption is valid is also one for which the maximum value of the geometric factor, G, is obtained. Moreover, for a radiation-cooled magnet the same design will be shown to provide a packing fraction, λ, very close to unity; for the presents, therefore, λ is assumed to be equal to one.

Figure 26 shows the resistivity of copper and aluminum as a function of temperature; as the temperature is increased, the resisitivity of each material increases. Thus, for fixed magnetic field strength and inner solenoid radius, the required input power increases with increase in solenoid temperature (Equation 2). Figure 27 presents the magnet power input for a field strength of 1 kilogauss as a function of temperature, normalized to an inner radius of 1-inch. The power requirements for an aluminum solenoid are clearly seen to be greater than for a corresponding copper solenoid, but the total subsystem weight penalty will be seen to be somewhat smaller due to the reduced magnet coil weight obtained by the use of aluminum with its smaller mass density. In the next section the magnet weights associated with the two materials in a radiation-cooled configuration are considered.

2. Radiation-Cooled Magnet Subsystem

In this section, estimates of the weight of a radiation-cooled magnet subsystem are presented. The weight of a magnet is given by

$$W_{mag} = 2\pi r_i^3 \, W(\alpha^2-1) \, \beta\lambda \qquad (3)$$

where r_i is the inner solenoid radius, W is the density of the magnet material, and α, β, and λ have the same meanings as above. For the radiation-cooled magnet, λ is assumed to be equal to 1, α and β are assumed to have values in the range 2 to 3. To a first approximation, then, the coil weight is given by

$$W_{mag} \approx 75 \, r_i^3 \, W \qquad (4)$$

For copper, $W \approx 550$ lb/ft^3, and the magnet weight is

$$W_{mag,cu} \approx 23.5 \, r_i^3 \text{ pounds } (r_i \text{ in inches})$$

For aluminum, $W \approx 165$ lb/ft^3, and the magnet weight is

$$W_{mag,al} \approx 7.2 \, r_i^3 \text{ pounds } (r_i \text{ in inches})$$

Figure 28 presents the total weight of the magnet subsystem, as a function of coil temperature, assuming a power supply weight of 50 lb/Kw, a 1 kilogauss magnetic field strength at the coil core and an inner radius of 1-inch. It is seen that for coil temperatures below 600°C, the smaller weight of an aluminum

magnet coil compensates for the increased power input required and appears to be a somewhat more attractive system from the point of view of weight penalty accuring to the use of the external magnetic field.

A major consequence from figure 28 is a result that, provided the coil can be operated at temperatures below 600°C, neither system imposes a weight penalty of as great as 50 pounds. The power requirement is less than 600 watts. For an engine operating in the 30 to 50 kilowatt range, the engine power supply weight is of the order of 1500-2500 pounds. The entire magnet subsystem then represents only of the order of 2 to 3 percent of the engine power supply weight. Except for ease in fabrication, therefore, there is little reason to choose one of the materials considered over the other.

The one point which has not yet been determined is whether a radiation-cooled magnet can be operated at temperatures below 600°C. For a radiation-cooled magnet, all the input power must be radiated from the magnet exterior surface. The radiation area of the coil is given by

$$A = 2\pi r_i^2 \, (2\alpha\beta + \alpha^2 - 1) \qquad (5)$$

and for the assumed values of α and β, the radiating area becomes

$$A \simeq 100 \, r_i^2 \ (cm^2) \qquad (6)$$

For a 1-inch inner radius, the radiating area is thus of the order of 650 cm^2, and the total power which can be radiated is given by

$$P = 3.66 \times 10^{-9} \times \varepsilon t^4 \text{ watts} \qquad (7)$$

Figure 29 shows the power which can be radiated for both aluminum and copper as a function of temperature, super-imposed upon a replot of thesolenoid power versus temperature presented in figure 27. The emissivity of copper has been taken as 0.6, that of oxidized aluminum has been taken to be in the range 0.11 to 0.19 in the temperature range of interest. The figure shows, in a rather dramatic fashion, that a copper magnet will operate at a temperature of the order of 300°C, will require approximately 225 watts of solenoid power, and will entail a total magnet power supply weight of the order of 35 pounds. An aluminum magnet, on the other hand, would melt, it being incapable of radiating all the input power unless its emissivity could be increased.

Several methods for increasing the emissivity suggest themselves. Probably the simplest consists of placing a plating on the radiating surfaces of the aluminum magnet coil (such as aluminum oxide). At the temperatures of interest, no problems would be encountered with this plating process. The coating would increase the emissivity of the aluminum magnet coil, say, to 0.6, and the curve of power radiated shown in figure 29 for copper would

be equally valid for the aluminum magnet coil. For this configuration, then, an aluminum magnet would operate at 425°C requires an input power of 525 watts, and entails a total magnet and power supply weight of the order of 33 pounds. To within the approximations utilized for this discussion, the two materials impose the same weight penalty (approximately 35 pounds), this total weight includes provision for the power supply based on a specific power supply weight of 50 lb/Kw.

Since the solenoid power is porportional to the square of the magnet field strength, the temperatures and power requirements associated with lower magnetic field strengths are much reduced. For lower magnetic field strengths, aluminum becomes more attractive a material than copper. Figure 30 presents the total magnet and power supply weight penalties incurred as a function of field strength for field strengths up to 1.4 kilogauss.

For field strengths below about 1 kilogauss, aluminum appears to be the more attractive magnet material. For field strengths above 1 kilogauss, the weight of the power supply for a aluminum magnet coil, as well as its operating temperature, rapidly increases. For field strengths of the order of 1 kilogauss, the absolute difference in system weight is entirely negligible, and either magnet coil could be utilized.

3. Magnet Coil Design

This section presents a brief outline of the differences between the normal "wire-wound" solenoid design, and a more efficient and compact design which was originally suggested by Bitter[22] and has most recently been improved by Johansen[23].

The two geometries are most simply compared by considering the methods of fabrication and the resulting current distributions. The "normal" configuration is obtained by winding a square conductor into a solenoid, thereby achieving a uniform current density throughout the conducting coil. Each turn of the coil must be insulated from all other windings in both the radial and the axial directions, and the volume taken up by this insulation reduces the fraction of the coil volume which carries current, i.e., this design has a value of λ which is clearly less than 1. Moreover, radial heat conduction is inhibited by the insulation between the individual turns.

The axial magnetic field strength at the coil core, and the input power may be related by the Fabry relation

$$B = G_1 \left(\frac{P\lambda}{\rho r_i}\right)^{\frac{1}{2}}$$

where

$$G_1 = \frac{\mu_o}{2\pi} \left(\frac{\beta}{\alpha^2 - 1}\right)^{\frac{1}{2}} \ln \frac{\alpha + \alpha^2 + \beta^2}{1 + 1 + \beta^2} \qquad (8)$$

a result first obtained by Fabry[21]. Values of G_1 have been tabulated by Cockcroft[24]. The maximum value which G_1 can attain is 0.18 and occurs for values of α and β in the vicinity of 2-3.

A more efficient design, generally attributed to Bitter[22], is one in which the current density in the coil is inversely proportional to the radius, and is fabricated by making pancake disks of conductor which are cut through along a radius and joined to form a spiral-like surface. Figure 31 shows several disks; the coil is obtained by joining edges A to B and C to D in the illustration.

The radial heat conduction in this configuration is not inhibited by insulating materials, since the only insulation required is between pancake sections. A further improvement suggested by Johansen[23], is obtained if aluminum is used; in this case each disk can be anodized and the insulation volume is then negligibly small. Thus, this design yields a value of λ very close to unity. Even if copper is used, the value of λ for this configuration is still much closer to unity than for the "normal" coil configuration.

For this configuration, the Fabry relation is given by

$$B = G_2 \left(\frac{P\lambda}{\rho r_i}\right)^{\frac{1}{2}} \tag{9}$$

where

$$G_2 = \frac{\mu_o}{2\pi} (\beta \ln \alpha)^{-\frac{1}{2}} \ln \frac{\beta + 1 \quad \beta^2}{\beta + \alpha^2 \beta^2} \tag{10}$$

Values of G_2 are given in Reference 22. The maximum value attained by G_2 is 0.21 for $\alpha = 6$ and $\beta = 2$. For α and β is the vicinity of 2-3, the value of G_2 is 0.2, and this is the value which has been used in the sections above. If λ had the same value for this and the "normal" coil geometry, this configuration would still be about 10 percent more efficient. In practice, λ is greater for this design as well, and the radial heat conduction is also improved. This magnet configuration is thus more efficient from all considerations and it forms the basis of the analysis above.

Finally, with the assumption that all the input power is radiated from the outer edge of the magnet coil, it is readily shown that the difference in temperature between the inner and outer coil surfaces is given by

$$\Delta T = \frac{p \ \ln \alpha}{8\pi \ k\beta \ r} \qquad (11)$$

For the situations considered above, this difference is of the order of only 1-10°C, and the previous assumption of constant coil temperature is completely valid.

V. PROGRAM DIRECTION

The effort during the second half of the program on the research and development of a magnetoplasmadynamic-arc thrustor will be directed as follows:

1. Studies of heat transfer with large radiation-cooled thrustors will continue with the aim of raising the radiative ability through achievement of higher surface temperature or increased surface emissivity.

2. Further performance measurements will be made with the objective of understanding better the interaction with the environment.

3. Engine endurance and integrity will be explored through extended time and recycling tests with particular attention directed toward reaching an understanding of and a solution to the problem of anode mechanical failure.

4. The analysis of the MPD arcjet will continue with efforts directed toward a better understanding of the supersonic portion of the flow. Attempts will be made to theoretically predict the voltage characteristic.

5. Additional work will be performed on the radiation-cooled magnet design and the subsystem requirements. Such effects as heat loading from the radiating thrustor will be examined.

VI. REFERENCES

1. Finger and Shulman, in Space Power Systems, Academic Press, (1961) pg. 615.

2. Lazar, J., and J. P. Mullin, A Review of the Role of Electric Propulsion, AIAA Paper 66-1025 (1966). AIAA Third Annual Meeting.

3. Ritchie, D., P. Toms and W. Menetrey, "Potentials of Solar Power for Electric Propulsion," Paper No., 66-210, AIAA Fifth Electric Propulsion Conference (March 1966).

4. Ramirez, P., and D. Tollefson, "Design and Analysis of Power Conditioning for Ion Propulsion Systems, "Paper No. 66-215, AIAA Fifth Electric Propulsion Conference (March 1966).

5. Molitor, J. H., D. Berman, R. L. Selizer and R. N. Olson, "Design of a Solar-Electric Propulsion System for Interplanetary Spacecraft," Paper No. 66-215, AIAA Fifth Electric Propulsion Conference, (March 1966).

6. Ducati, A., G. M. Giannini, and Muehlberger, Experimental Results in High Specific Impulse Thermo-Ionic Acceleration, AIAA J. 2 (1964) 1452-1454.

7. Cann, G. L., Annular Magnetic Hall Current Accelerator, AIAA Paper No. 64-670, Fourth Electric Propulsion Conference, Philadelphia, Penn. (August 1964).

8. Kelly, A. J., N. M. Nerheim, J. A. Gardner, "Electron Density and Temperature Measurements in the Exhaust of an MPD Source," AIAA Fifth Electric Propulsion Conference, San Diego (March 1966).

9. Grossman, W., H. A. Hassan, Hess, R. V., and Oertel, G., Experiments with a Coaxial Hall Current Plasma Accelerator, AIAA Paper No. 64-697, Fourth Electric Propulsion Conference, Philadelphia, Penn. (August 1964).

10. Hess, R. V., Fundamentals of Plasma Interaction with Electric and Magnetic Fields, Proceedings of the NASA-Electric and and Magnetic Fields, Proceedings of the NASA-University Conference on the Science and Technology of Space Exploration, Paper No. 59, Volume 2, (November 1963).

11. Seikel, G. R., and E. Reshotoko, Hall Current Ion Accelerator, Bul. Am. Phys. Soc., 7, No. 6 (1962).

12. Powers, W. E., and R. M. Patrick, A Magnetic Annular Arc, Avco Everett Research Laboratory Report RR-129 (May 1962).

13. John, R. R., Bennett, S., and Connors, J. F., Experimental Performance of a High Specific Impulse Arcjet Engine," Astronautica Acta 11, 97 (1965).

14. Bennett, S., R. R. John, G. Enos, and A. Tuchman, Experimental Investigation of the MPD Arcjet, AIAA Paper No. 66-239, AIAA Fifth Electric Propulsion Conference, San Diego, (March 1966).

15. W. E. Moeckel, Promises and Potentialities of Electric Propulsion Status of Thrustor Performance, AIAA Paper No. 66-1024, AIAA Third Annual Meeting, (December 1966).

16. Avco/RAD Arcjet Technology Research and Development, Final Report NASA CR-54687, RAD-TR-65-37 on Contract NAS3-5900 (December 1965).

17. John, R. R., and S. Bennett, "Arcjet Research and Technology, NASA CR-5752 (1965).

18. Jones, R. E., and E. L. Walker, Status of Large Vacuum Facility Tests of MPD Arc Thrustor, AIAA Third Aerospace Sciences Meeting, AIAA Paper No. 66-117, (January 1966).

19. Avco/RAD Thirty Kilowatt Plasmajet Rocket Engine Development, Third Year Development Program Summary Report NASA-CR-54079, RAD-TR-64-42, on Contract No. NAS 3-2593 (July 1964).

20. Powers, W. E., "Measurements of the Current Density Distribution in the Exhaust of an MPD Arcjet," AIAA Third Aerospace Sciences Meeting, AIAA Paper No. 66-116, (January 1966).

21. Fabry, Eclairage Electrique, 17, 133 (1898).

22. Bitter, Rev. Sci. Instr. 7, 482 (1936).

23. Johansen, to be presented at AIAA 5th Aerospace Sciences Meeting, 1967.

24. Cockcroft, Phil. Trans. Roy Soc. 227, 235 (1928).

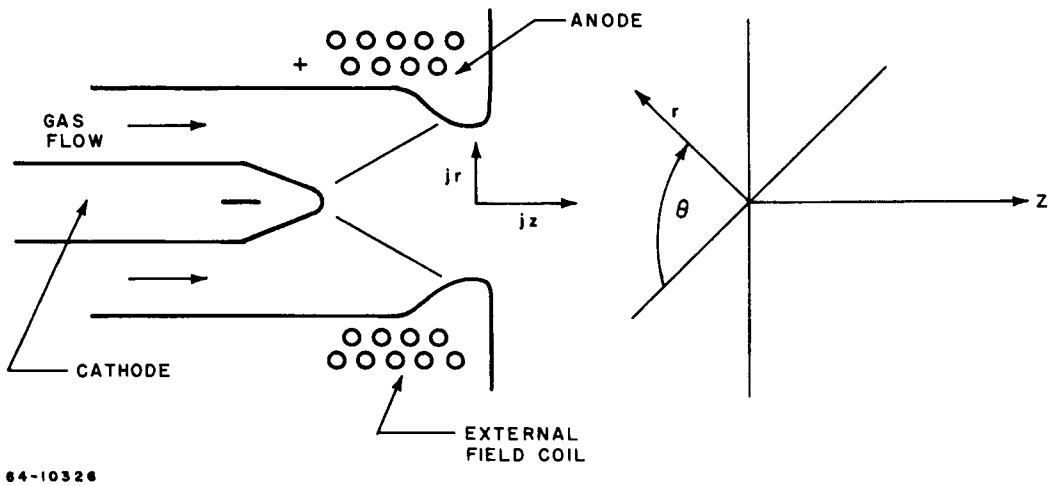

Figure 1 SKETCH OF GENERALIZED MPD THRUSTOR CONFIGURATION

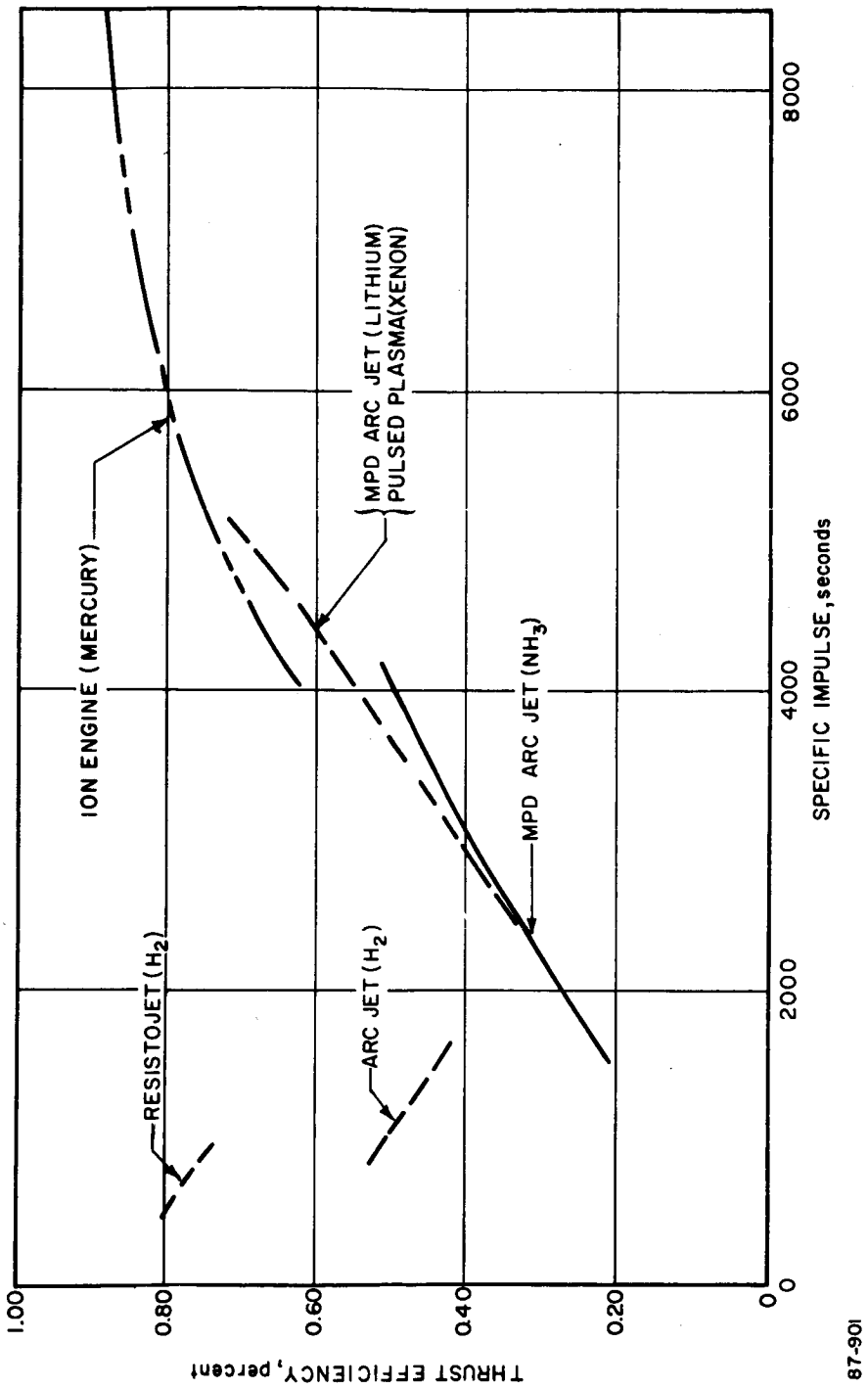

Figure 2 OVERALL EFFICIENCY VERSUS SPECIFIC IMPULSE

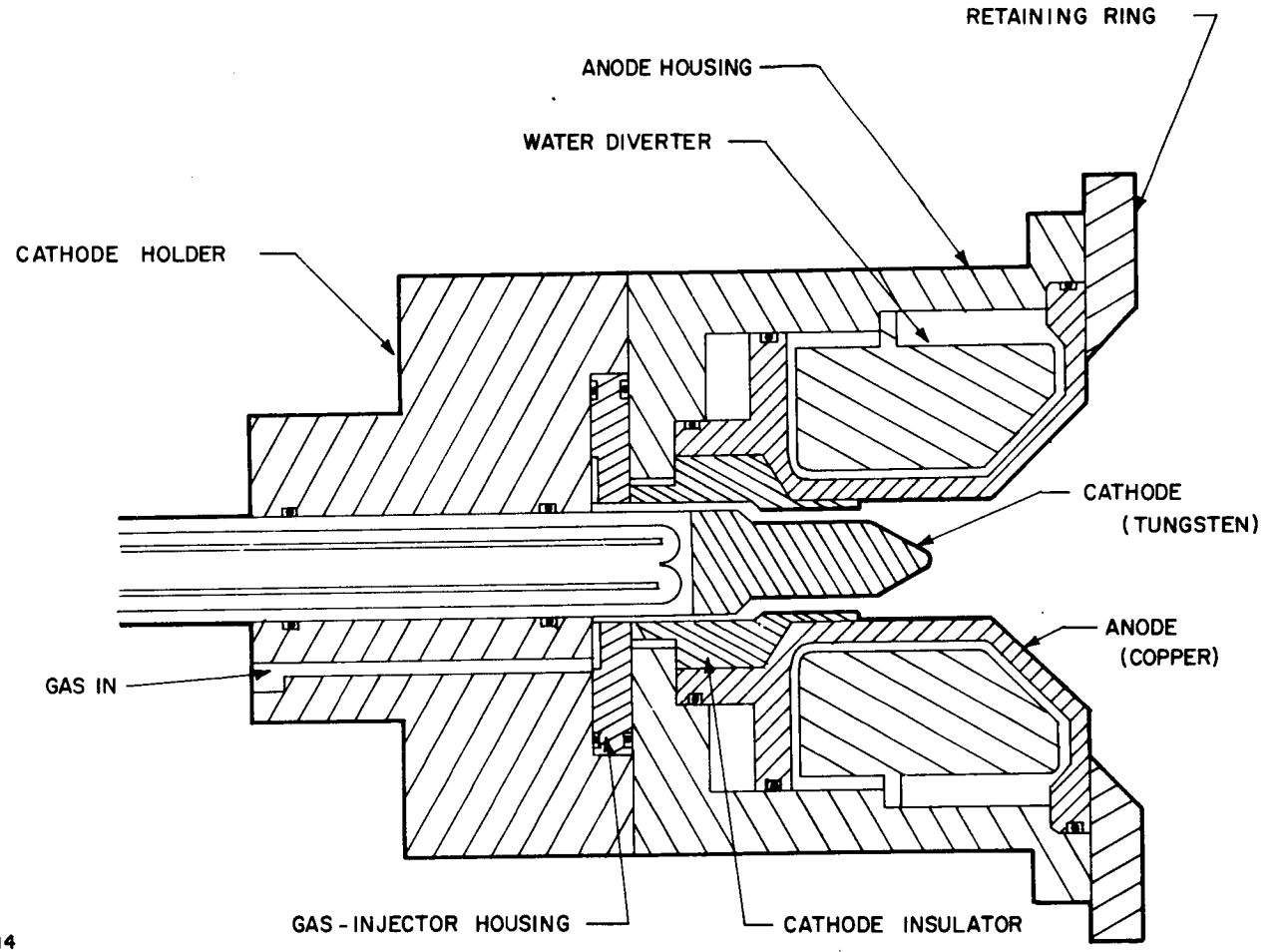

Figure 3 SCHEMATIC DRAWING OF THE MPD CONFIGURATION X-7C USED FOR TESTS OF SENSITIVITY OF PERFORMANCE TO CONFIGURATION

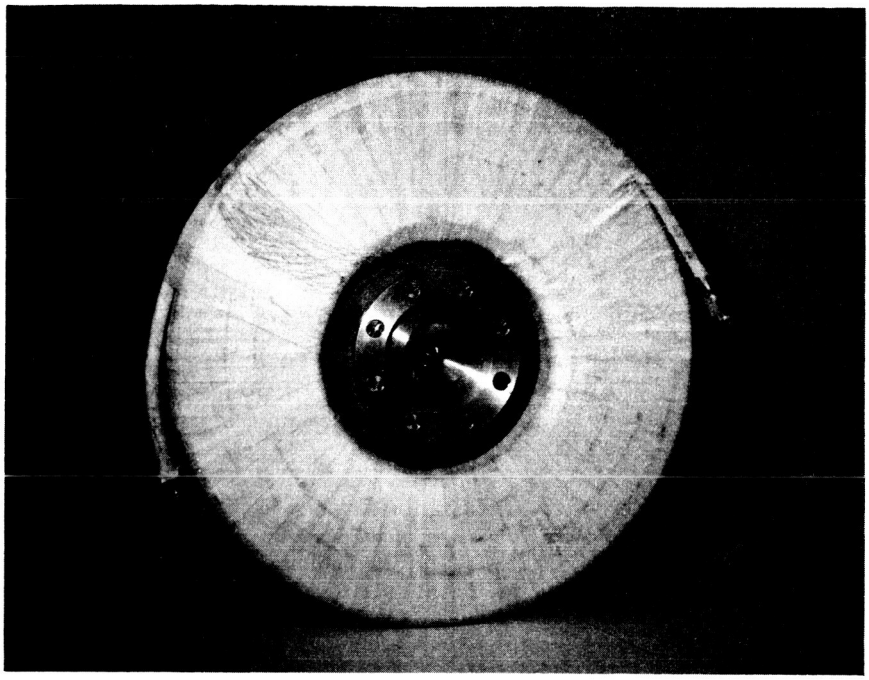

Figure 4: Photograph of X-7C MPD Thrustor

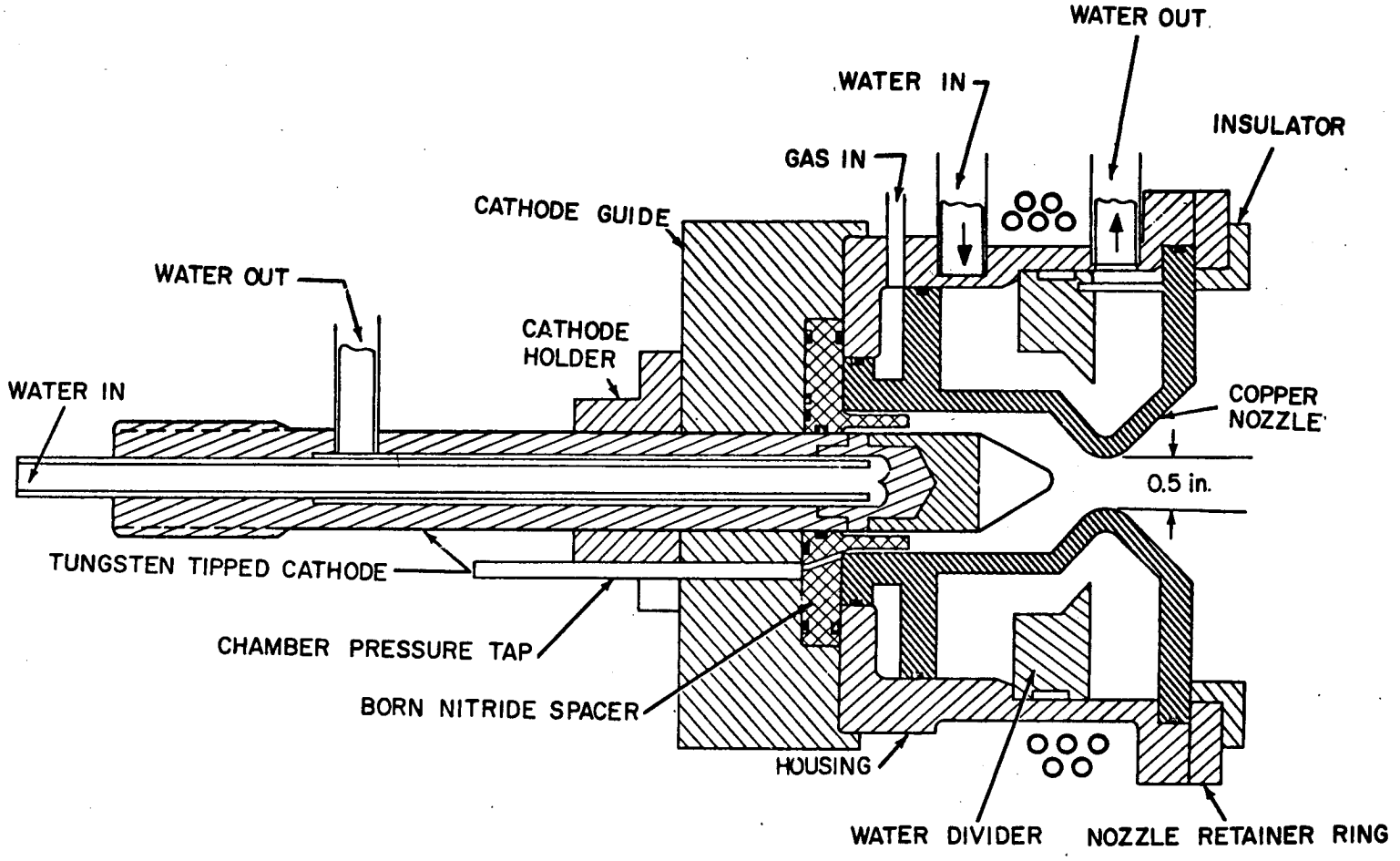

Figure 5: Schematic Drawing of the X-2C MPD Thrustor

Figure 6: Anode Voltage versus Arc Current for X-7C-4 Engine

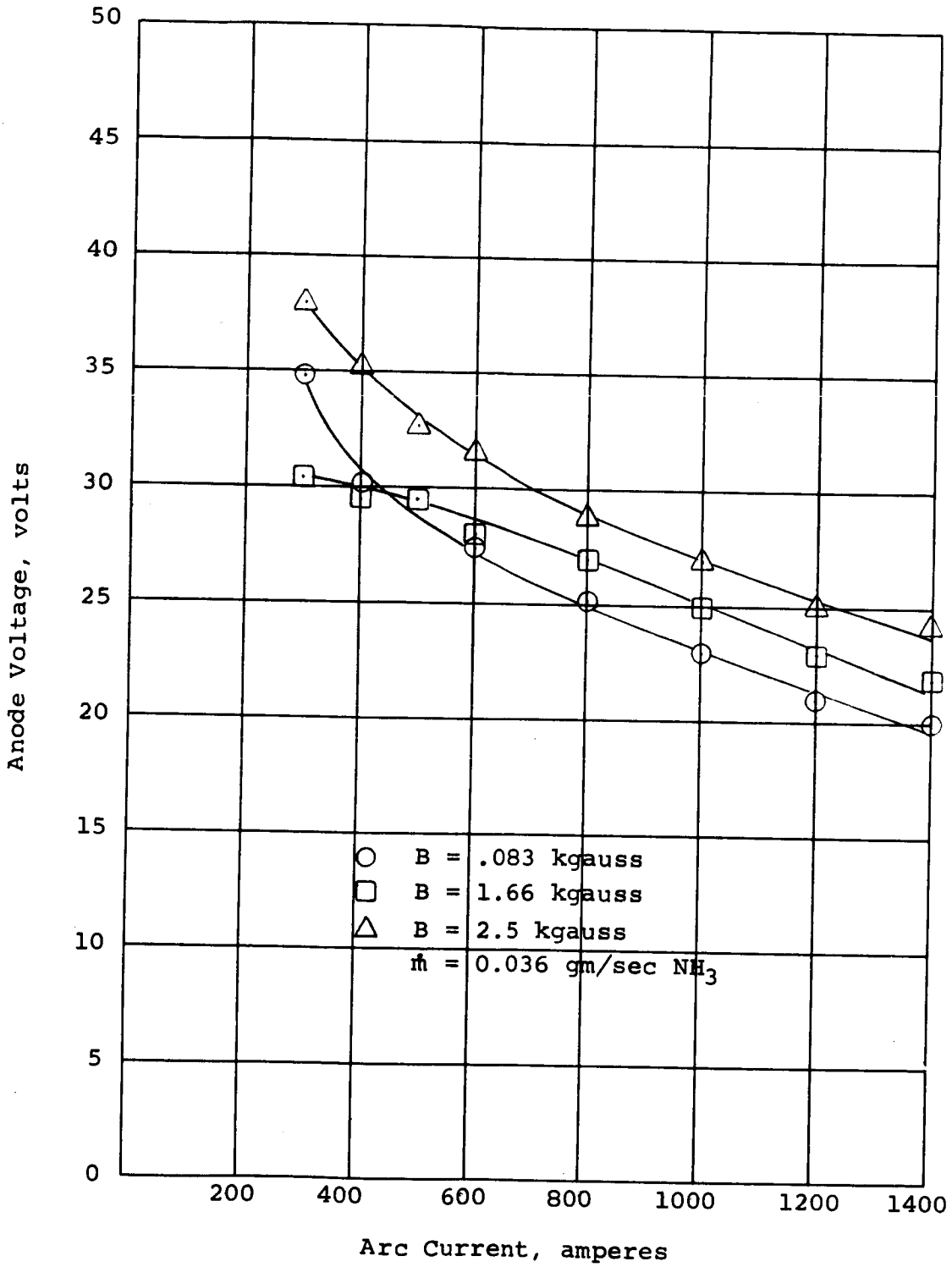

Figure 7: Arc Voltage versus Arc Current for X-7C-4 Engine

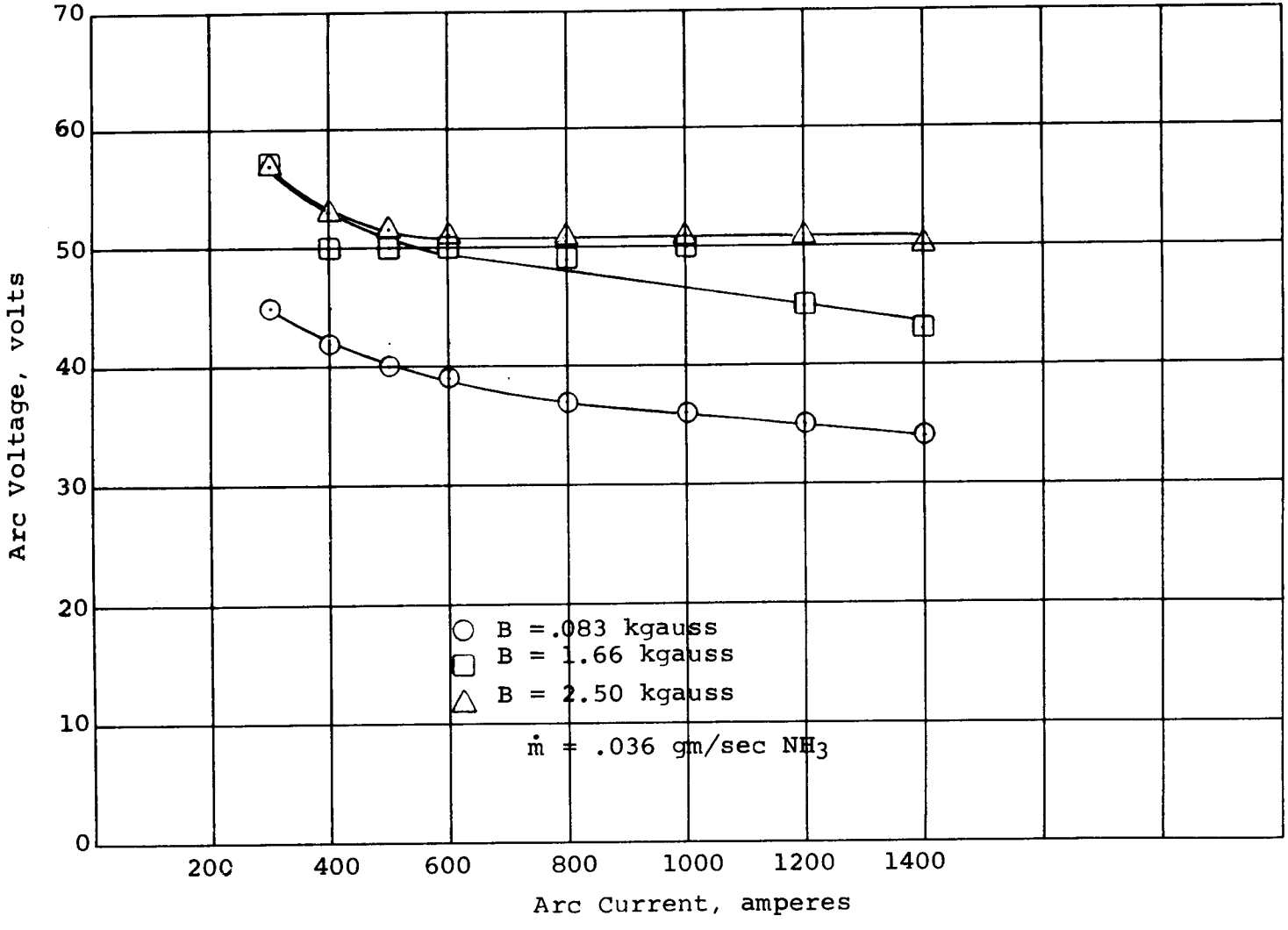

Figure 8: Thermal Efficiency versus Arc Current for X-7C-4 Engine

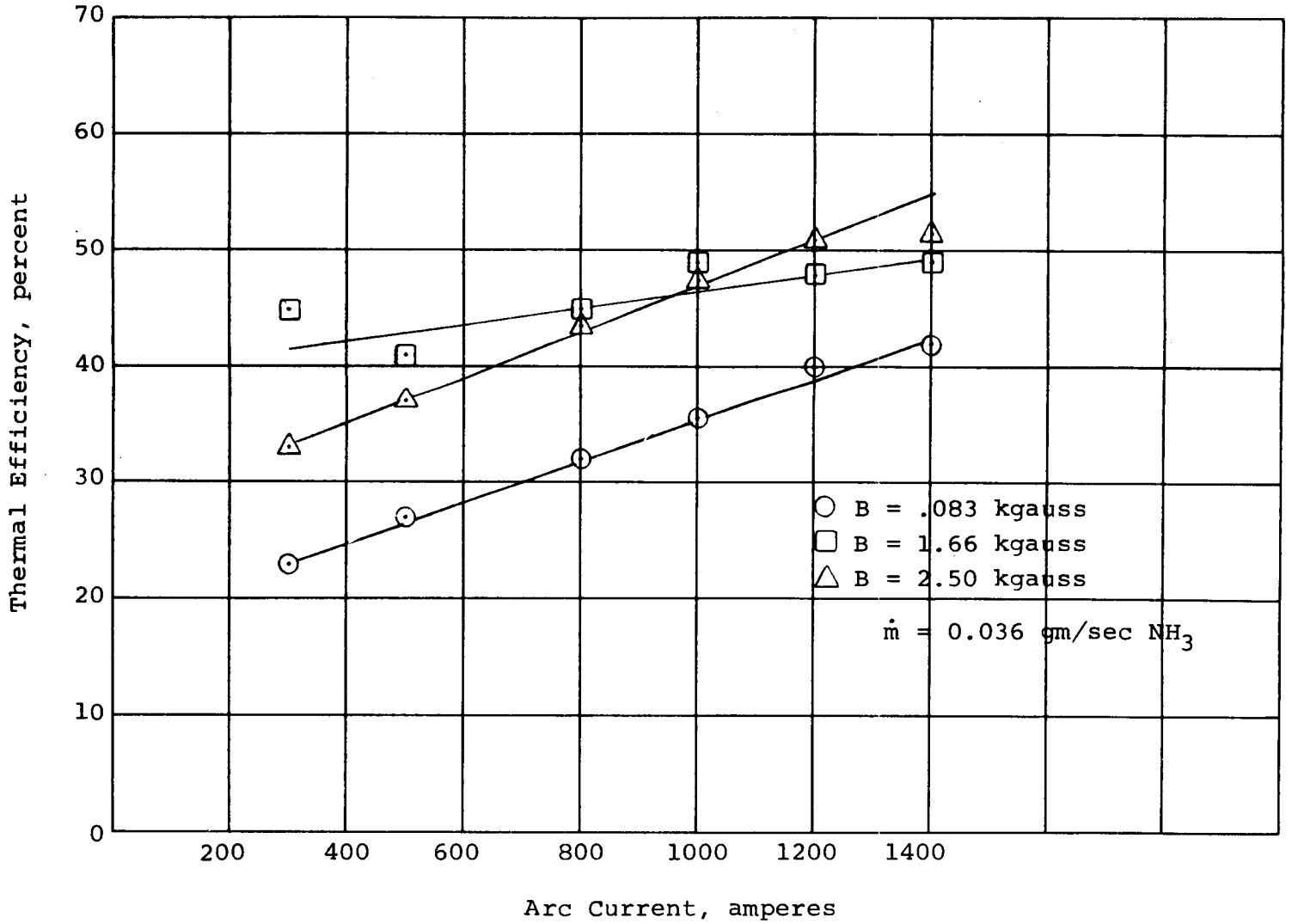

Figure 9: Thrust Efficiency versus Specific Impulse for X-7C-Engines

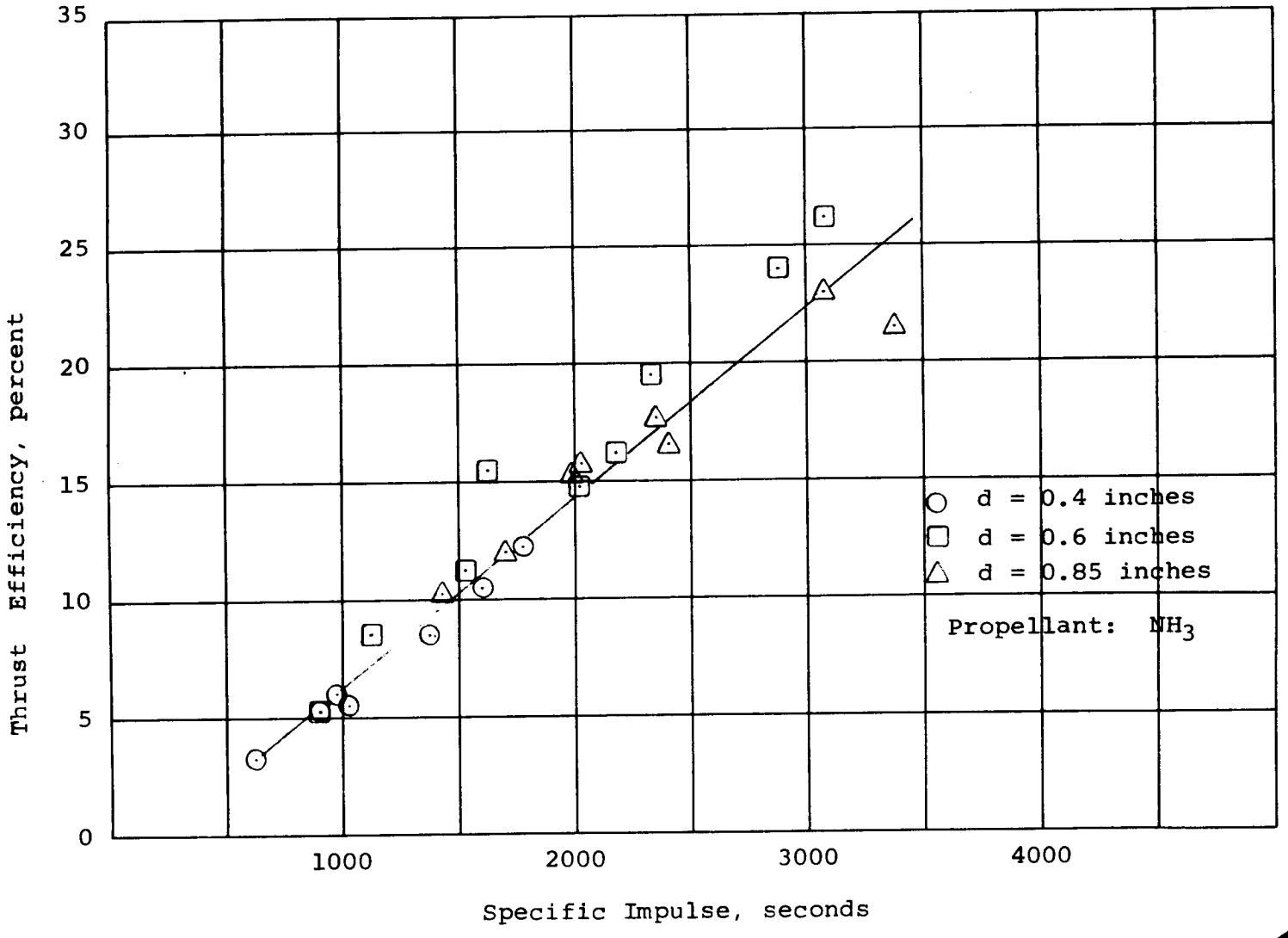

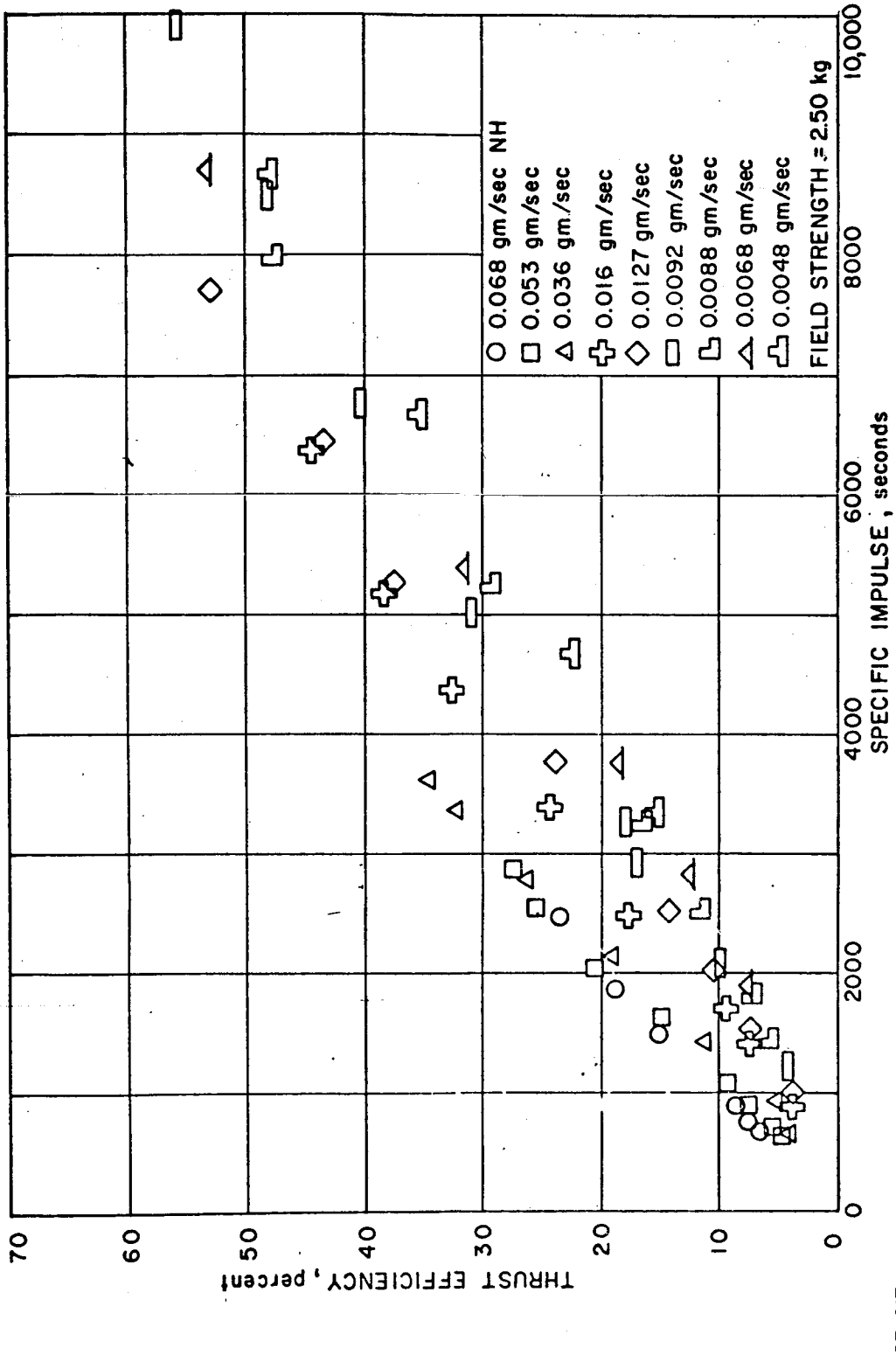

Figure 10: Thrust Efficiency versus Specific Impulse for X-2C Engine B = 2.50 kgauss

Figure 11: Thrust Efficiency versus Specific Impulse for X-2C Engine B = 0.83 kilogauss

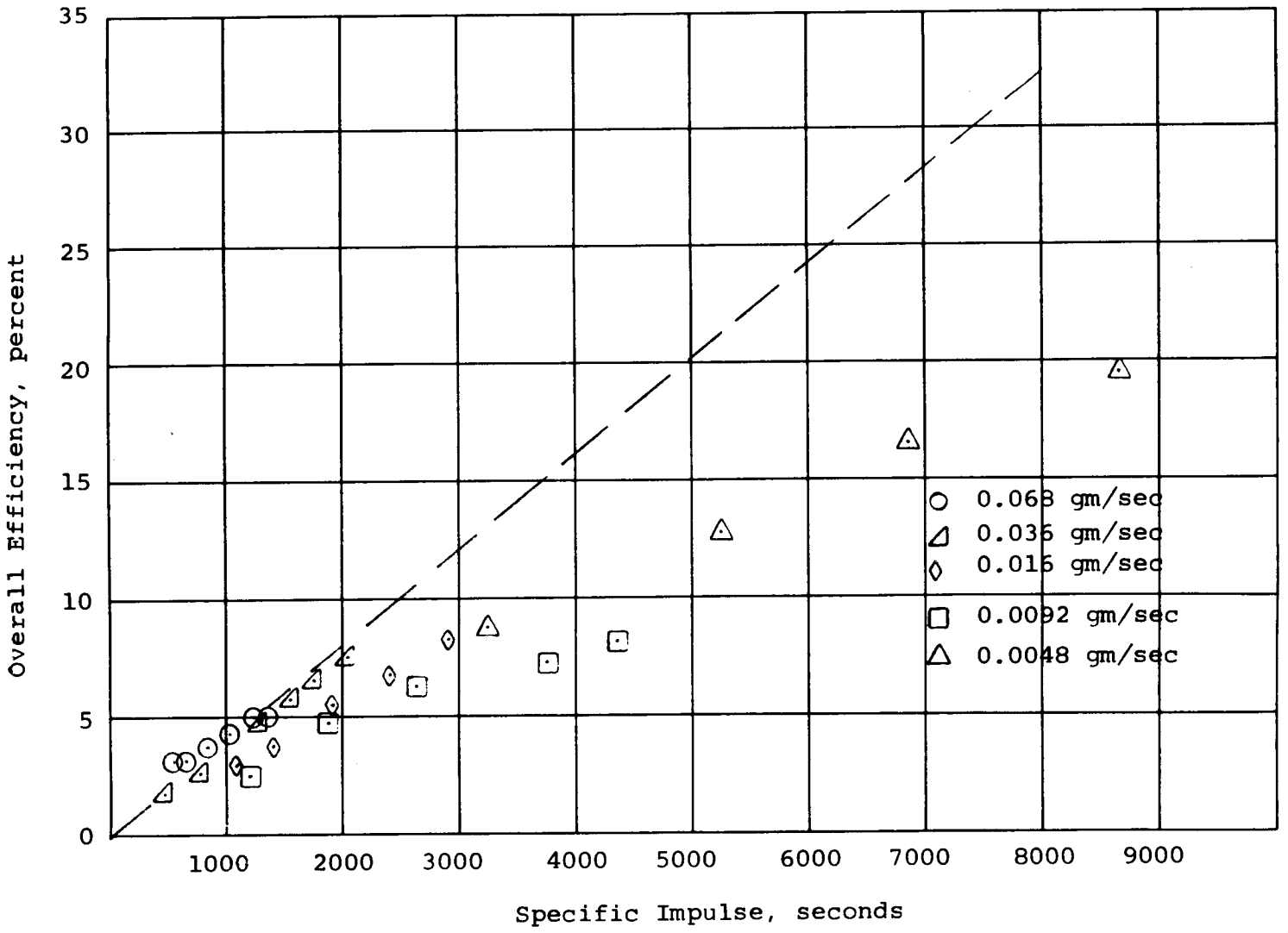

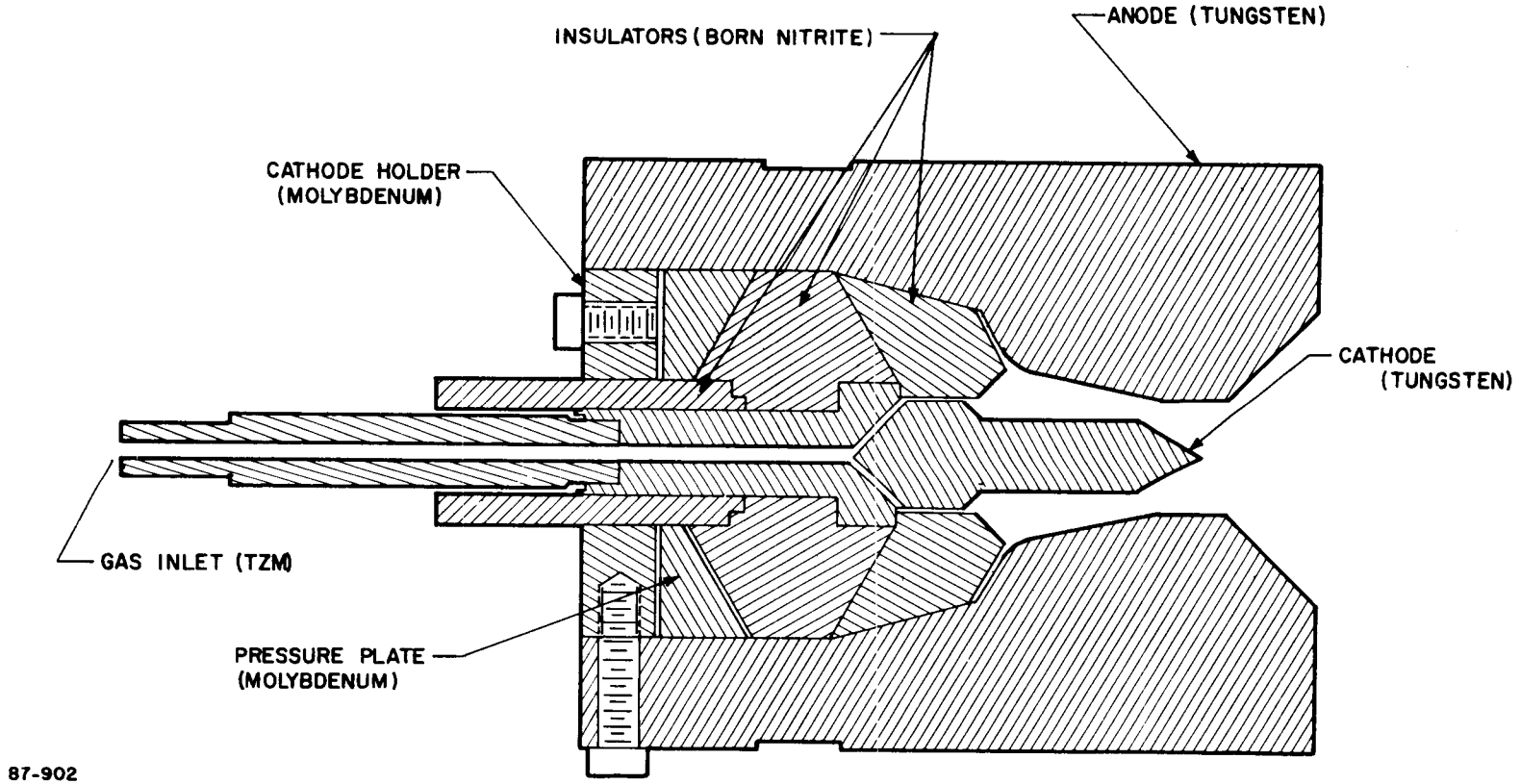

Figure 12 SCHEMATIC DRAWING OF X-7CR MPD RADIATION COOLED THRUSTOR

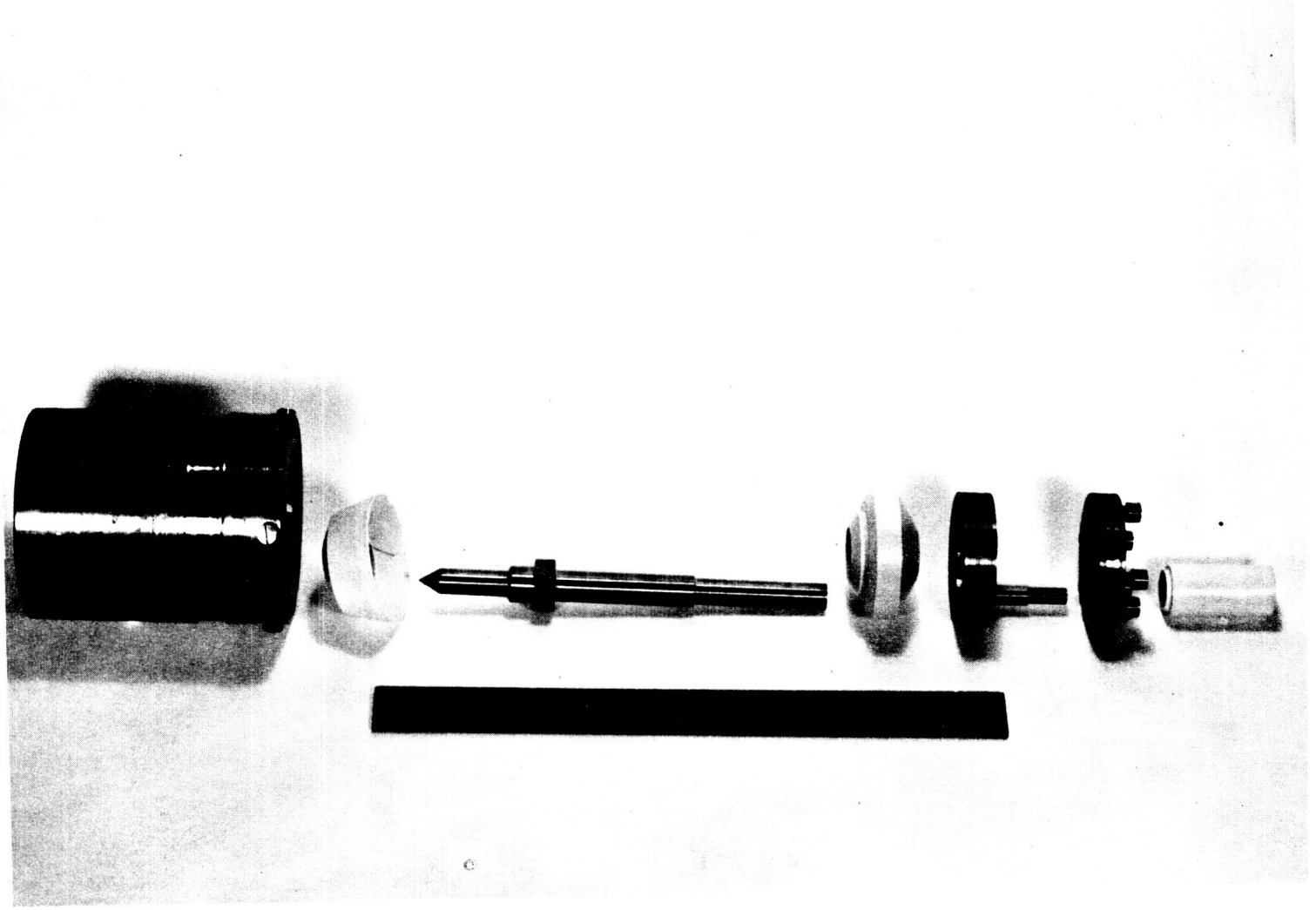

Figure 13: Photograph of X-7C-R MPD Thrustor Disassembled

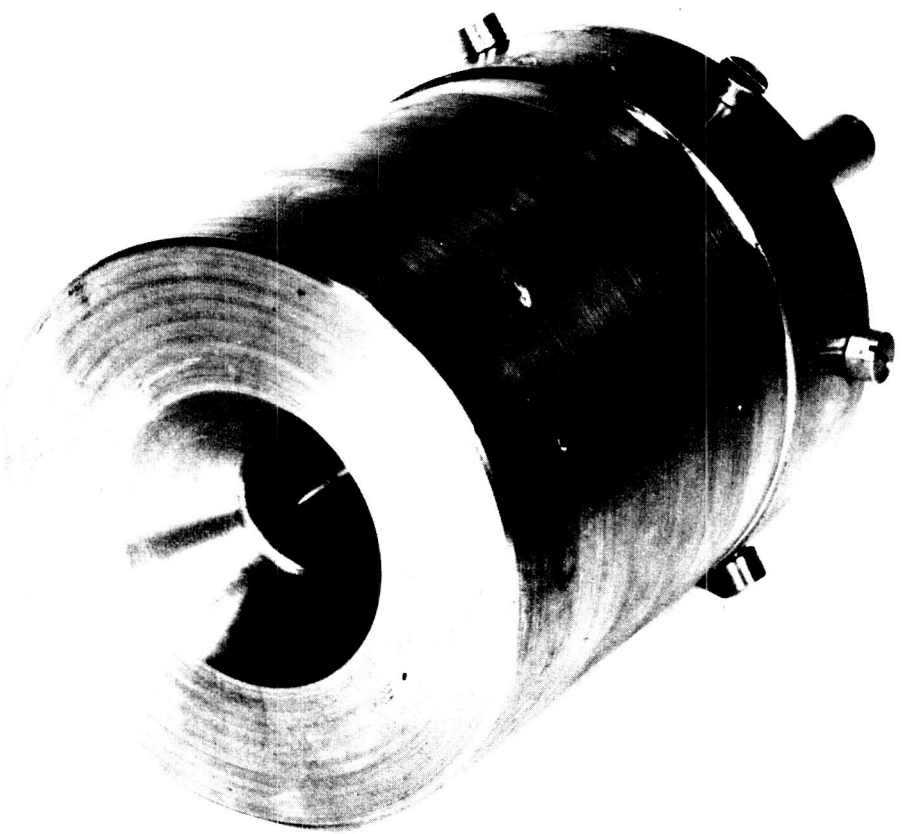

Figure 14: X-7C-R MPD Thrustor Assembled

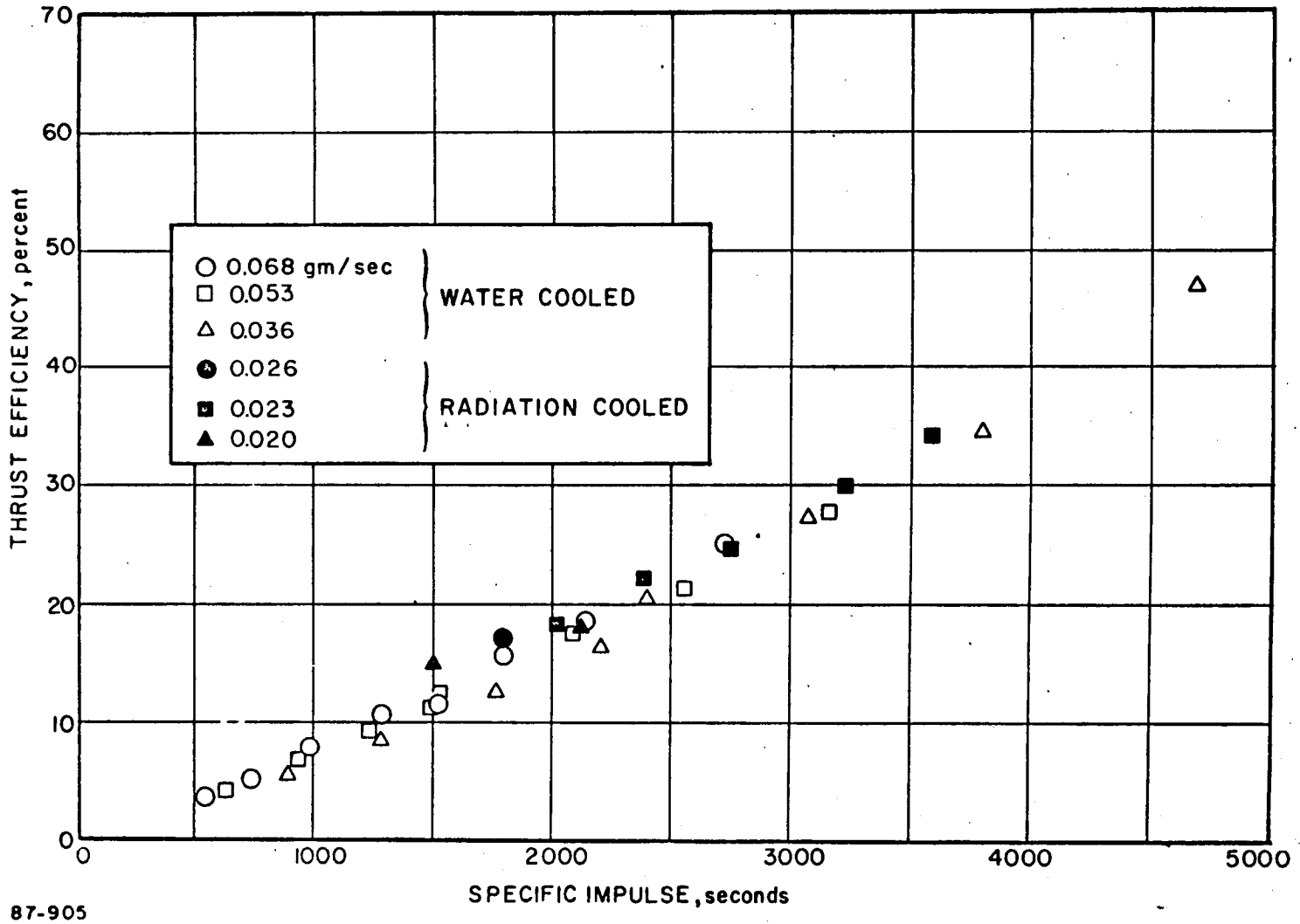

Figure 15: Comparison of Measured Efficiency of 4-inch Diameter Water-Cooled and Radiation-Cooled MPD Thrustor

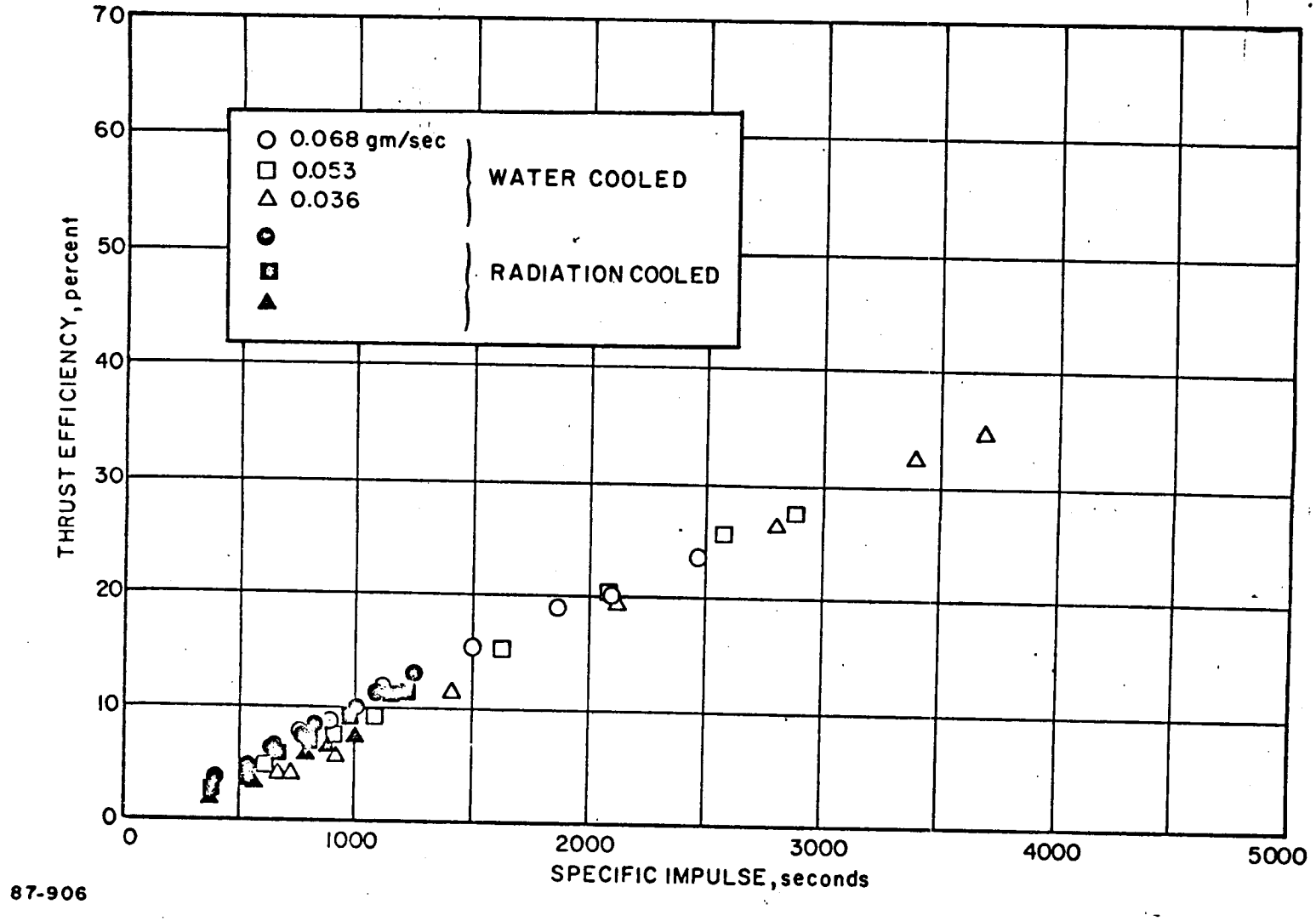

Figure 16: Comparison of Measured Efficiency of 3-inch Diameter Water-Cooled and Radiation-Cooled MPD Thrustor

Figure 17: Arc Voltage versus Current for the 3-inch Diameter Water-Cooled and Radiation Cooled Thrustor

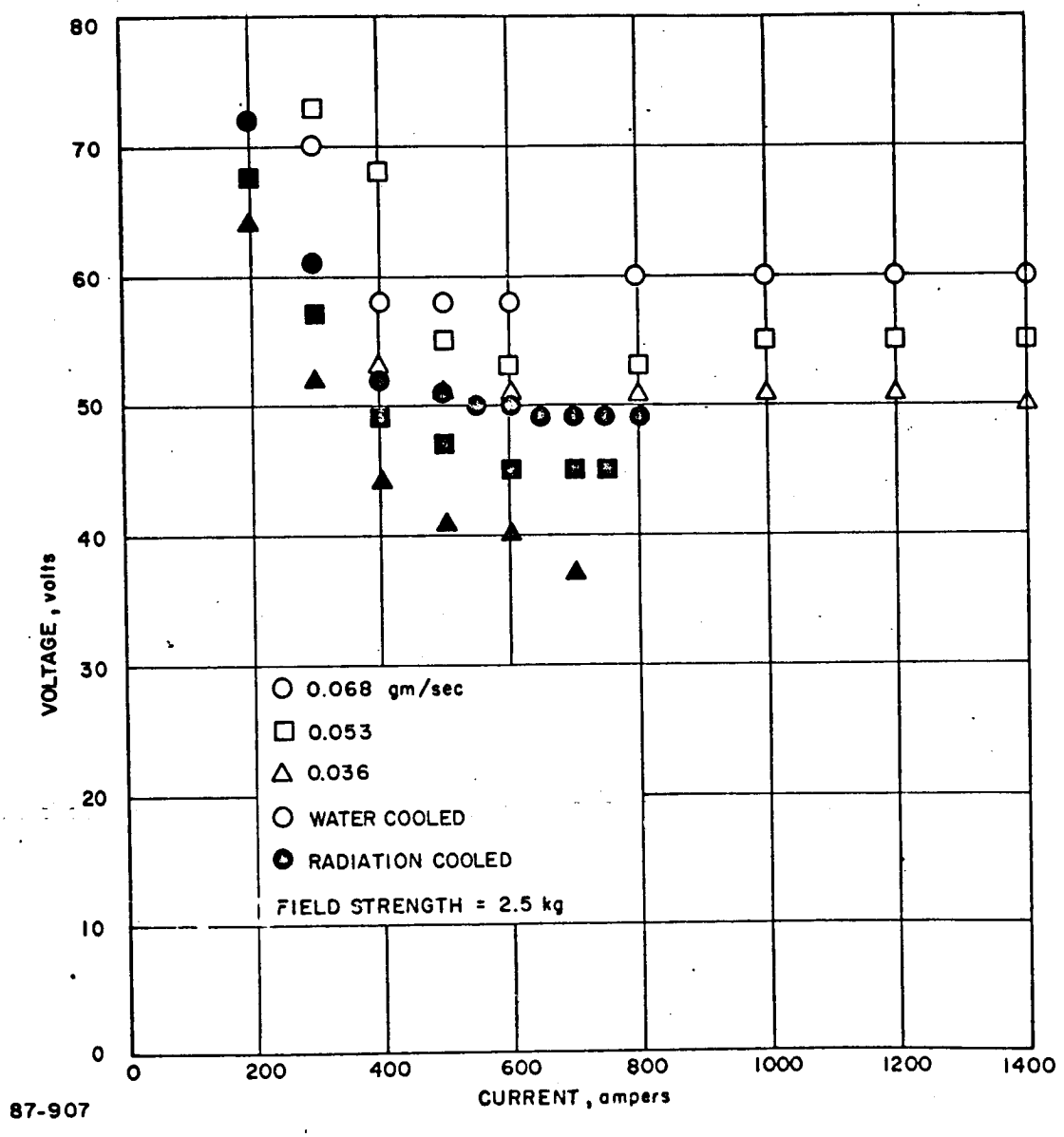

Figure 18: Measured Surface Temperature versus Power for Radiation Cooled Thrustors

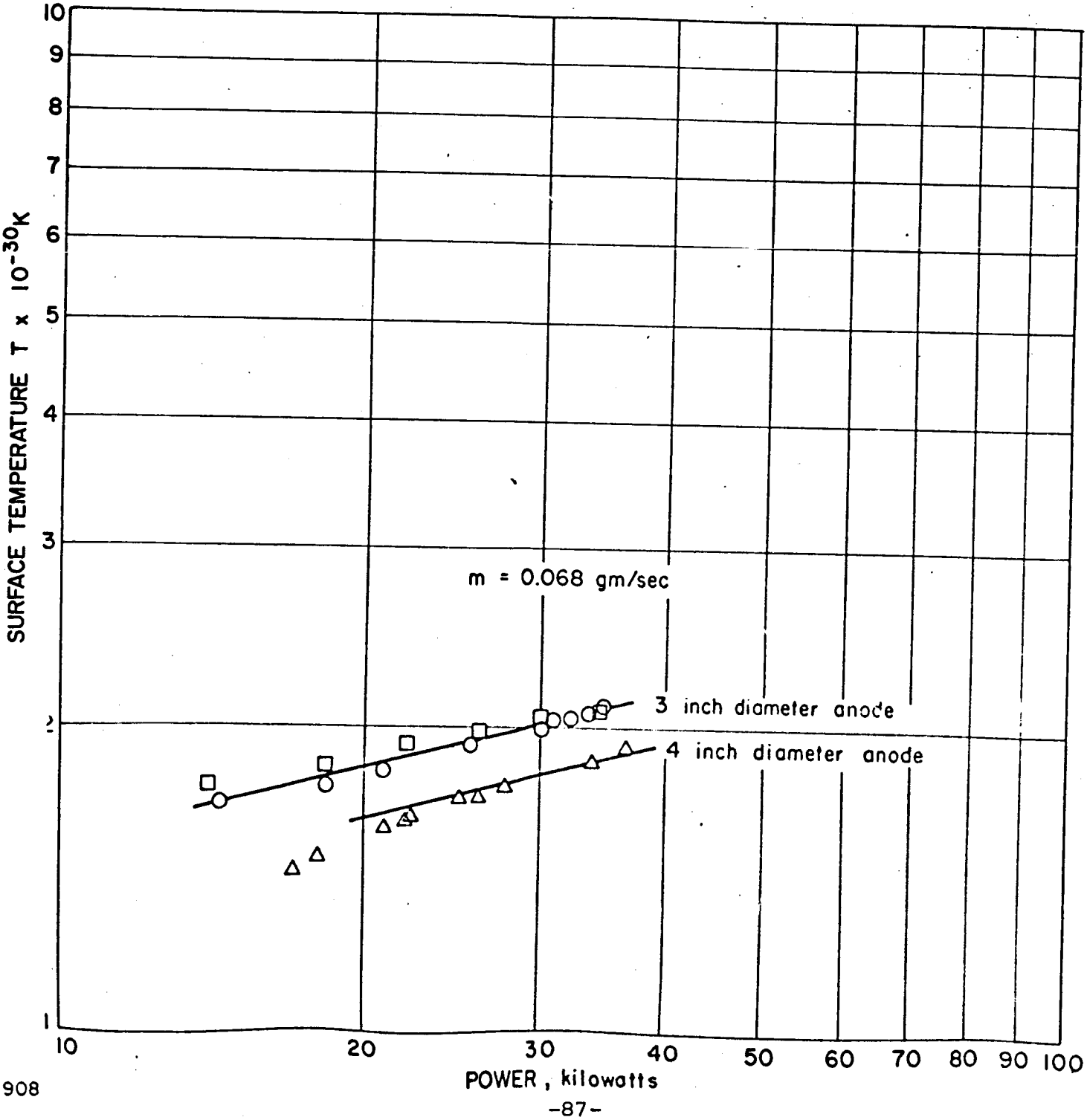

7-908

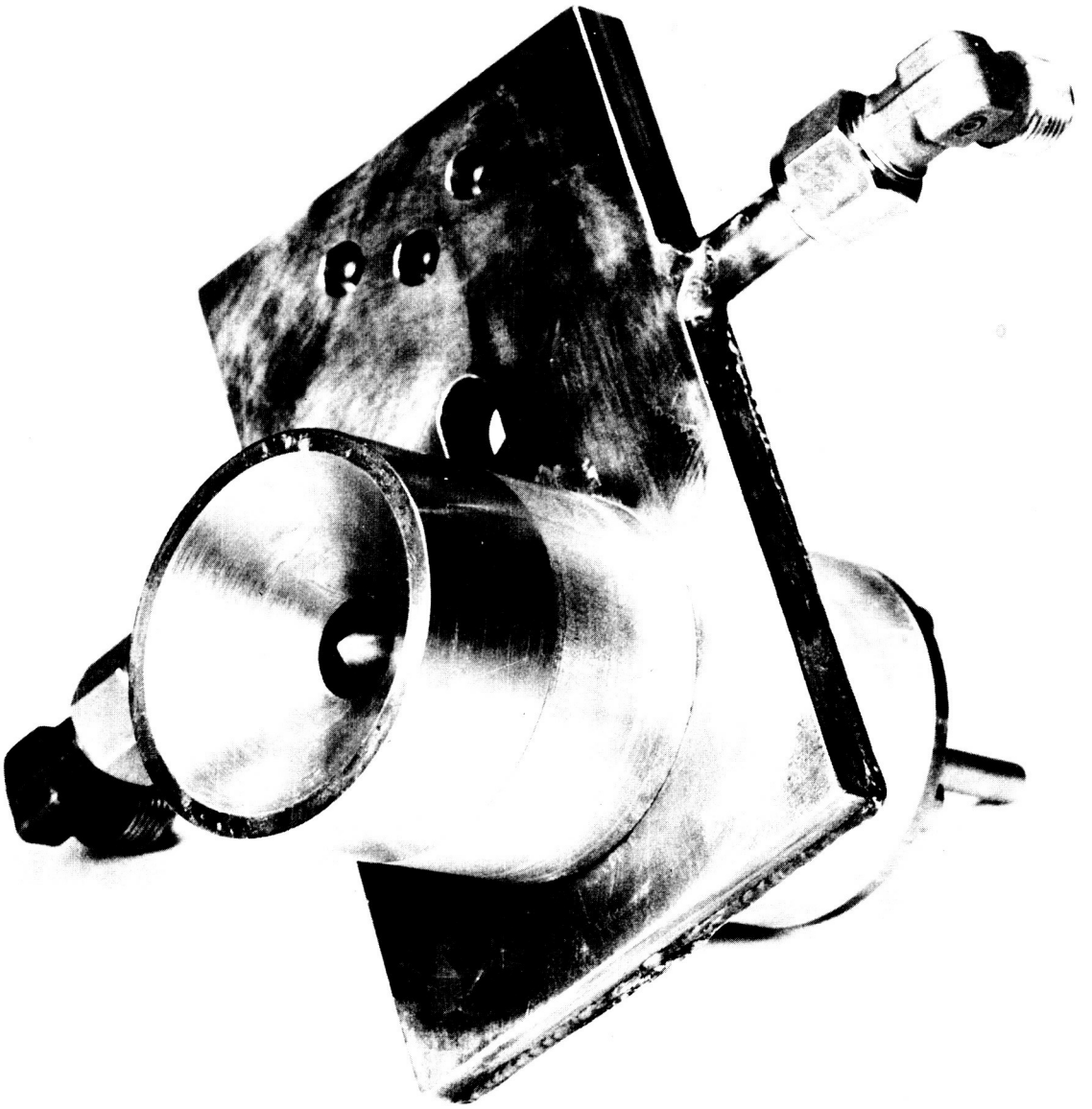

87-909

Figure 19 PHOTOGRAPH OF RADIATION COOLED ALKALI METAL MPD ARCJET MODEL L-2

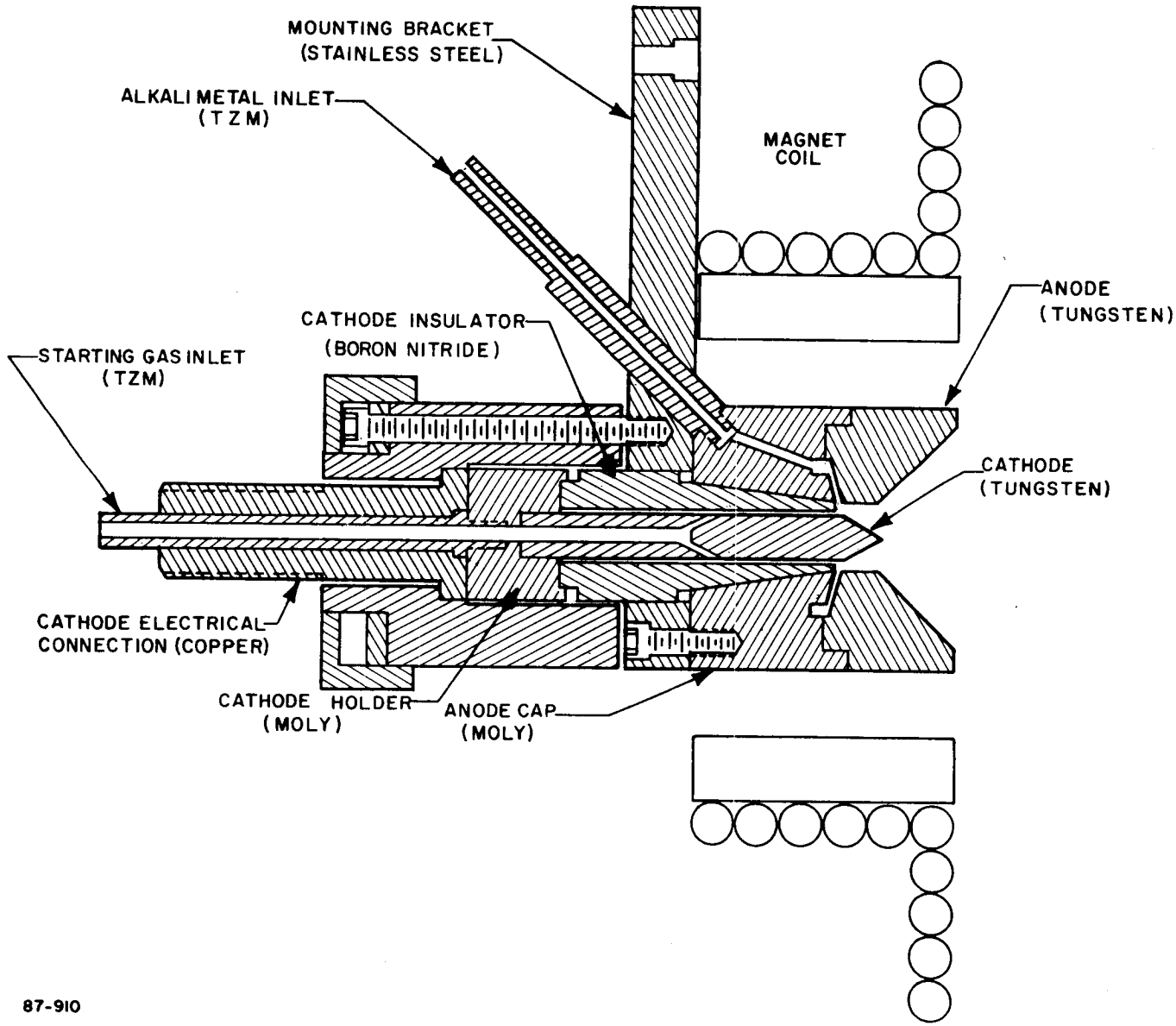

Figure 20 SCHEMATIC OF RADIATION COOLED ALKALI METAL MPD ARCJET MODEL L-2

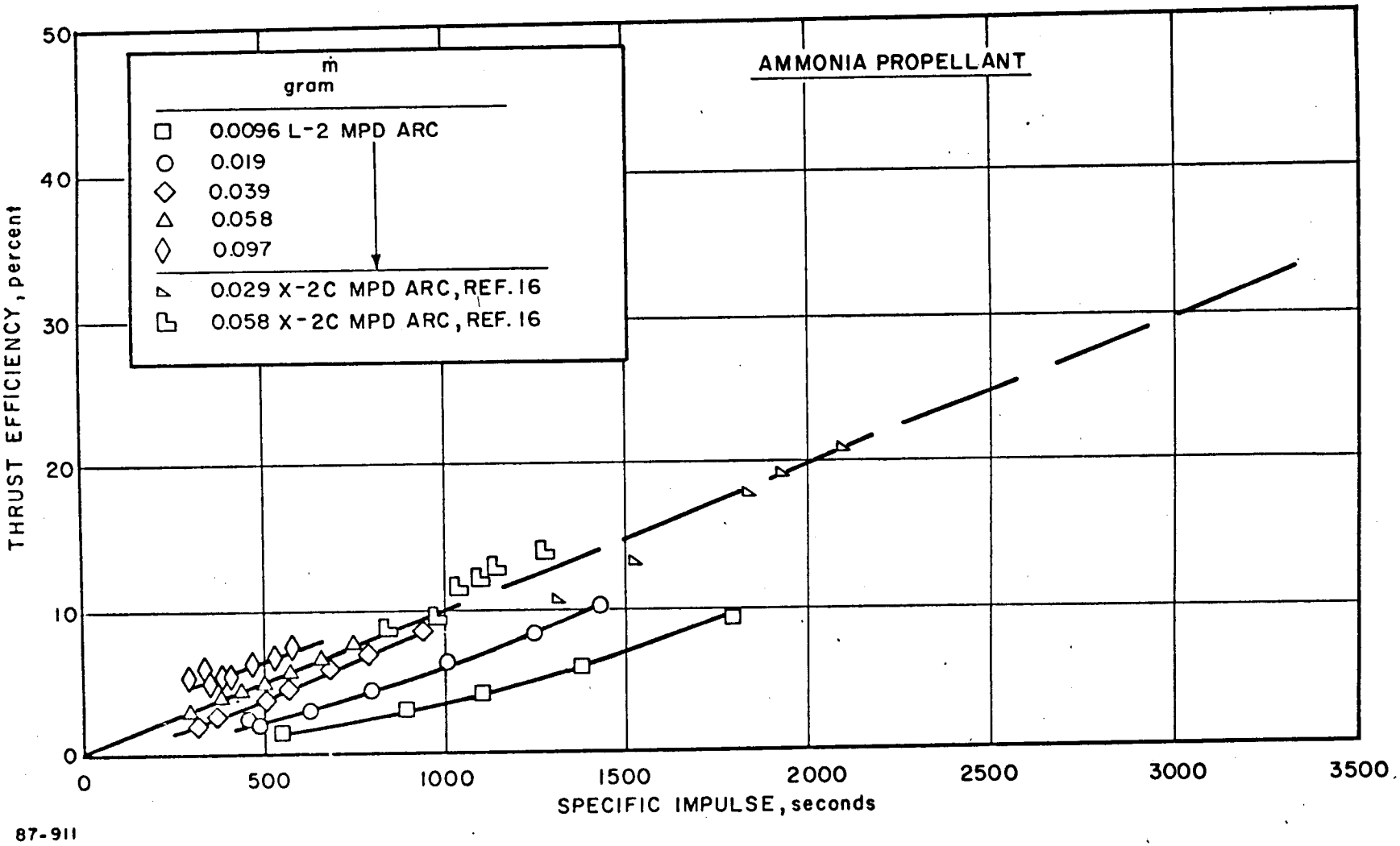

Figure 21: Thrust Efficiency versus Specific Impulse for the Model L-2 Thrustor

Figure 22: Anode Diameter versus Maximum Power for Radiation Cooled MPD Thrustors

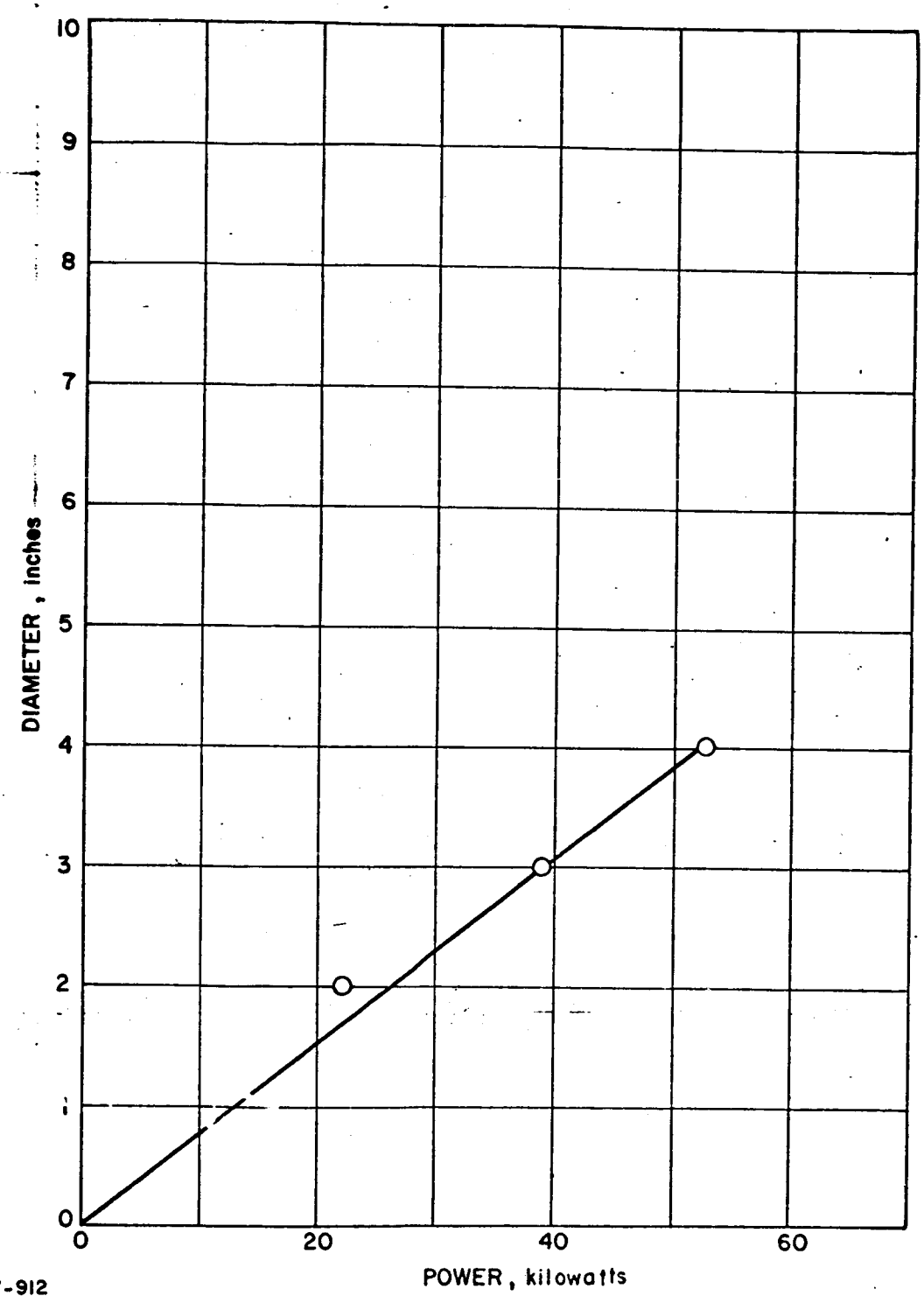

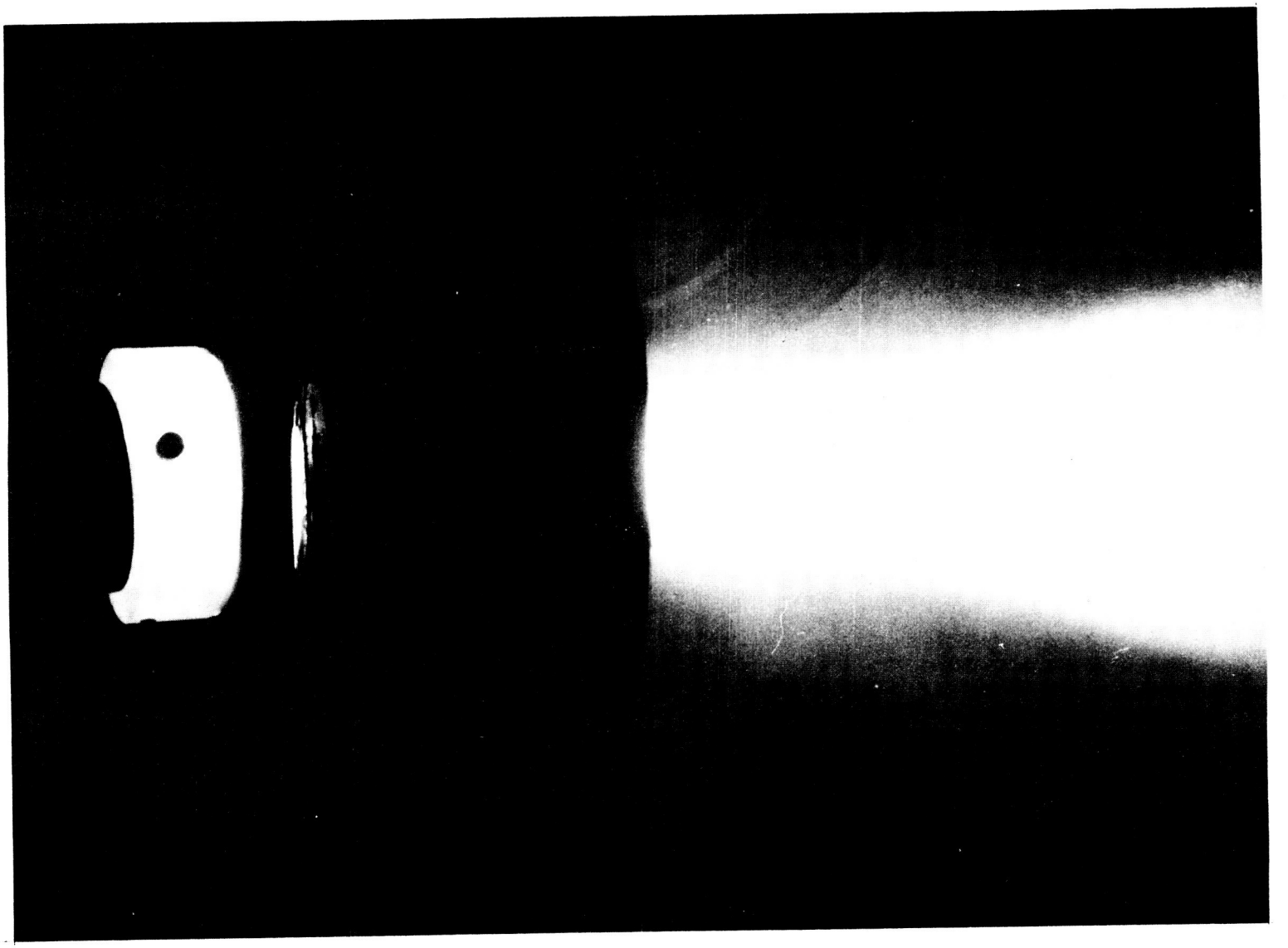

Figure 23: Photograph of X-7C-R MPD Thrustor During 75-Hour Life Test

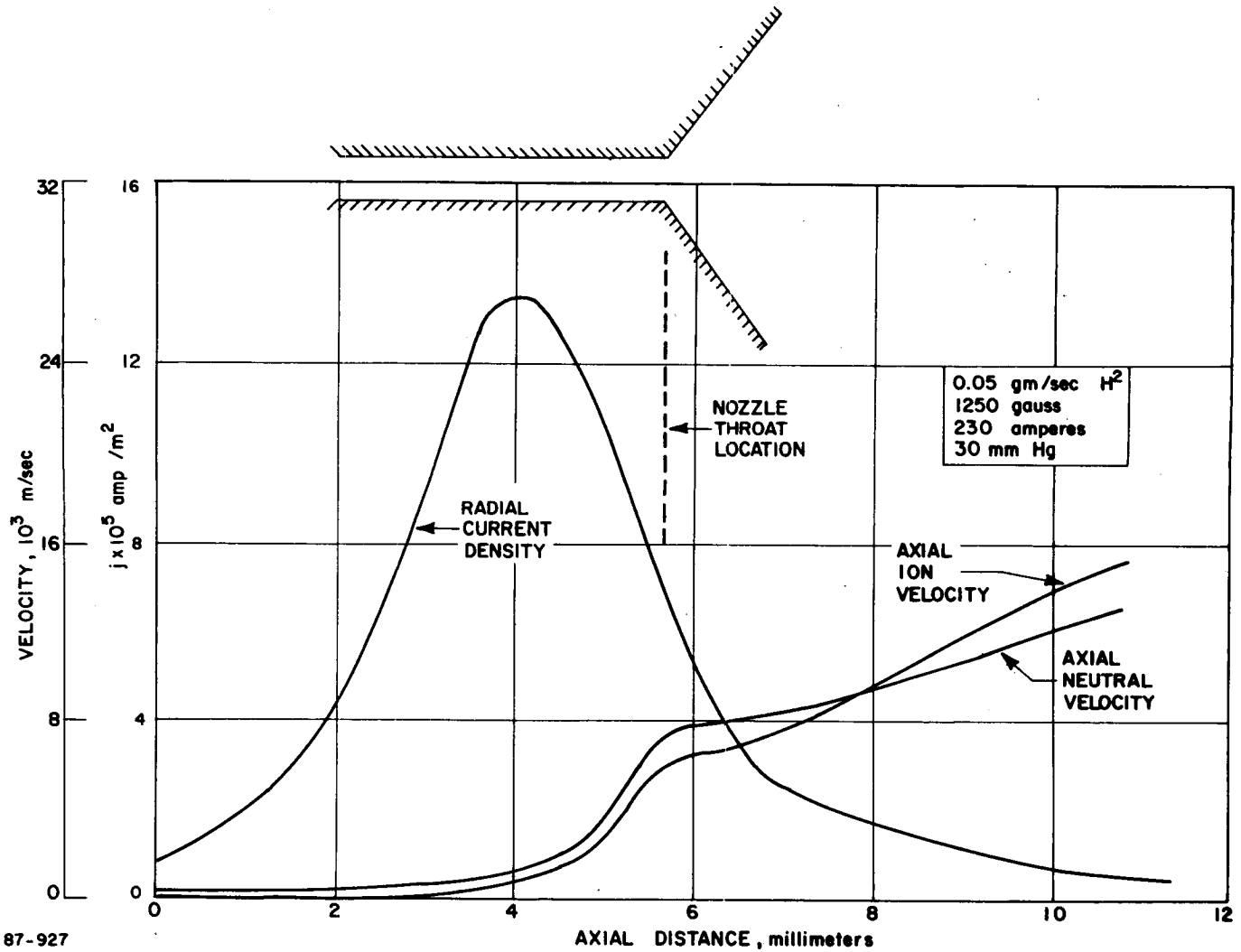

Figure 24 CALCULATED CURRENT DENSITY AND VELOCITY DISTRIBUTION FOR THE MPD ARC DISCHARGE

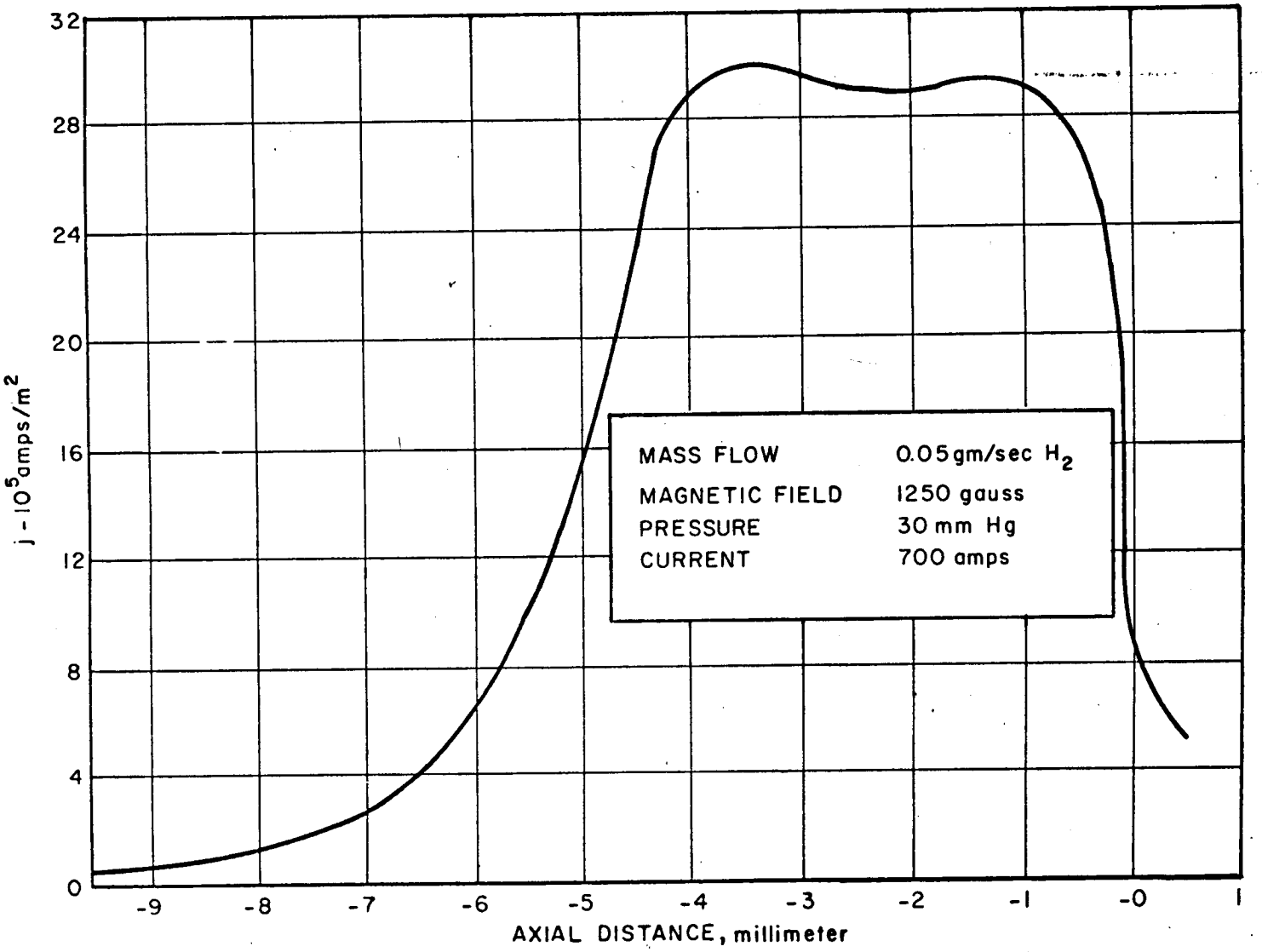

Figure 25: Calculated Current Density Distribution for High-Current Discharge

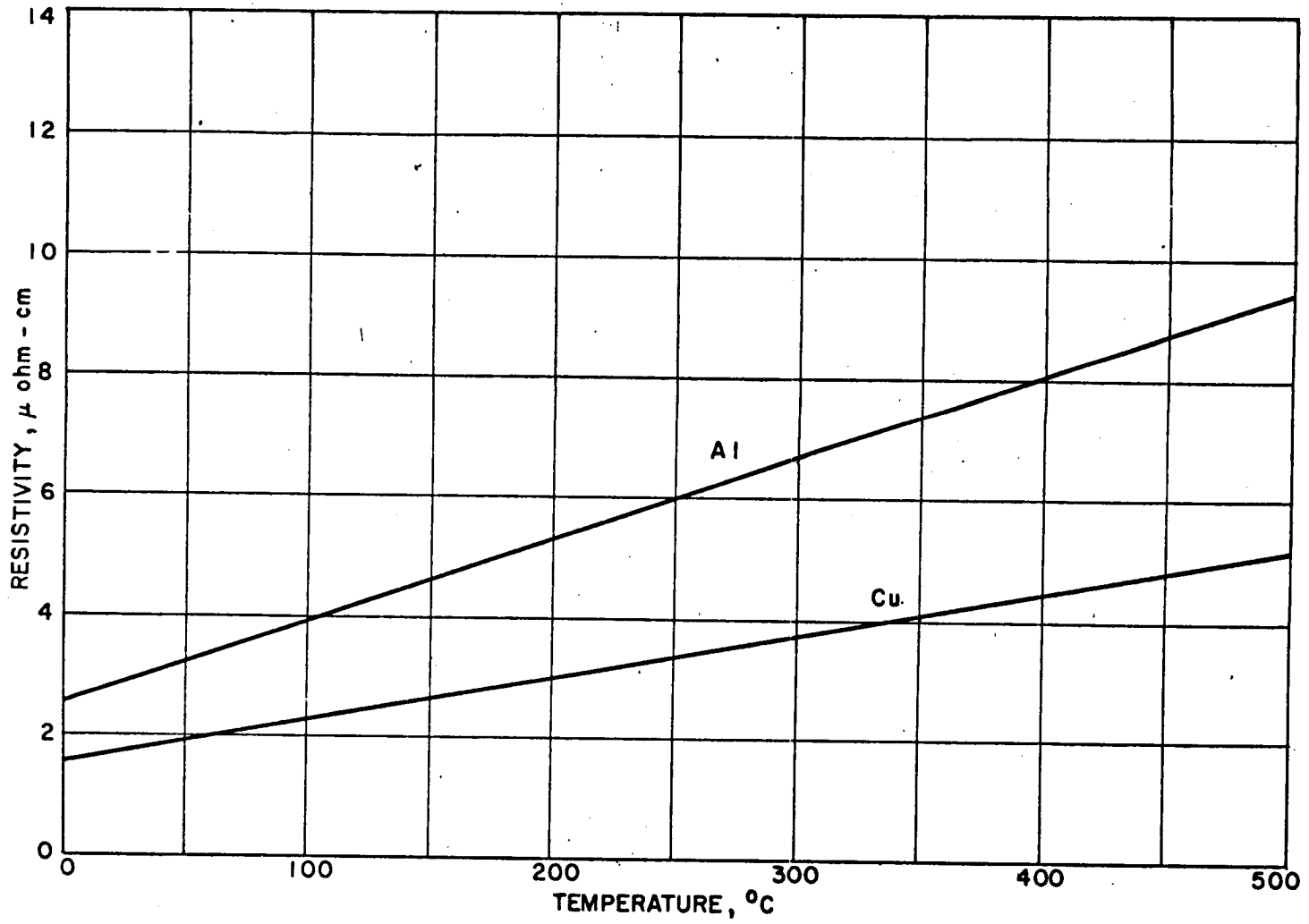

87-929

Figure 26: Resistivity versus Temperature for Copper and Aluminum

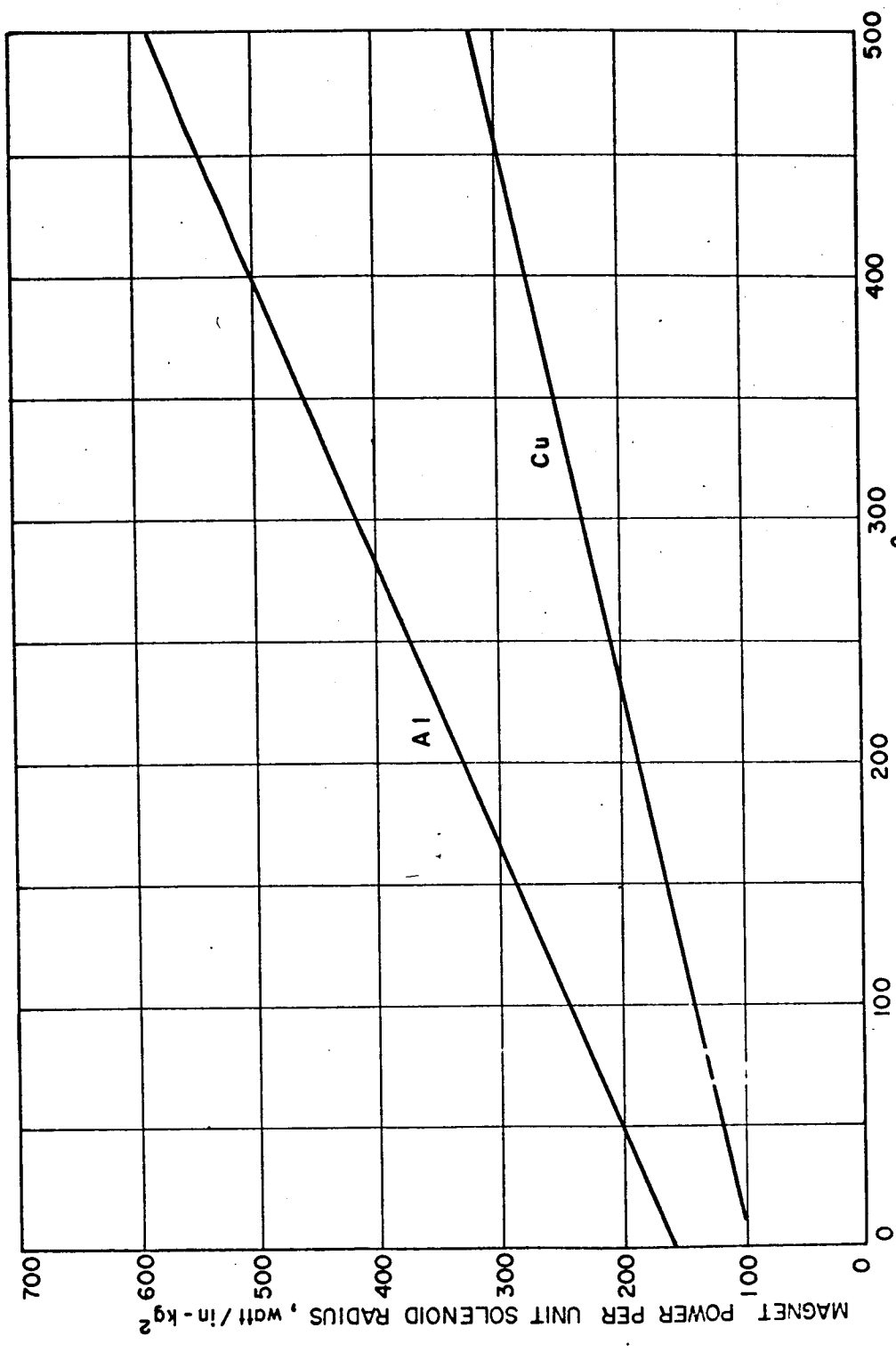

87-930

Figure 27: Normalized Magnet Power versus Temperature

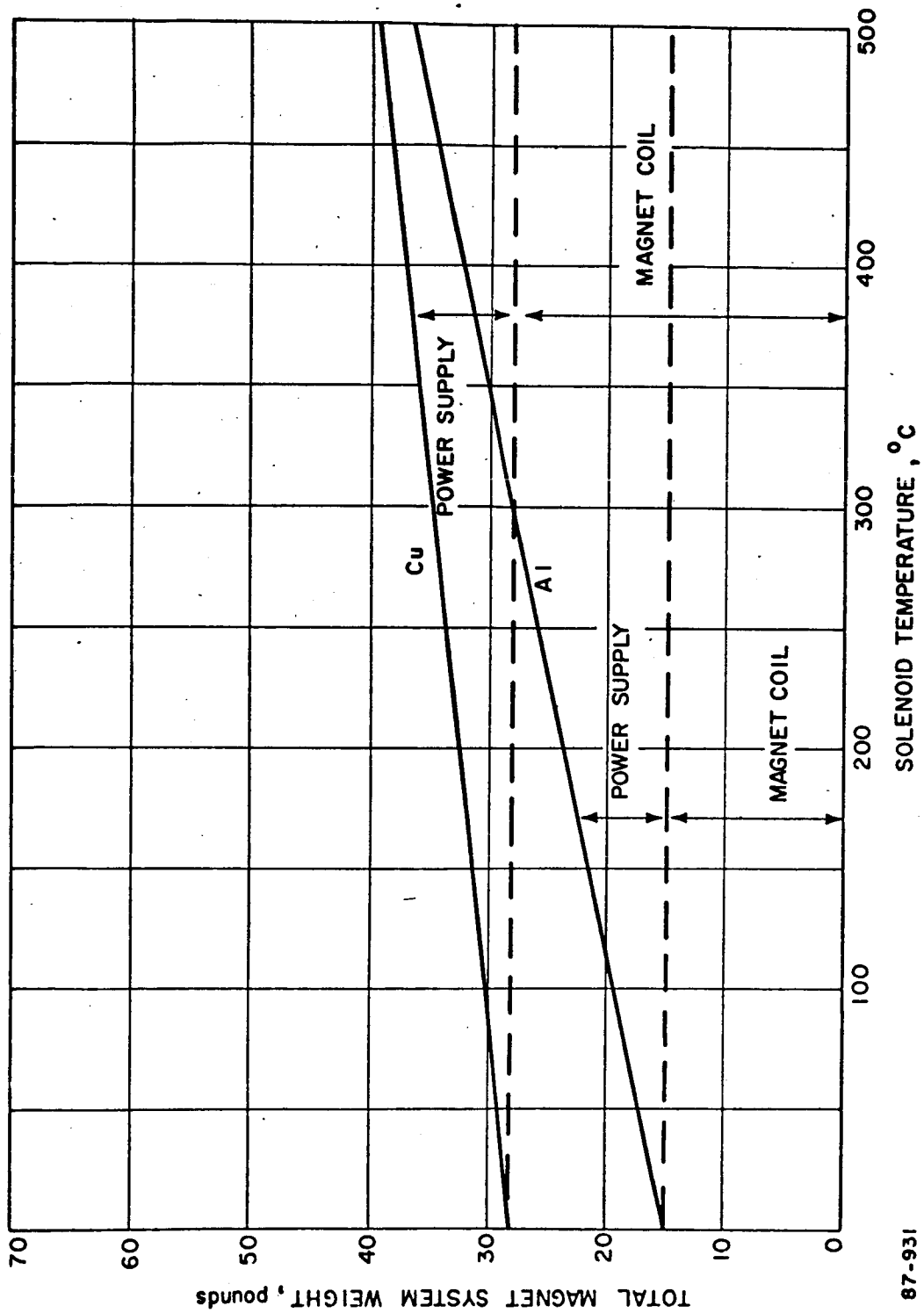

Figure 28: Total Magnet System Weight versus Solenoid Temperature

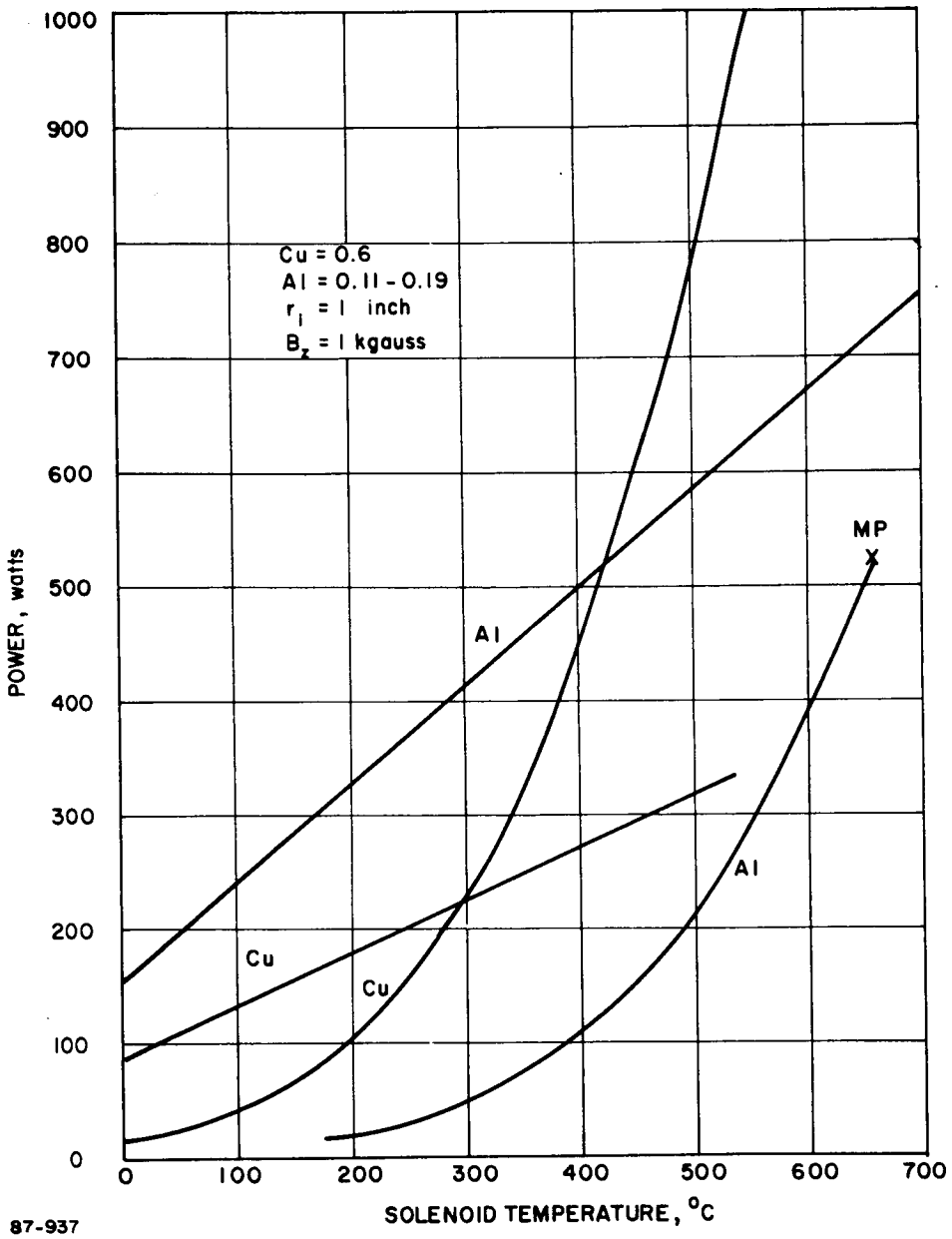

Figure 29 MAGNET POWER VERSUS TEMPERATURE

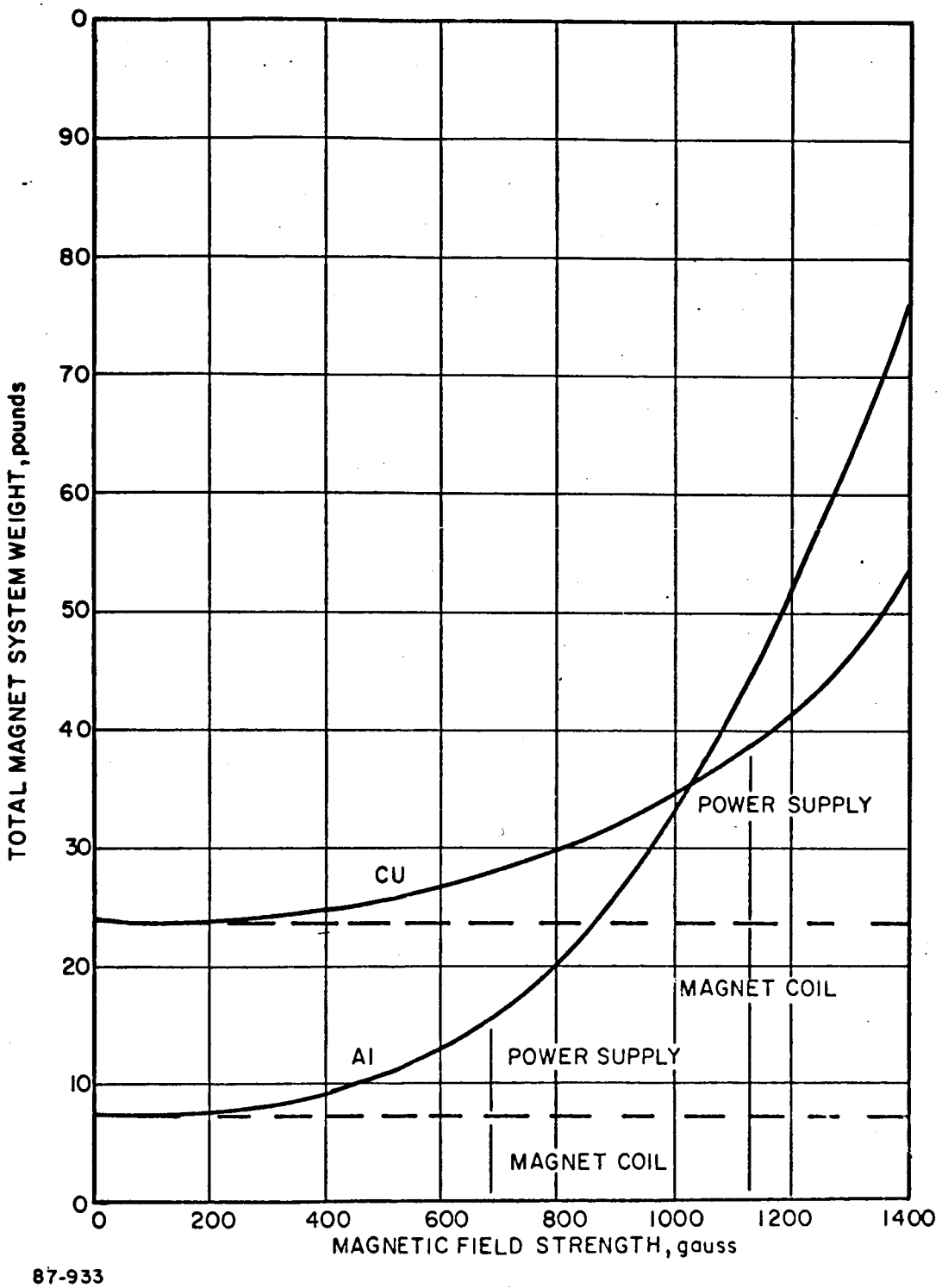

Figure 30: Magnet System Weight versus Magnetic Field Strength

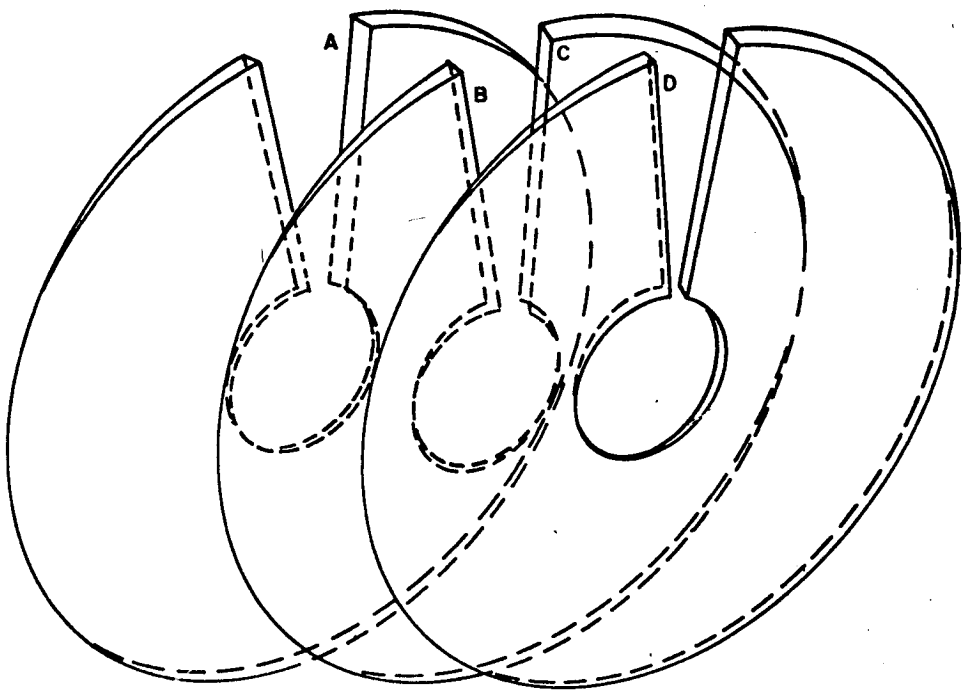

Figure 31: Fabrication of Bitter Solenoid

DISTRIBUTION

Addressee	No. of Copies
National Aeronautics and Space Administration Washington, D. C. 20546	
Attn: RNT/James Lazar	1
RRP/Dr. K. H. Thom	1
RNT/J. Mullin	1
NASA-Lewis Research Center 21000 Brookpark Road Cleveland, Ohio 44135	
Attn: Spacecraft Technology Procurement Section (M.S. 54-2)	1
Technology Utilization Office (M.S. 3-19)	1
Technical Information Division (M.S. 5-5)	1
Library (M.S. 60-3)	2
Spacecraft Technology Division	
C. C. Conger (M.S. 54-1)	1
H. Hunczak (M.S. 54-3	1
S. Domitz (M.S. 54-3	9
E. W. Otto (M.S. 54-1)	1
Electric Propulsion Laboratory (M.S. 301-1	
W. Moeckel	1
G. Seikel	1
D. Connolly	1
Report Control Office (M.S. 5-5)	1
NASA Scientific and Technical Information Facility P.O. Box 33 College Park, Maryland 20740	
Attn: NASA Representative RQT-2448	6
NASA-Marshall Space Flight Center Huntsville, Alabama 35812	
Attn: Ernest Stuhlinger (M-RP-DIR)	1
Research and Technology Division Wright-Patterson AFB, Ohio 45433	
Attn: AFAPL (APIE-2)/P. Lindquist	1
Jet Propulsion Laboratory 4800 Oak Grove Drive Pasadena, California 91103	
Attn: J. J. Paulson	1

Addressee	No. of Copies
Electro-Optical Systems, Inc. 300 North Halstead Street Pasadena, California 91107 Attn: G. L. Cann	1
General Dynamics/Convair P.O. Box 1128 San Diego, California 92112 Attn: Dr. A. V. Larson	1
NASA-Ames Research Center Moffett Field, California 94035 Attn: G. Goodwin	1
Princeton University Forrestal Research Center Princeton, New Jersey 08540 Attn: Dr. R. G. Jahn	1
NASA-Langley Research Center Langley Field Station Hampton, Virginia 23365 Attn: M. Ellis R. Hess	1 1
Avco-Everett Research Laboratory A Division of Avco Corporation 2385 Revere Beach Parkway Attn: Dr. R. M. Patrick	1
United States Air Force Office of Scientific Research Washington, D. C. 20025 Attn: M. Slawsky	1
Space Sciences, Incorporated 301 Bear Hill Road Waltham, Massachusetts 02154 Attn: J. M. Proud	1
Ford Motor Company Aeronutronics Newport Beach, California 92660 Attn: R. M. Spongberg	1

Addressee	No. of Copies
General Electric Company Missile and Space Division Space Sciences Laboratory P.O. Box 8555 Philadelphia, Pennsylvania 19101 Attn: P. Gloersen	1
Thermal Mechanical Research Laboratory OAR USAF Wright-Patterson Air Force Base, Ohio 45433 Attn: Eric Soehngen	1
Giannini Scientific Corporation 3839 South Main Street Santa Ana, California 92702 Attn: Adriano Ducati	1
Los Alamos Scientific Laboratories P.O. Box 1663 Los Alamos, New Mexico 87544 Attn: Dr. Stratton	1
Catholic University of America Department of Space Sciences and Applied Physics Washington, D. C. 20017 Attn: Prof. C. C. Chang	1
University of Minnesota Department of Mechanical Engineering Heat Transfer Laboratory Minneapolis, Minnesota 55435 Attn: Dr. E. Pfender	1
McDonnell Aircraft Corporation P.O. Box 516 St. Louis, Missouri 63166 Attn: Dr. W. van Camp	1
Research Library - Wilmington (+ 1 reproducible)	3
Research Library - Lowell (+ 1 reproducible)	1
Reports Distribution Center - Wilmington	33

DISTRIBUTION

Addressee	No. of Copies
W. Bade	1
S. Bennett	5
L. Cass	1
G. Enos	1
M. Goriansky	1
R. John	1
R. Krauss	1
A. Malliaris	1
J. Maxwell	1
M. Malin	1
A. Ogden	1
R. Patrick (Avco/Everett)	1
W. Powers	5
R. Schlier	1
A. Schneiderman (Avco/Everett)	1
C. Simard	1
A. Tuchman	1
R. Wetherby	1
J. Workman (Avco/Everett)	1
J. Yos	1
Central Files	1
Research Library - Wilmington	1
Research Library - Lowell	1
Reports Distribution - Wilmington	1
Reports Distribution - Lowell	1